

# Evaluation of pore water pressures and breach growth in an existing dike during an in situ test at Wichelen (Belgium)

Lode De Vriese

Supervisors: Prof. dr. ir. Tom De Mulder, Prof. Adam Bezuijen

Counsellors: Ir. Patrik Peeters (Waterbouwkundig Laboratorium), Dr. ir. Leen De Vos (Afd. Geotechniek)

Master's dissertation submitted in order to obtain the academic degree of  
Master of Science in Civil Engineering

Department of Civil Engineering  
Chair: Prof. dr. ir. Peter Troch  
Faculty of Engineering and Architecture  
Academic year 2015-2016



# Preface

As a student in Civil Engineering, I've always been interested in geotechnics. Dike construction and breaching is something that was limitedly seen in the different courses. Living close to the river Scheldt, this master dissertation was the ideal opportunity to deepen myself into this matter.

I would like to express my gratitude towards all persons who have contributed to the realization of this thesis.

My supervisors from Ghent University: Prof Adam Bezuijen and Prof Tom De Mulder and my counsellors: from the geotechnics division of the Flemish government dr. ir. Leen De Vos and from Flanders Hydraulics Research ir. Patrik Peeters. I thank them for their feedback, advice, patience and willingness to support. Further I would like to thank all the people at the geotechnics division for their support during my thesis. In particular: Elke Declercq and Hannes Quintens.

Finally, I want to thank my parents, brother and girlfriend, without their support it wouldn't have been possible to succeed in my study and this master dissertation.

Lode De Vriese, June 2016

# Permission for use of content

The author gives permission to make this master dissertation available for consultation and to copy parts of this master dissertation for personal use. In the case of any other use, the copyright terms have to be respected, in particular with regard to the obligation to state expressly the source when quoting results from this master dissertation.

Lode De Vriese, June 2016

# Toelating tot bruikleen

De auteur geeft de toelating deze masterproef voor consultatie beschikbaar te stellen en delen van de masterproef te kopiëren voor persoonlijk gebruik. Elk ander gebruik valt onder de bepalingen van het auteursrecht, in het bijzonder met betrekking tot de verplichting de bron uitdrukkelijk te vermelden bij het aanhalen van resultaten uit deze masterproef.

Lode De Vriese, juni 2016

# Evaluation of pore water pressures and breach growth in an existing dike during an in situ test at Wichelen (Belgium)

By

Lode De Vriese

Master's dissertation submitted in order to obtain the academic degree of

Master of Science in Civil Engineering

Academic year 2015-2016

Supervisors:

Prof. dr. ir. Tom De Mulder

Prof. dr. ir. Adam Bezuijen

Dr. ir. Leen De Vos

Ir. Patrik Peeters

Department of Civil Engineering

Faculty of Engineering and Architecture

## **Abstract**

In this master dissertation an in situ dike breach test is discussed. Discharge measurements are done and compared to formulas found in literature. A new coefficient of discharge is calculated and validated for this situation. The pore water pressures in the dike are measured during the test to see the effect of hindered erosion and the saturation of the dike. A simulation of the pore water pressure is done in SEEP/W and a comparison is made with the measured values. In literature the breaching process is usually discussed using specially made dikes as verification. This in situ test gave the opportunity to examine the breaching process in a real dike. Surface erosion and macro(in)stability are both analysed as the dominant breach growth processes. The slope stability calculation is linked to the calculated pore water pressure. The methods are evaluated and compared to the observations.

## **Keywords**

Dike breaching, Breach growth, Breach discharge

# Evaluation of pore water pressures and breach growth in an existing dike during an in situ test at Wichelen

Lode De Vriese

Supervisors: Tom De Mulder, Adam Bezuijen, Leen De Vos, Patrik Peeters

**Abstract**—In this article an in situ dike breach test is discussed. Discharge measurements are done and compared to formulas found in literature. A new coefficient of discharge is calculated and validated for this situation. The pore water pressures in the dike are measured during the test to see the effect of hindered erosion and the saturation of the dike. A simulation of the pore water pressure is done in SEEP/W and a comparison is made with the measured values. In literature the breaching process is usually discussed using specially made dikes as verification. This in situ test gave the opportunity to examine the breaching process in a real dike. Surface erosion and macro(in)stability are both analysed as the dominant breach growth processes. The slope stability calculation is linked to the calculated pore water pressure. The methods are evaluated and compared to the observations.

**Keywords**—Dike breaching, Breach growth, Breach discharge

## I. INTRODUCTION

### A. Situation

The breach test is part of the updated Sigmaplan which has as main objective to mitigate flood risks along the Scheldt estuary in Flanders (Belgium). This is done by making more flood control areas (FCA). Therefore new dikes have to be constructed more inland and the old dikes sometimes lose their function and have to be removed. This opportunity gave the possibility to execute overflow breach tests on these dikes. In this framework in Wichelen between Ghent and Antwerp a new FCA was constructed and an overflow breach test was staged on the old dike. This is marked in Fig. 1.



Fig. 1. Situation of the FCA in the Scheldt estuary [1]

### B. Geometry and composition

In Fig. 2 the geometry of the dike is shown. The dike consisted out of a sand core surrounded by a clay layer of approximately 30 cm. The sand core reached until the level of the polder. The clay layer of the polder stretched until the river. At the river side a riprap revetment is present almost until the crest, at the landward side an old grass cover is present.

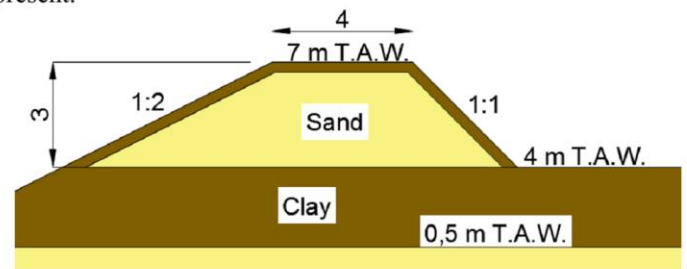


Fig. 2 Dike geometry

## II. BREACH TEST

Breaching of the dike was initiated by making a pilot channel in the dike. The dimensions of this channel were optimized to obtain the most successful test possible. The breach test was executed on two consecutive days: 16/11/2015 and 17/11/2015. The first test wasn't successful due to a too low water level in the river. The subsequent day, the depth of the pilot channel was increased and there was a higher water level. After the test on 17/11/2015, part of the riprap revetment was removed.

## III. DISCHARGE THROUGH THE BREACH

The formula given by Govinda and Murilidhar [2] is suggested to be a good approximation of the breach discharge.

$$Q = C_d \sqrt{g} B_e H^{3/2}$$

$$0,971 \sqrt{8/27} \left(\frac{H}{L_c}\right)^{0,022}$$

With:  $C_d$

The discharge through the breach is indirectly measured using a volume to height ratio made of the polder. When the measured discharge is compared to formula given in [2] it is noticed that the discharge in the breach is much smaller. The main reason for this is the rough bottom in the breach. It was noticed that part of the riprap protection on the river side was flowed into the breach. This causes a lot of friction decreasing the water flow.

A new coefficient of discharge is calculated. This coefficient of discharge is obtained by minimalizing the RMSE compared to the measured water volume and derivated discharge in the polder. An evaluation is done by performing an ADCP measurement in the breach. The best solution was obtained when using a constant value of Cd and optimizing it using the measured water discharge in the polder. In Fig. 3 the discharge calculations are shown.

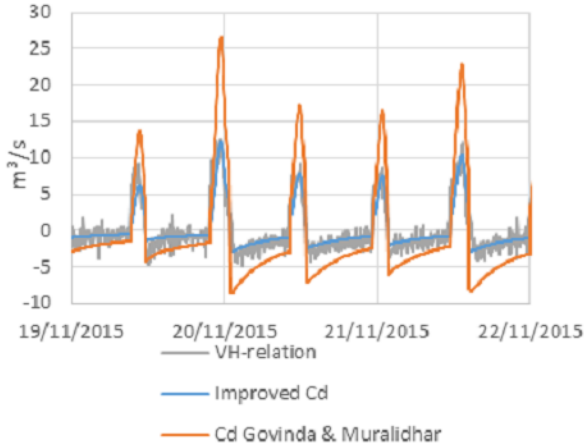


Fig. 3 Discharge calculations

#### IV. WATER PRESSURE IN THE DIKE

The water pressures in the dike are measured to examine the saturation of the dike in time and the effects of hindered erosion, as described in [3]. Hindered erosion causes an under pressure in the dike. A simulation is done of the water pressure in the dike using the SEEP/W and is compared to the measurements

##### A. Placement of sensors

The placement of the sensors in the dike are shown in Fig. 4. Most sensors are placed landward because most erosion is expected here as in [4] Two different types of sensors are used BAT and MEMS sensors. The MEMS sensors have a smaller logging interval (1 sec) compared to the BAT sensors (60 seconds).

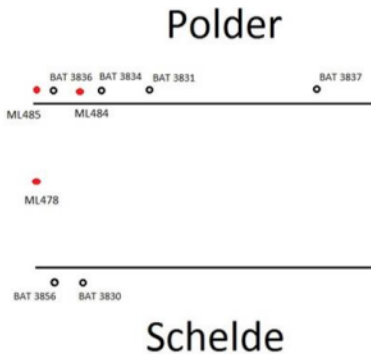


Fig. 4 Placement of the sensors

##### B. Hindered erosion

No suction pressures related to hindered erosion were measured. It is assumed that the flow velocities in the breach were too small and that the packing of the sand was too loose. Also the sensor has to be positioned just under the eroding layer.

#### C. Simulation pore water pressure

The measured water pressures are simulated using SEEP/W for a period from 8:07 h 17/11/2015 to 8:00 h 24/11/2015. The geometry inserted in SEEP/W consists out of three time steps 0-1200 sec, 1200-100380 sec, 100380 sec-end and is show in Fig. 5. These time steps are chosen in accordance with the observed breach growth. The crosses in the figure represent the sensors placed in the dike. The inserted soil properties were obtained by soil investigation.

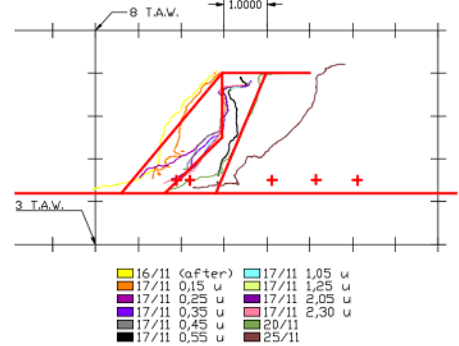


Fig. 5 SEEP/W model compared to observations

A good similarity was found between the measurements and the calculated values. The accuracy of the simulation is in direct relation to the inserted geometry. If there are fast changes in geometry the similarity between the simulation and the measurement is less.

#### V. BREACH GROWTH

##### A. Observations

There was mainly lateral breach growth due to the clay layer at the base of the breach. Therefore only breach phases IV and V were observed as described in [5]. The breach growth is split up into two different phases: the initial phase and the further breach growth. The initial phase is the breach growth during the first tide that flows through the breach. The subsequent growth is noted as the further breach growth. In the initial phase it is noticed that breach has a more O-shape because the sand core is more prone to erosion compared to the clay layer. In the further breach growth there is less direct erosion in the breach, the breach growth happens more due to slope failure. It is assumed that the riprap revetment that flowed into the breach protected the sides from further direct erosion. At the end of the breach test it could be seen that the breach growth was asymmetrical. The side where the riprap was removed had eroded more.

##### B. Analytical formulas

The breach growth is calculated using analytical formulas: the method of Van Rijn [6] and an excess shear strength equation. The inserted parameters in the formulas are obtained from ground research. Using the different obtained parameters a minimum and maximum value for erosion is given in Fig. 6. The method of Van Rijn [6] gives a good result when compared to the measured width. When the excess shear stress equation is used too large values are obtained (36-268 m).

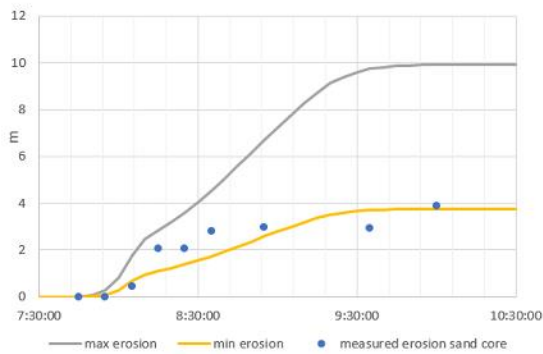


Fig. 6 Calculated erosion each side of the breach using Van Rijn[6]

The further breach growth is more prone to slope failure, therefore it is assumed that the formula of Van Rijn [6] isn't valid.

### C. Limit state equilibrium

The further breach growth is calculated using limit state equilibrium software, SLOPE/W, because SEEP/W and SLOPE/W are part of the same software suite: GEO Studio. The same model, with three geometries can be used and the results from the SEEP/W analysis are used as input. A Morgenstern Price analysis is performed for the same period. In the initial growth there is a lot of erosion, so at the end of each geometry a piece of the toe is removed. This is in correspondence with the observations and with the calculated erosion speed.

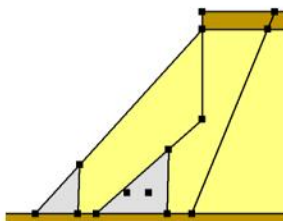


Fig. 7 Geometry in SLOPE/W

For the first geometry: 0-1200 sec, the factor of safety increases due to an increase in suction forces. When a piece of toe of 0,6 m is removed, a factor of safety of 0,995 is obtained so failure is likely to occur. The slip surface is in accordance with the observations as can be seen in Fig. 8.

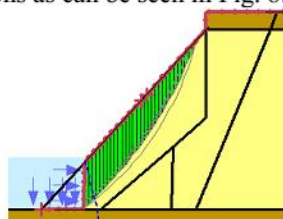


Fig. 8 Slip surface for first geometry

For the subsequent geometry the calculated factor of safety is shown in Fig. 9. The most critical moment in time is just after high tide when the water is flowing out of the sides causing a destabilizing gradient. A piece of toe of 1 meter was removed at the most critical moment (52000 seconds). This calculation gave a higher factor of safety. This can be explained due to model errors: the flow is modelled for the non-eroded part. If the toe is removed, the part where the destabilizing gradient occurs is removed. In reality the flow will penetrate deeper into the soil.

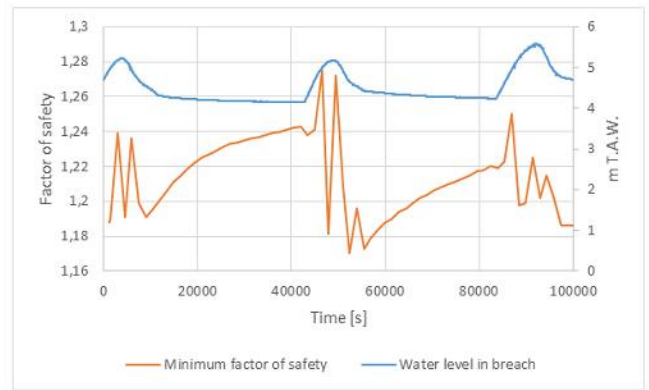


Fig. 9 Factor of safety second geometry 1200-100380 sec

When calculating the final geometry it was found that only shallow slip surfaces occurred. In Fig. 10 the factor of safety is given in time. The depth of these slip surfaces was approximately 0,3 m. This failure mechanism is in agreement with the observations.

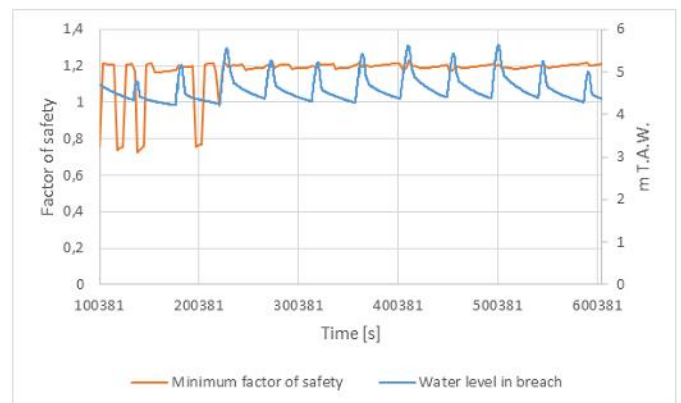


Fig. 10 Factor of safety second geometry 100380 min -end

## VI. CONCLUSION

The discharge in the breach was smaller compared to formulas found in literature. The riprap protection that has flowed into the breach is the main reason for this causing more friction also there was some influence of the riprap onto the breach growth noticed. The effects of hindered erosion weren't measured during the test. The breach growth is split up into: the initial phase, calculated using the method of Van Rijn, and the further growth, calculated using the limit state equilibrium. A good agreement is noticed between the calculations and the measurements.

## REFERENCES

- [1] Peeters, P., Visser, P., & Mostaert, F. (2012). Organisation of in situ dike breaching experiments in Belgium: Monitoring program. Version 2\_0. WL Rapporten, 706\_08e. Flanders Hydraulics Research & Delft University of Technology. Antwerp, Belgium.
- [2] Govinda Rao, N. S., & Muralidhar, D. (1963, Aug/Sept). Discharge characteristics of weirs of finite crest width. *La Houille blanche No. 5*, 213-232.
- [3] Van Rhee, C. (sd). Sediment entrainment at high flow velocity. *Journal of hydraulic engineering, ASCE, vol. 136 no. 9*, (pp. 572-582).
- [4] Peeters, P., Zhao, G., Visser, P., & De Vos, L. (2012). Large-scale Dike Breaching Experiments at Lillo in Belgium. *Proceedings of the 7th international conference on Scour and Erosion, Chapter 32* (pp. 289-297). Perth, Australia: CRC Press.
- [5] Visser, p. (1994). A model for breach growth in sand-dikes. Proc. 24th Int. Conf. coastal Eng., (pp. 2755-2769). Kobe, Japan.
- [6] Van Rijn, L. (1993). Principles of Sediment Transport in Rivers, Estuaries and Coastal Seas. Amsterdam: Aqua publications.

# Table of contents

Preface.....	I
Permission for use of content .....	II
List of abbreviations and symbols .....	XI
1 Introduction .....	1
1.1 Situation test.....	1
1.2 Geometry and composition of the dike .....	2
1.3 Aim of the thesis.....	4
1.4 Outline of the thesis .....	4
2 Previous breach experiments .....	6
2.1 Zwin '94 breach experiment.....	6
2.1.1 Breach test.....	6
2.1.2 Hindered erosion.....	8
2.2 Model test on sand dike with clay liner.....	9
2.3 Model test on embankment with inclined clay core.....	10
2.4 Model test of cohesive embankments .....	11
2.5 Large-scale dike breaching experiments at Lillo in Belgium .....	12
2.6 Conclusion .....	14
3 Considerations before breach test .....	15
3.1 Timing test .....	15
3.2 Pilot channel .....	16
3.2.1 Situation of channel .....	17
3.2.2 Angle of the side slopes.....	17
3.2.3 Width.....	18
3.2.4 Depth.....	18
3.2.5 Hydraulic grade line calculation program .....	18
3.2.6 Conclusion .....	26
3.3 Discharge measurement.....	26
3.3.1 Height to volume relation .....	26
3.3.2 Extra dike.....	27
3.4 Piezometers .....	27
3.4.1 Saturation .....	28



3.4.2	Suction tests of BAT and MEMS sensors.....	30
3.4.3	Installation.....	32
3.4.4	Location of sensors in the dike.....	32
3.5	Other measurements/tests .....	33
3.5.1	Before the breach test .....	34
3.5.2	During breach test.....	34
3.5.3	After breach test .....	34
4	Preparations test.....	35
4.1	Installation sensors.....	35
4.2	Soil tests.....	36
4.3	Pilot channel .....	36
4.4	Grid .....	36
5	Observations during the breach test .....	37
5.1	Breach test I on 16/11/2015.....	37
5.2	Breach test II on 17/11/2015.....	38
5.3	Further progress of the breach.....	40
6	Flow rate through the breach .....	42
6.1	Surface floats .....	42
6.1.1	Water velocity using GPS floats .....	42
6.1.2	Water velocity using camera images .....	44
6.1.3	Conclusion .....	44
6.2	Divers .....	44
6.2.1	Discharge calculation .....	44
6.2.2	Conclusion .....	50
6.3	Water velocity calculation .....	50
6.3.1	Estimation.....	50
6.3.2	Conclusion .....	51
6.4	ADCP measurement.....	52
6.5	Evaluation of coefficient of discharge .....	53
6.6	Conclusion .....	55
7	Water pressures in the dike.....	56
7.1	Breach test I on 16/11/2015.....	56
7.2	Breach test II on 17/11/2015.....	57

7.3	Further progress of the breach.....	58
7.4	Calculation with SEEP/W .....	58
7.4.1	Model .....	59
7.4.2	Boundary conditions .....	60
7.4.3	Soil properties .....	61
7.4.4	Results .....	62
7.4.5	Sensitivity analysis.....	65
7.5	Conclusion .....	68
8	Breach growth.....	69
8.1	3D models.....	69
8.2	Initial phase.....	69
8.2.1	Breach growth in top view .....	69
8.2.2	Vertical breach growth.....	70
8.2.3	Calculation.....	71
8.2.4	Conclusion .....	74
8.3	Further breach growth .....	75
8.3.1	Breach growth in top view .....	75
8.3.2	Vertical breach growth.....	77
8.3.3	Calculation.....	77
8.3.4	Conclusion .....	78
8.4	Calculation of breach growth in SLOPE/W .....	78
8.4.1	Model .....	78
8.4.2	Soil properties .....	79
8.4.3	Forces on the soil .....	80
8.4.4	Calculation.....	80
8.4.5	Results .....	83
8.4.6	Sensitivity analysis.....	87
8.5	Conclusion .....	89
9	Conclusion and recommendations .....	90
10	References.....	92
11	Annexes .....	97
	Annex A: Soil characteristics dike .....	97
	Annex B: Plan of sensors and tests.....	102

Annex C: Water pressures recorded after the breach experiments .....	103
Annex D: Calculated water pressures with lower water level .....	106

# List of abbreviations and symbols

$\alpha$	Angle of the side slopes of the breach
$\rho_s$	Density of sand
$\rho_w$	Density of water
$\sigma_n$	Normal stress in soil
$\tau$	Shear stress
$\tau_{b,cr}$	Critical shear stress
$\tau_b$	Near bed shear stress
$\varphi'$	Effective angle of internal friction
$\varphi^b$	Angle indicating the rate of increase in shear strength relative to matric suction
$\Delta$	Relative density
3D	Three dimensional
ADCP	Acoustic Doppler current profiler
ATO	General technical support division from the Flemish government
BAT	Type of piezometer
$B_b$	Bottom width of the breach
$B_e$	Effective width
$c'$	Effective cohesion
$C_d$	Discharge coefficient
CPT	Cone penetration test
$D^*$	Dimensionless particle diameter
DOV	Database of the subsoil of Flanders
$D_{xx}$	Diameter corresponding with the xx% cumulative percentile value
E	Pick-up rate
F	Factor of safety
FCA	Flood control area
FHR	Flanders Hydraulic Research

g	Gravitational constant (9,81 m/s <sup>2</sup> )
GEO	Geotechnics division of the Flemish government
GPS	Global Positioning System
H	Water height above the beach
H <sub>w</sub>	Water height at the higher part of a broad crested weir
HET	Hole erosion test
HIC	Hydrological information centre
JET	Submerged jet erosion test
k <sub>d</sub>	Coefficient of erosion
L <sub>c</sub>	Crest length
MEMS	Type of piezometer
m <sub>v</sub>	Coefficient of volume change
n	Mannings roughness coefficient
N.A.P.	Normaal Amsterdams peil: General reference height in the Netherlands This is 2,33 m higher than T.A.W, the general reference height in Belgium
N <sub>i</sub>	Interslice normal force
n <sub>o</sub>	In-situ porosity
Q	Discharge
R	Hydraulic radius
RMSE	Root mean square error
T.A.W.	Tweede Algemene Waterpassing: General reference height in Belgium
TUD	Technical University Delft
U	Mean water velocity
U <sub>b</sub>	Water velocity at the bed
u <sub>a</sub>	Soil-air pressure
u <sub>w</sub>	Pore water pressure
VBA	Visual Basic for Applications
v <sub>e</sub>	Erosion rate

VH	Volume to height
WC	Water content
z	$H/\tan(\alpha)$
$Z_{br}$	Depth of the breach

# 1 Introduction

## 1.1 Situation test

This breach test is part of the updated Sigmoplan. The main objective of the updated Sigmoplan is to mitigate flood risks along the Scheldt estuary in Flanders (Belgium). This is done by making more flood control areas (FCA) with or without controlled reduced tide, (non-)tidal wetlands,... Therefore new dikes have to be constructed more inland and the old dikes sometimes lose their function. This opportunity gave the possibility to execute overflow breach tests on these dikes. Figure 1-1 gives an overview of the updated Sigmoplan and an overview of the measures taken. (Peeters, Zhao, Visser, & De Vos, 2012)

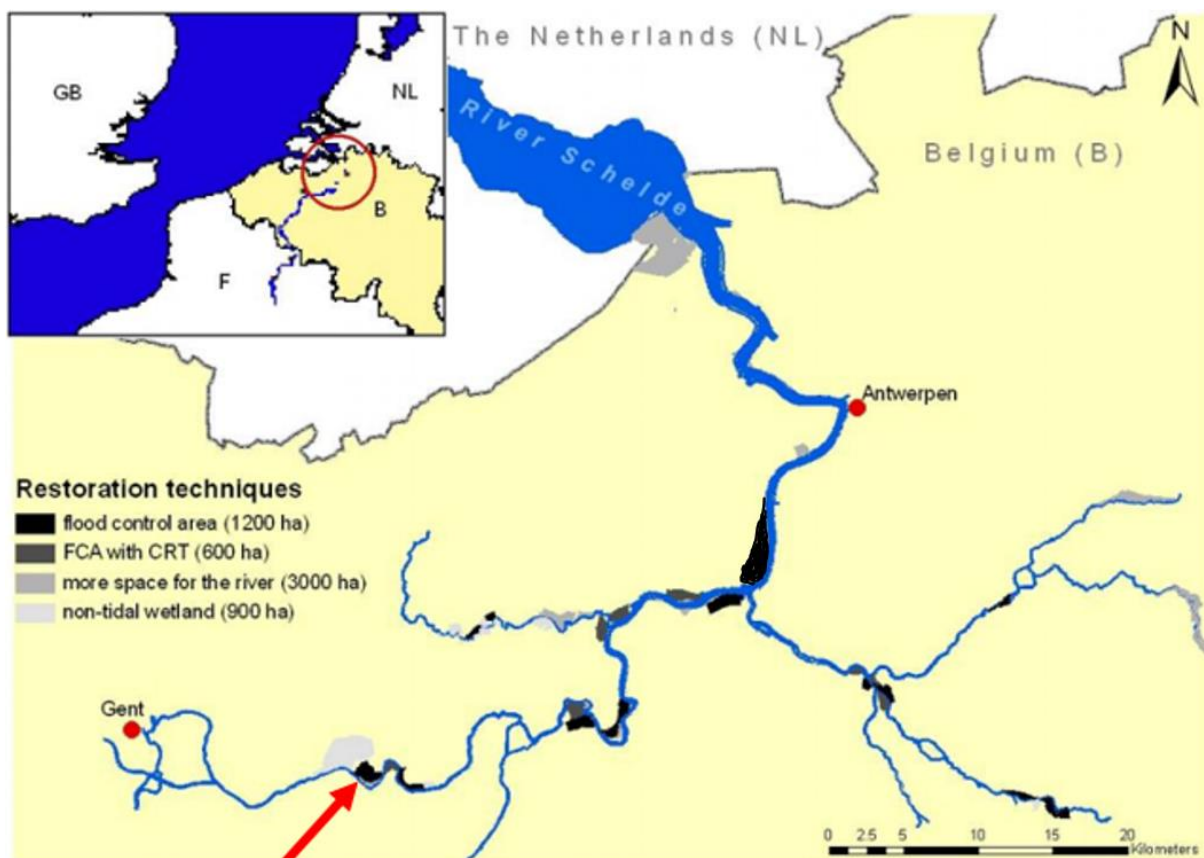


Figure 1-1 General overview of the updated Sigmoplan (Peeters, Visser, & Mostaert, 2012)

In Wichelen, situated along the Sea Scheldt between Ghent and Antwerp a new FCA was constructed. The location is indicated in Figure 1-1 by the red arrow. Part of this FCA consisted of a 22 hectare tidal wetland. Therefore a new ring dike was constructed landward and the old dike had to be partially removed. This gave the opportunity to execute some tests on the latter dike. A breach test was one of them. In Figure 1-2 an overview of the breach location is given. There is a zone of 100 meter on the dike where tests have been executed, at both ends riprap covered with concrete was installed to limit further damaging of the dike. The breach experiment is performed in association with TU Delft and Flanders Hydraulics Research (FHR).

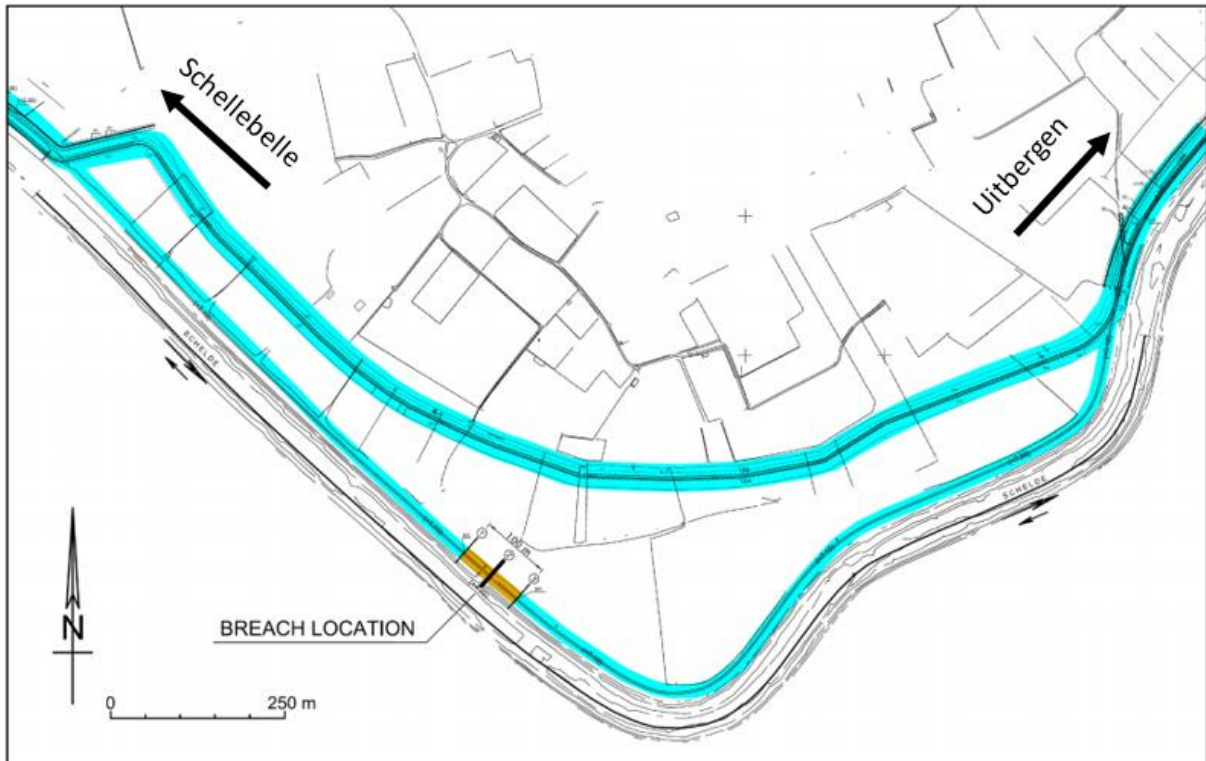


Figure 1-2 Overview breach location (Peeters, Visser, & Mostaert, 2012)

## 1.2 Geometry and composition of the dike

The dike geometry and composition is given in Figure 1-3. The difference between the mean high water level and the level of the FCA is approximately 1,3 meter.

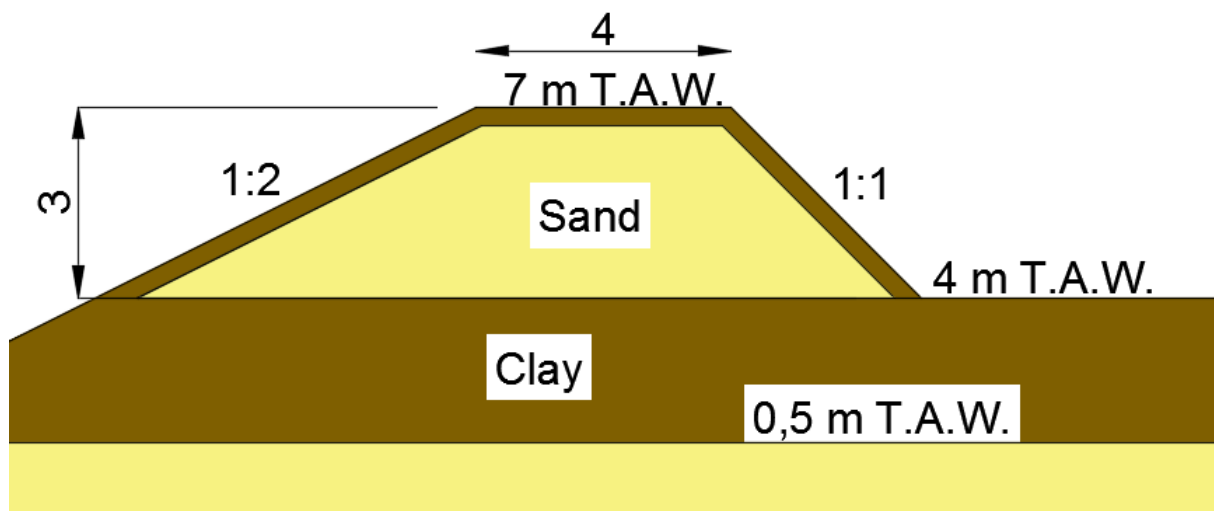


Figure 1-3 Geometry and composition of the dike

The dike consists of a cover layer of clay with grass on top of approximately 30 cm thick with an inner sand core. This can be seen in Figure 1-4. To have an indication of the soil of which the dike consists 9 CPT-tests are conducted (DOV, 2016), 3 at each side of the crest and 3 in the polder. There was a lot of scatter in the result of the different CPT-tests. This can be explained by the fact that this dike was probably made by using different batches of ground. Some general remarks can be made:



- At a level of 4 m T.A.W a clay layer is present
- The dike consists of a sand core.
- Under this sand core there is a clay layer that extends in the polder.
- Under this clay layer there is another sand layer.

The soil properties of the clay layer and sand core can be found in Annex A.



*Figure 1-4 clay lining and inner sand core (Irstea, 2015)*

In Figure 1-5 the dike is shown at the breach location. At the river side a rip rap revetment is present almost until the crest. There is also some vegetation at the river side mainly consisting out of reed. At the polder side an old grass cover is present. On the dike crest there is a bicycle path made out of small stone chippings.



*Figure 1-5 Dike at location breach experiment*

## 1.3 Aim of the thesis

In this thesis three main subjects are discussed: the flow through the breach, the pore water pressure in the dike and the breach growth caused by surface erosion and macro(in)stability.

The breach test is done by making a pilot channel in the dike during low tide in the river. During high tide the dike will encounter overflow and fail. The timing of the test and pilot channel dimensions were examined in order to have the best possible test conditions.

The flow through the breach is measured (indirectly) to compare it to different formulas found in literature. The coefficient of discharge is estimated and validated to make a prediction of the water velocities in the breach. These water velocities are necessary to calculate the erosion rate.

The pore water pressure in the dike is measured to see the effects of hindered erosion. This should cause a suction pressure in the dike. The saturation of the dike is also studied. This saturation is calculated and compared to the software.

Other breach experiments are discussed and compared to the situation in Wichelen to see if it is possible to make a prediction. In literature the breaching process is usually discussed using specially made dikes as verification. This in situ test gave the opportunity to examine the breaching process in a real dike. The dike in Wichelen is covered by a clay layer and a riprap revetment is present at the river side. The influence of these factors on the breach growth are examined.

The breach growth is compared to the breach phases as described by Visser. (Visser P. , 1998) The possibility to predict the breach growth is investigated using the formula given by Van Rijn (Van Rijn, 1993) and a slope stability analysis is used. The results are compared to the observations.

## 1.4 Outline of the thesis

In the first chapters some preliminary research of the breach test is presented. In chapter 2, other breach experiments are discussed and compared to the situation at Wichelen to make a prediction of the breach growth. In chapter 3 some calculations and considerations are given to attain an optimal test: the best possible timing is examined. The dimensions of the pilot channel that initiates the breach are discussed. The pore water pressure sensors that will be placed in the dike are tested prior to the breach experiment. The best situation of the sensors is given. In chapter 4 the in situ preparations are discussed.

In the following chapters results are described. In chapter 5 the observations and impressions of the breach test are given. In chapter 6 the flow through the breach is discussed using different measuring methods and a comparison is made using existing formulas. In chapter 7 the pore water pressures in the dike are discussed. The pore water pressures are simulated using finite-element software SEEP/W and compared to the measurements. Chapter 8 discusses the breach growth. The breach growth is modelled using the formula of Van Rijn and in SLOPE/W using the pore water pressure calculation. A comparison is made with the

observations. Finally a conclusions and recommendations for further research are presented in chapter 9.

## 2 Previous breach experiments

By investigating previous (model) breach tests insight is gained in the breaching process. A comparison is made between these experiments and the situation in Wichelen. The first test discussed, Zwin '94' breach experiment, is used to explain the mechanism of hindered erosion.

### 2.1 Zwin '94 breach experiment

#### 2.1.1 Breach test

The Zwin '94 breach experiment consisted out of two tests, the most successful one is considered here. A sand dike was constructed in the Zwin Channel, a tidal inlet at the Dutch-Belgian border. This dike was breached due to water overflow. The high tide at the inlet ranges from 2,85 m NAP at neap tide to about 4,35 m NAP at spring tide. During the experiment the weather conditions were good and the waves against the dike were negligible. (Visser P. , 1998)

The dike tested was 3 m high and its width at the top was 8 m. A cross-section of the dike is given in Figure 2-1. It was constructed with local sand ( $D_{50}$  approx. 0,20 mm). A small pilot channel, 2 m wide and 0,8 m deep, was made to ensure breaching of the dike near the middle of the inlet.

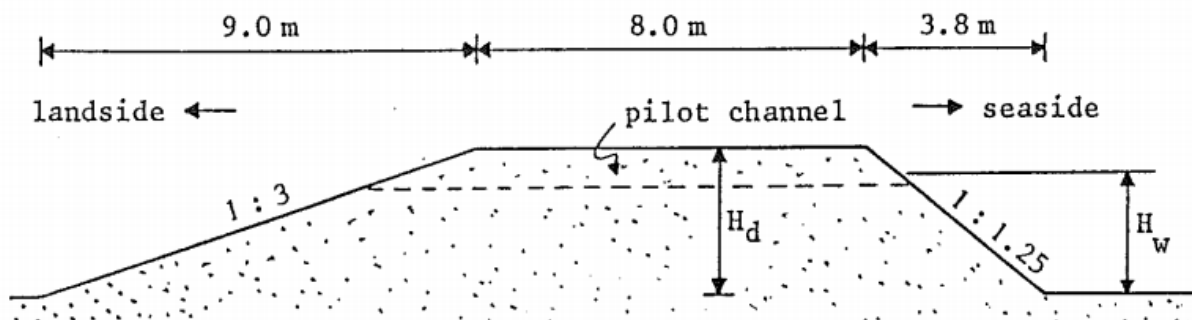


Figure 2-1 Cross section (Visser, Kraak, Bakker, & Smit, 1995)

The experiment was started approximately 20 minutes before high tide by removing a small temporary dike in the pilot channel. The breach erosion process lasted for approximately 60 minutes. The width of the breach at the end of the test was 42 meters.

During the experiment five different stages of breach growth were noticed as previously described in (Visser p. , 1994). The transition between each phase is given in Figure 2-2.

- I. Steepening of the landside slope (0-1,5 min)
- II. Retrograde surface erosion of the land-side slope (1,5-6,5 min)
- III. Lowering of the dike crest, vertical breach growth and increase of flow (6,5-8,5 min)
- IV. Mainly lateral breach growth with critical flow conditions (8,5-23 min)
- V. Mainly lateral breach growth with subcritical flow conditions until breach growth stops (23-60 min)

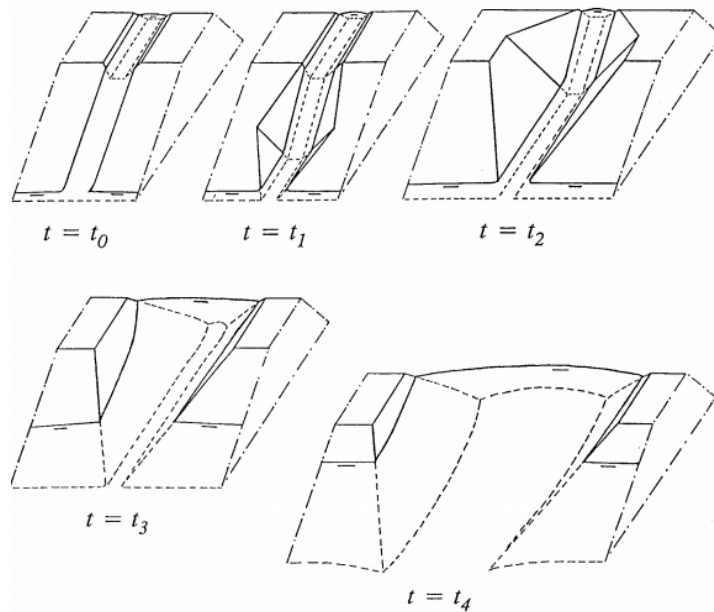


Figure 2-2 Five-step breaching mechanism (Visser P. , 1998)

During the test the flow velocities were measured using Ott-propellers. The sensors were situated at a depth of 1,5 NAP, this is approximately one meter below the water level of high tide. Sensors MS-4 and MS-5 are placed on the land side of the breach so they weren't fully submerged in the beginning of the test. Only the submerged results are depicted.

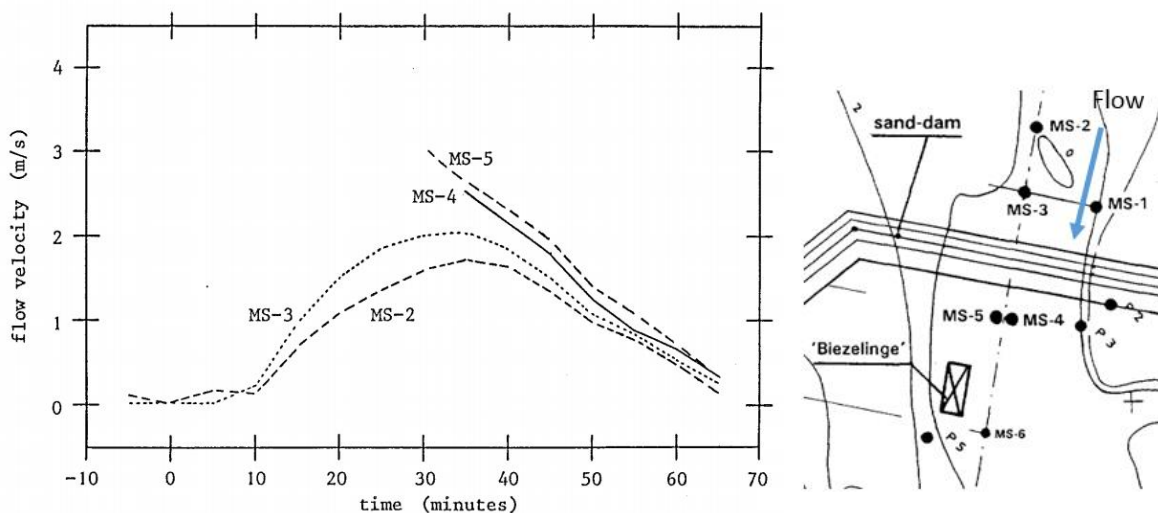


Figure 2-3 Flow velocities and positioning of sensors (Visser, Kraak, Bakker, & Smit, 1995)

## Comparison

In this experiment a dike is constructed using local sand, this is different to the experiment in Wichelen where an in situ dike will be tested. On the Wichelen dike vegetation is present, a clay lining and bicycle path. These elements will slow down the erosion, therefore it can be expected that the breach growth will be much slower and more limited. When the soil properties are compared, the sand core in Wichelen is approximately the same as the sand in the Zwin '94 breach experiment  $D_{50} = 0,15 \text{ mm} \leftrightarrow 0,2 \text{ mm}$ .

The water level differences are in this experiment approximately 1,5 meter. This is comparable to the difference expected in Wichelen (1,3 m). The water level difference in Wichelen will be lower but the length of the breach is smaller so there will be less friction, therefore it is expected that the flow velocities will be comparable with these in the breach experiment in Wichelen.

### 2.1.2 Hindered erosion

Conventional models, for example the model of Van Rijn (Van Rijn, 1993), to calculate the erosion rate for non-cohesive sediments tend to make an overestimation when high flow velocities are present. These flow velocities occur, for instance, in breaching of dikes or in jetting sand with a trailing suction hopper dredger. At these flow velocities the erosion process is significantly influenced by the soil properties. In (Bisshop, Visser, Van Rhee, & Verhagen, 2010) is explained that the erosion will be hindered: “faster than the grains move upward they cannot erode”. The concept of hindered erosion is explained by two properties of granular soils: dilatancy and permeability.

If erosion occurs at low flow velocities grains are picked up one at a time. If the flow velocity increases layers of grains are picked up at a time. The top layer is subjected to shear. During shearing the arrangement of the grains will change. If sand is densely packed, during shearing the porosity will increase. This is shown in Figure 2-4. This increase in volume needs to be compensated by a flow of water to increase the pore volume. This can only happen if the pore water pressure decreases in the sheared zone introducing a hydraulic gradient. This gradient sucks the top layer on the bed and hinders erosion. It is dependant of the erosion rate and permeability and initial density. If the sand is loosely packed less dilatation will occur compared to a densely packed sand. (Bisshop, Visser, Van Rhee, & Verhagen, 2010)

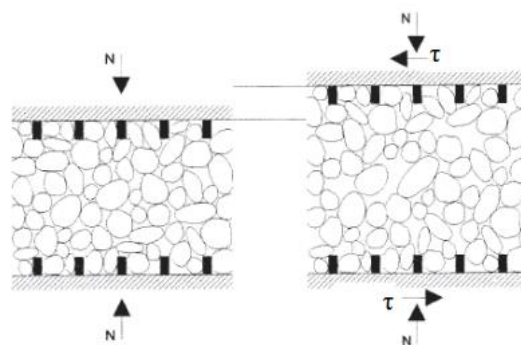


Figure 2-4 Increase in porosity during shearing of sand (CROW, 2004)

Van Rhee (2007,2010) derived an erosion formula that includes the effect of hindered erosion. This formula is evaluated using the erosion rates measured in the Zwin 94' breach experiment. Only the erosion rates measured during breach phase IV and V were used. Different side slope angles of the breach are given. The results of this comparison is given in Figure 2-5. The results of the formula of Van Rijn (Van Rijn, 1993) tend to overestimate the erosion rate at flow velocities larger than 1 m/s for these flow velocities better agreement is obtained using Van Rhee's formula. In (Bisshop, Visser, Van Rhee, & Verhagen, 2010) it is suggested to make use of the formula of Van Rhee when the flow velocities are larger than 1 m/s.

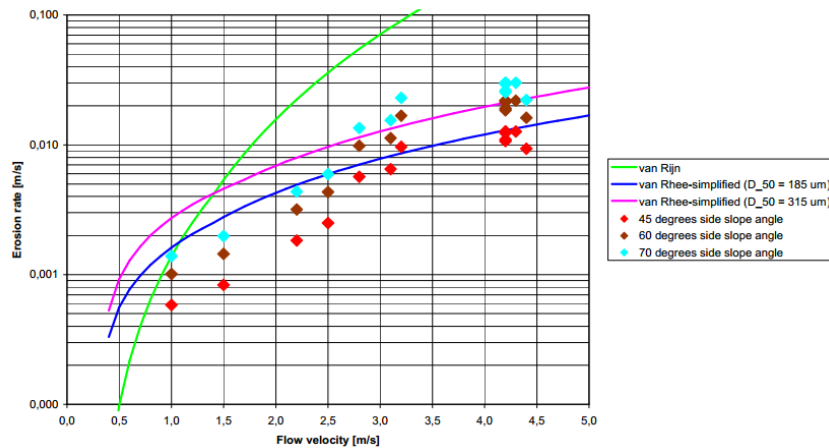


Figure 2-5 Experimental data vs. model calculations

## 2.2 Model test on sand dike with clay liner

In (Geisenhainer & Kortenhaus, 2006) the results are given of model tests conducted on a sand dike with a clay lining. This is done to have information on the influence of wave overtopping and overflow regarding the initiation of breaching of sea dikes at the landward side. The clay used in the models was taken from an existing dike. The sand core was 60 cm high and made out of different compacted layers, the clay liner on the top of the dike was 10 cm thick and 6 cm on both sides. The inclination of the landward slope is 1:3 and of the seaward slope 1:6.

The test conducted was a wave overtopping test. Wave parameters were selected to cause wave overtopping in the range of less than 0.1 l/(s.m)



Figure 2-6 Dike model view from seaward side

The dike failed due to erosion which started from the landward dike toe at the connection with the concrete flume. The sand had been removed, chunks of the clay layer on top failed consecutively and fell downwards so that a backward erosion of the clay layer occurred on the landward side of the dike.



Figure 2-7 Model after breach test (Geisenhainer & Kortenhaus, 2006)

### **Comparison**

The dike in Wichelen has similar characteristics as in this experiment but there are some differences. To initiate the breach test, a pilot channel will be dug in the dike so the clay lining on the dike will be partly damaged. The test conducted was a wave overtopping test. The breach test in Wichelen is an overflowing test. The clay lining itself will be more stable in Wichelen due to the presence of vegetation. In Wichelen there is a good transition between the polder clay and the clay lining of the dike so it is less likely to expect failure starting from the landward toe of the dike.

Because the pilot channel crosses the sand core, it can be expected that the erosion will start from the position at the landward side of the dike where the clay lining is still intact. The flow will erode the sand core causing a decrease in support of the clay lining at the landward side causing failure.

## 2.3 Model test on embankment with inclined clay core

In the test described by (Hunt, Hanson, & Temple, 2005) and (Hunt S. L., Hanson, Crook, & Kadavy, 2005) the lateral breach growth is examined. This is done by making an embankment and performing an overflow test. The completed embankment had a height of 1,3 m and crest width of 1,8 m, with upstream and downstream faces of the embankment sloped at 3:1. An inclined clay core was installed at the waterside and had a width of 0,9 m. A Stage IV breach process (Visser P. , 1998) was simulated by making a notch 0,30 m wide through the centre of the entire height of the embankment. Prior to testing, the notch was backfilled within 0,30 m of the top of the embankment with a sand plug to protect the notch opening as the reservoir filled. On the day of testing, the reservoir was filled to the level of overtopping the sand plug. The sand in the pre-cut notch quickly eroded, and the stage IV breach widening event began.



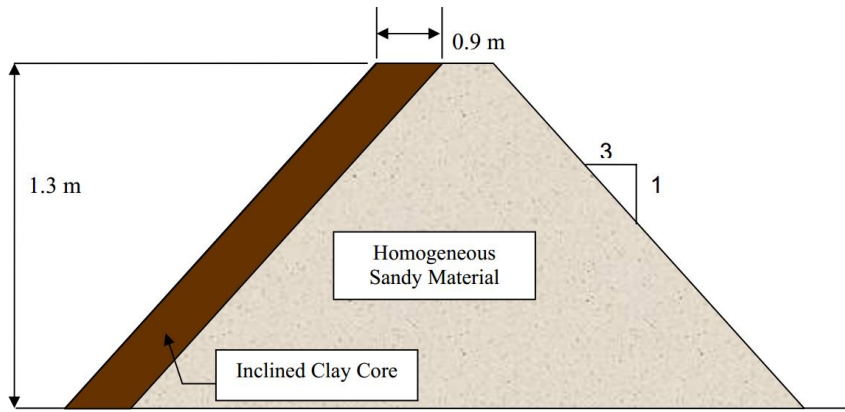


Figure 2-8 Schematic of embankment test with inclined clay core (not to scale) (Hunt, Hanson, & Temple, 2005)

The breach widening during the test was approximately 2,1 m/hour. It was found that the rate of widening did not vary significantly to that of a homogeneous sand dike. This is due to the fact that the loss of support of the clay material due to the eroded core caused the breach through the inclined core to widen as well.

### **Comparison**

In Wichelen a clay lining fully covers the dike. In this paper only the influence of an inclined clay core at the water side was examined. It is found that the influence is negligible. In Wichelen the riverside consists out of a clay lining with on top a riprap revetment and vegetation. The vegetation will support the clay lining, causing less erosion of the outer layer.

It is expected that the sand core will erode faster than the clay lining therefore an O-shaped breach can be expected. The lateral breach growth will mainly depend on the resistance to erosion of the outer clay lining.

## 2.4 Model test of cohesive embankments

Three large-scale physical cohesive embankment models were constructed and tested. The description of these tests is given in (Hanson, Cook, & Hunt, 2005). The different parameters of each embankment are given in Table 2-1. Soil 1 and 2 are made of silty sand. Soil 3 is a lean clay.

No.	Embankment			Notch		
	Height (m)	Slope	Soil	Depth (m)	Width (m)	Crest Length (m)
1	2.29	3:1	1	0.46	1.83	4.6
1	2.29	3:1	2	0.46	1.83	4.6
1	2.29	3:1	3	0.46	1.83	4.6
2	1.52	3:1	1	0.30	1.22	3.7
2	1.52	3:1	2	0.30	1.22	3.7
2	1.52	3:1	3	0.30	1.22	3.7
3	2.29	3:1	2	0.46	8.23	4.5

Table 2-1 Embankment parameters (Hanson, Cook, & Hunt, 2005)

During these tests the breach phases provided by literature (Visser P. , 1998) are noticed. In Table 2-2 the duration between each phase is given and the final erosion width.

Embankment	Soil	Breach			Peak Outflow (m <sup>3</sup> /s)	Final Erosion Width (m)	Erosion Side Slopes
		Initiation, $t_i$		Formation, $t_f$			
		Stage I ( $t_1 - t_0$ , min)	Stage II ( $t_2 - t_1$ , min)	Stage III ( $t_3 - t_2$ , min)			
1	1	16	15	20	6.5	6.9	Vertical
1	2	54	266	112	1.8	6.2	Vertical
1	3	164	>1036	--	1.0	4.2	Vertical
2	1	18	22	68	2.3	3.3	Vertical
2	2	80	1092	361	1.3	3.3	Vertical
2	3	166	>4200	--	0.3	2.4	Vertical
3	2	51	256	52	4.2	4.5	Vertical

Table 2-2 results (Hanson, Cook, & Hunt, 2005)

During all three tests the breach channel widened to a large extent as the breach slopes became undermined, causing mass failures to occur. The undermining was observed to occur as a detachment process, resulting in an overhang developing. This is in accordance with (Coleman, Jack, & Melville, 1997). A crack along the surface was observed at the initiation of mass failure of the bank. The breach widening happened in steps, the average speed was between 0,022 and 0,88 m/hour.



Table 2-3 Tension crack (Hunt S. L., Hanson, Crook, & Kadavy, 2005)

**Comparison**

The dike in this test consists out of cohesive soil, in Wichelen a sand core is present, so a faster erosion can be expected. It is expected that the same erosion process occurs: there will be a flow in the breach that will undermine the sides of the sand core causing chunks of the sides to fall in the breach. In the beginning of the breach most erosion will occur in the middle. At the landward and river side, the clay lining will be more difficult to erode.

2.5 Large-scale dike breaching experiments at Lillo in Belgium

An in situ dike breach test following overflow is executed along the tidal river Scheldt and described in (Peeters, Zhao, Visser, & De Vos, 2012). This test is executed in the same

framework as the breach test in Wichelen. It took place in Lillo just downstream of Antwerp where a 13 ha piece of land will be developed into a tidal marsh giving more space to the river. A new ring dike was constructed and on the old dike a breach test was executed. The dike had a height of 3 m and a crest width of 6 m. The inclination of the inner and outer slopes equals 3:1. A trapezoidal pilot channel with a bottom and top width of 1 m and 2 m respectively, was made. The bottom of this initial breach was 1,5 m above ground level. The dike consisted out of sand to about 5 m below the crest where there was a clay layer. At the riverside, a riprap revetment and reed vegetation is present. There was no grass cover present on the dike. The Lillo experiment confirms the breach stages described in literature (a.o. Visser, 1998; Zhu, 2006; Hahn et al., 2000; Oumeraci et al., 2005; Temple et al., 2005; Morris et al., 2009). Prior to the lateral breach growth, headcut migration precedes a V-shaped growth of the pilot channel. This can be seen in Figure 2-9. The breach sides remain vertical during the lateral growth in stage IV and stage V of the breach growth.

Different intersects were made along the dike width and the breaching speed was derived. This is seen in Figure 2-9, the widening speed goes from 0,64 to 0,32 m/min. The polder side erodes slower but longer than the riverside. The total erosion is approximately the same. The erosion of the breach was stopped after 50 min when the water level inland became equal to the river.

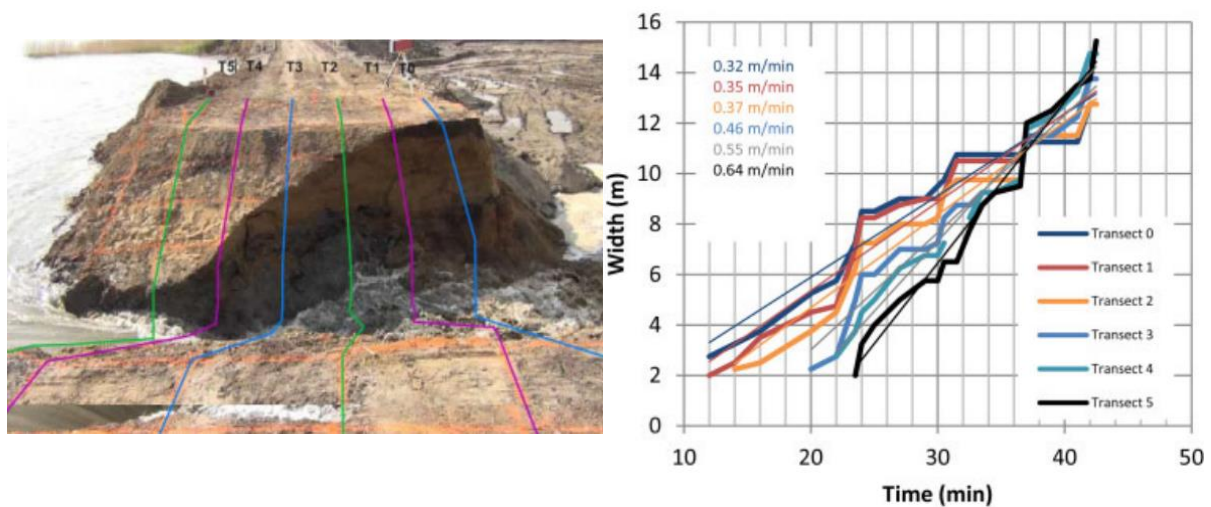


Figure 2-9 Breach width in time (Peeters, Zhao, Visser, & De Vos, 2012)

## **Comparison**

This test is very similar to the one executed in Wichelen. It makes use of an in situ dike where a pilot channel is dug to initiate the breach and the dike fails due to overflowing. This dike however had no clay lining or grass cover on it, this can make a significant difference in the erosion process. It can be expected that the breach widening speed is lower in the experiment in Wichelen.

In the breach experiment in Wichelen it is possible that there is a headcut formed. A V-shaped breach growth as in the breach experiment in Lillo can occur but this is much dependent of the erosion resistance of the outer clay lining.

## 2.6 Conclusion

It is expected that the breach growth is in accordance to the difference breach phases described by Visser (Visser p. , 1994). From the different tests it can be concluded that the inner sand core will be more prone to erosion. Because a pilot channel is dug in the dike there will be direct contact between the sand core and the flow of water. This unprotected sand will erode first and cause a loss in support of the clay lining similar to the breach experiment explained in section 2.3. It is possible that the breach will be V-shaped but more likely is the O-shape because the inner sand core will be most prone to erosion and will erode due to undermining as described in 2.4.

The water velocity in the breach will be comparable to the Zwin '94 breach experiment because the conditions are approximately the same.

It is difficult to predict an exact value for the breach growth. The tests indicate a large difference due to the difference in soils of which the dike consists. The water level at the two sides of the dike is different in each test. The influence of the vegetation on the dike is also not negligible. The range of values found for the breach growth is when assuming a breach time of 2 hours ranging from 0,022-42 m/h. The experiment of (Hunt, Hanson, & Temple, 2005) is most similar to the situation in Wichelen so a breach growth smaller than 4 m/h is expected.

# 3 Considerations before breach test

In advance of the breach test some considerations are made and some calculations are done to have the most successful test possible at the test location. The river Scheldt next to the dike is tidal so the timing is investigated. In the dike a pilot channel will be made to initiate the breach. The best possible dimensions of this pilot channel are calculated using the theory of hydraulic grade lines. It is suggested to make an extra dike in the polder to have a more accurate estimate of the flow through the breach. In the dike piezometers will be installed, these are tested in advance and their position in the dike is discussed.

## 3.1 Timing test

The water that will flow through the breach comes from the river Scheldt. This is a tidal river therefore the best timing of the test is investigated. This is done by examining the astronomical predictions of the water level in the river Scheldt in Uitbergen provided by Flanders hydraulic research (FHR). Uitbergen is two kilometres away from the test location so the difference is negligible. The water level in Uitbergen is given in m T.A.W. for every minute of the month of November. The maximum water level each tide is important, a higher water level is more beneficial for breach growth, because the water will have more energy and more erosion will occur.

A graph is made of the high water levels during the month of November in Figure 3-1. The red line indicates the mean high water level (5,16 m T.A.W.). It can be seen that the high water level differs in time this is due to the tidal influence. On 13/11/2015 and 27/11/2015 there are peaks, this is around the time of new moon (11/11/2015) and full moon (25/11/2015). The low water level of the river is more constant due to the base flow of the river. Note that these water levels are just an estimation because the weather also has an influence. The best intervals, taking only the water level in consideration, are 9-17/11/2015 and 23-30/11/2015.

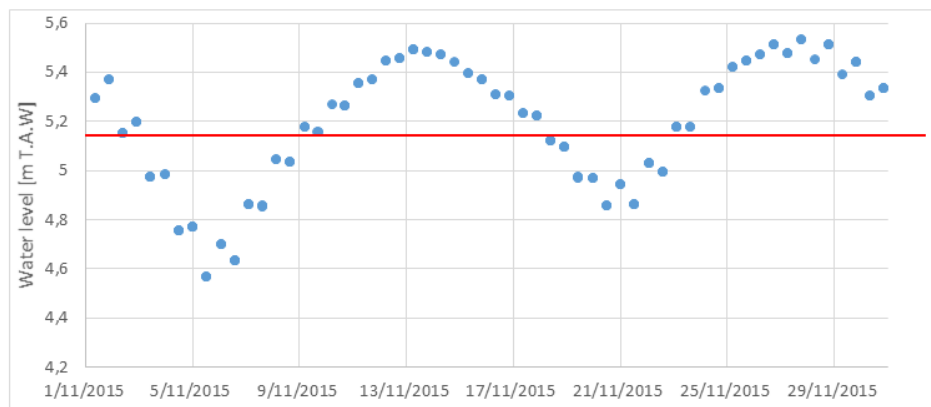


Figure 3-1 Waterlevels at Uitbergen

Not only the water level in the river Scheldt is important, but also the sunrise and -set times during this period are important. If the test is executed during daylight there is no need for electrical lighting of the test site. In Table 3-1 the sunrise and -set times are given for the month of November in Wetteren (5 km away of test location). Sunrise is the moment when

the sun is just above the horizon, so approximately half an hour earlier it is possible to make use of natural daylight.

The interval of dates that have a high water level naturally lit, is 1-9/11/2015 and 15-24/11/2015. It is more beneficial to have a high water level early in the day because then it is a certainty that whole the test can be performed in daylight.

To conclude: The best dates for the test are 15 to 17 November. The high water level will be above average and there can be made use of natural daylight, if the test is initiated half an hour before high water.

Date	Sunrise	Sunset	Day time
1/nov	7:37	17:19	9:41
2/nov	7:38	17:17	9:38
3/nov	7:40	17:15	9:35
4/nov	7:42	17:13	9:31
5/nov	7:43	17:12	9:28
6/nov	7:45	17:10	9:24
7/nov	7:47	17:08	9:21
8/nov	7:49	17:07	9:18
9/nov	7:50	17:05	9:14
10/nov	7:52	17:04	9:11
11/nov	7:54	17:02	9:08
12/nov	7:55	17:01	9:05
13/nov	7:57	16:59	9:02
14/nov	7:59	16:58	8:59
15/nov	8:01	16:57	8:56
16/nov	8:02	16:55	8:53
17/nov	8:04	16:54	8:50
18/nov	8:06	16:53	8:47
19/nov	8:07	16:52	8:44
20/nov	8:09	16:50	8:41
21/nov	8:10	16:49	8:39
22/nov	8:12	16:48	8:36
23/nov	8:14	16:47	8:33
24/nov	8:15	16:46	8:31
25/nov	8:17	16:45	8:28
26/nov	8:18	16:45	8:26
27/nov	8:20	16:44	8:24
28/nov	8:21	16:43	8:21
29/nov	8:22	16:42	8:19
30/nov	8:24	16:42	8:17

Table 3-1 Sunrise and -set times in Wetteren (Zonsopgang en zonsondergang Wetteren, 2015)

## 3.2 Pilot channel

The following parameters can be adjusted for the pilot channel:

- Situation of channel
- Angle of the sides
- Width
- Depth

A program is written in Visual basic for applications (VBA) to examine the influence of the depth on the different hydraulic parameters.

### 3.2.1 Situation of channel

The zone where the breach test can be executed has a length of 100 m. At both ends of this zone in the dike a concrete plug is installed. This is done to prevent any further erosion of the dike after the breach test. The initial plan was to make the breach in the middle of the test zone at S4 & S5 on Figure 3-2.



Figure 3-2 CPT-tests on dike crest (DOV, 2016)

Sand is easier to erode compared to clay and it is easier to measure pore water pressure differences in sand. Hence the most sandy conditions are best. These are found more near S1 & S2. Therefore it is decided to place the pilot channel more towards these locations. An example of the CPT-test S1 is given in Figure 3-3.

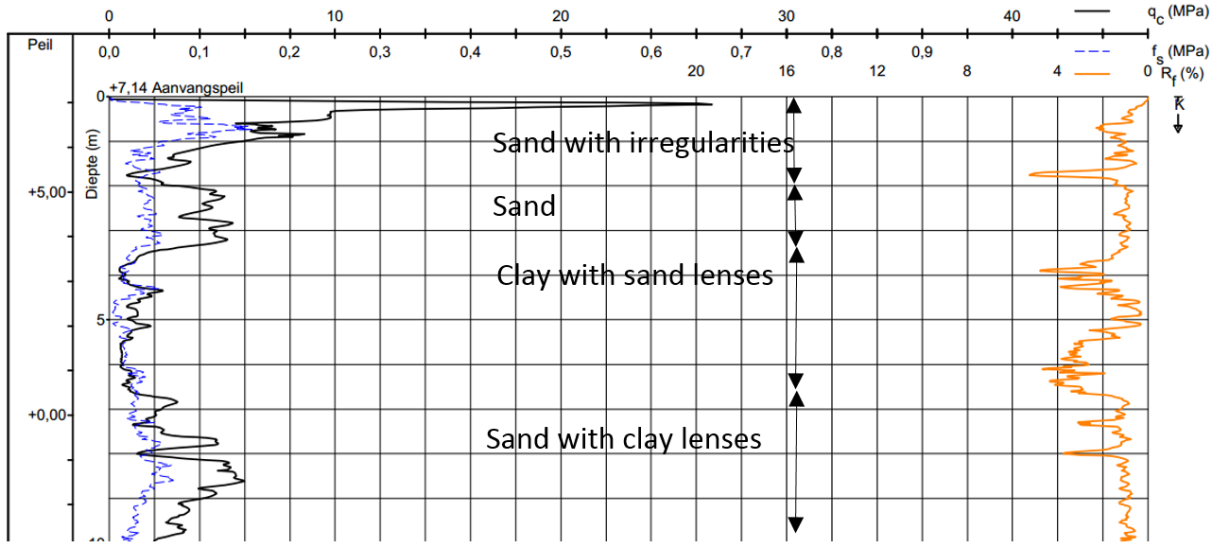


Figure 3-3 CPT-test S1

### 3.2.2 Angle of the side slopes

Because the pilot channel will be made a day before the experiment, it is important that it is stable during one day. The dike is a sand dike with a clay cover. After some consideration with GEO a side slope angle of the pilot channel of 45° is assumed to be stable enough. This is the same angle as in the breach experiment in Lillo as described in section 2.5.

### 3.2.3 Width

During the breaching experiment it is important that the breach stays open when soil falls from the sides into the pilot channel. Therefore the width of the channel has to be sufficient. If the pilot channel is very wide, the polder will be directly inundated and the duration of flow will be small. Therefore a good balance is necessary. A bottom width of 1 m is chosen. This width is still easy to dig with an excavator and large enough to do some testing in the pilot channel (e.g. infiltration test).

### 3.2.4 Depth

The influence of depth is examined using the theory of hydraulic grade lines. It is assumed that there is a gradually varying flow so the theory of Bresse is valid. The flow of the water over the dike consists of two parts: the crest section and the side of the dike. These sections have a different hydraulic grade line. The crest section is the actual pilot channel that is dug in the dike. It is assumed that the manning roughness coefficient is  $0,022 \text{ s/m}^{1/3}$ , this corresponds with excavated earth (Whipple, 2002). The old grass cover on the side of the dike is assumed to have a manning roughness coefficient of  $0,03 \text{ s/m}^{1/3}$ . (De Mulder, 2015)

The goal is to maximize the shear stress and the velocity at the toe of the dike. In this case the dike is most susceptible to erosion during the breach experiment. The depth of the pilot channel also has an influence on the duration of the test. If the depth is small, the water will only flow during a small period with a small force. If the pilot channel is too deep it will be difficult to notice breach phases I till III as described by (Visser P. , 1998), because no headcut will be formed. The breach will only grow sideways and not deepen because of the clay layer at the level of the polder.

### 3.2.5 Hydraulic grade line calculation program

A program is written in VBA to automatically calculate the hydraulic grade lines in the breach in time. The calculation is performed for the high tide of 16/11/2015 in the morning. The hydraulic parameters can be derived from each model. If the depth is changed, the influence can be evaluated and the best depth of the pilot channel can be chosen.

#### 3.2.5.1 Input

The input parameters of the program are: the dimensions of the pilot channel and the manning roughness coefficients for the different sections, the geometry of the dike and the height of the polder. The inserted parameters are:

$B_b$  Base width of breach

$H_w$  The water level, This is taken equal to the astronomical water levels of 16/11/2015 provided by FHR.

$\tan(\alpha)$





$L_c$  Crest length is calculated for each pilot channel depth. This is done assuming a width at the top of the dike (7 m T.A.W.) of 4 meter and the angles of the side of the dike are  $45^\circ$

$Z_{br}$  The depth of the breach

### 3.2.5.2 Breach discharge

The dike and the pilot channel can be seen as a weir with a trapezoidal cross section. There are many different formulas for calculating the flow for this kind of weir. The breach can be seen as a broad or sharp crested weir but because there is a large crest length the best approximation will be a broad crested weir. A weir is defined as broad crested according to De Mulder if: (De Mulder, 2015, p. 234)

$$\frac{H}{L_c} \leq 0,5$$

If this ratio become smaller then 0,07 the friction losses can't be neglected, because the large crest length ( $L_c \approx 10 \text{ m}$ ) friction will have an influence on the flow in the breach.

In most formulas found in literature the same coefficients appear:

$C_d$  Discharge coefficient

$g$  Gravitational constant,  $9,81 \text{ m/s}^2$

$H$  ( $H_w - Z_{br}$ ) Water height above the crest level.

$B_e$  Effective width, The pilot channel is a trapeze so  $B_e = B_b + H / \tan(\alpha)$

$B_b$  Base width of breach

$z$   $H / \tan(\alpha)$

$B_w$  Width of breach at water level

$L_c$  Crest length

For the same boundary conditions different formulas were calculated and a comparison was made between different discharge formulas to choose the best possible fit. The chosen boundary conditions are:

- $H = 0,5 \text{ m}$
- $\tan(\alpha) = 4$
- $B_b = 5 \text{ m}$
- $B_e = 5,125 \text{ m}$
- $B_w = 5,25 \text{ m}$
- $L_c = 10 \text{ m}$

### Cippoletti weir (Horton, 1907)

This formula is for sharp crested weirs, the breach is better approximated by a formula for broad crested weirs. This formula is calculated to see the difference between broad and sharp crested.

The theoretically derived formula is:

$$Q = \frac{2}{3}\sqrt{2g}B_bH^{3/2} + \frac{8}{15}z\sqrt{2g}H^{5/2} = 5,32 \text{ m}^3/\text{s}$$

This formula will give a too large result because there is no contraction taken into account. Therefore the formula is adjusted using experiments to have a better result:

$$Q = C_d B_e H^{3/2} = 3,367 B_e H^{3/2} = 3,27 \text{ m}^3/\text{s}^*$$

Other coefficients for  $C_d$  in literature are found according to (Flinn & Dyer, 1894):

$$Q = C_d B_e H^{3/2} = 3,301 B_e H^{3/2} = 3,22 \text{ m}^3/\text{s}^*$$

\*The input values for these formulas is in feet.

The result of these formulas will be too large because they are derived for a sharp crested weir. In a sharp crested weir the flow isn't influenced by the weir itself. In a broad crested weir the flow lines become parallel to the crest. In minimum one section of the weir critical flow conditions can be found. The theoretical flow over a broad crested weir is used in the formula of Sing and Scarlatos.

### Singh and Scarlatos (Singh & Scarlatos, 1988)

This flow formula is part of the Chang and Zhang breach model.

$$Q = 1,7 B_e H^{3/2} = 3,08 \text{ m}^3/\text{s}$$

Chang and Zang compared this formula to measurements of a real dam breach experiment. This showed a good similarity as can be seen in Figure 3-4.

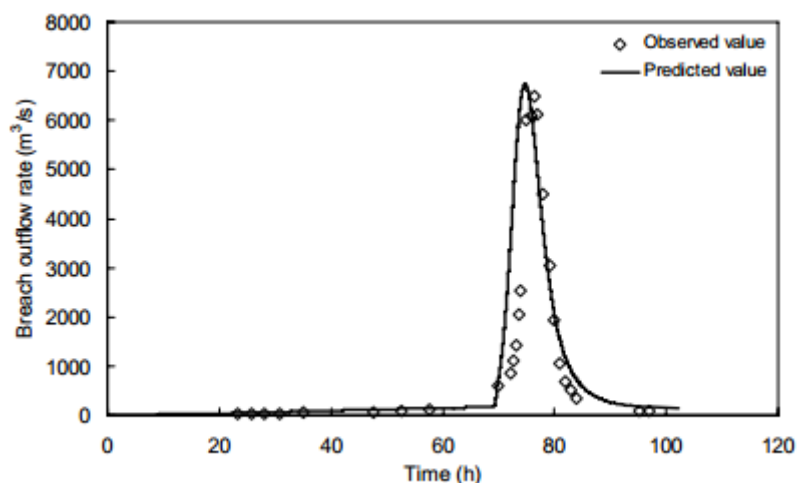


Figure 3-4 Predicted and measured breach outflow (Chang & Zang, 2010)

This formula can be theoretically derived by assuming that there the water level becomes critical in the breach. (Claydon , 2016) It doesn't take into account the friction of the flow on the crest. This friction will cause a smaller flow.

**Breach flow during breach phase IV and V** (Visser P. , 1998)

The formula of Visser is incorporated in the BRES breach model.

$$Q = C_d \left(\frac{2}{3}\right)^{3/2} \sqrt{g} B_e H^{3/2} = 3,09 \text{ m}^3/\text{s}$$

With:  $C_d = \frac{3}{2+B/B_w} \left[ \frac{3}{1+2B_w/B} \right]^{1/2} = 1$

In this formula the friction on the outer and inside of the breach is neglected. Therefore a smaller flow can be expected.

**Singh and Quiroga** (Singh & Quiroga, 1987)

This flow formula is part of the BEED breach model.

$$Q = (C_r B_b + C_t z) H^{3/2} = 3,065 \text{ m}^3/\text{s}$$

With:  $C_r = 1,7$

$C_t = 1,35$

**Fritz and Hager** (Fritz & Hager, Hydraulics of embankment weir, 1998)

This formula is made for broad crested weirs. The side of this weir has an angle of 1/1.

$$Q = C_d \sqrt{2g} B_e H^{3/2} = 2,97 \text{ m}^3/\text{s}$$

With:  $C_d = 0,43 + 0,06 \sin(\pi(\xi - 0,55)) = 0,37$

$\xi = \frac{H}{H+L_c} = 0,0476$

**Tracy** (Tracy, 1957)

This formula is made for broad crested weirs. The side of this weir has an angle of 1/1. The coefficient  $C_d$  is read from a graph.

$$Q = 2,87 B_e H^{3/2} = 2,78 \text{ m}^3/\text{s}^*$$

\*The input parameters of the formula are in feet.

**Govinda Rao and Muralidhar** (Govinda Rao & Muralidhar, 1963)

$$Q = C_d \sqrt{g} B_e H^{3/2} = 2,81 \text{ m}^3/\text{s}$$

With:  $C_d = 0,971 \sqrt{8/27} \left(\frac{H}{L_c}\right)^{0,022} = 0,495$

### Floodsite (Néelz, 2008)

Floodsite does research for integrated flood risk analysis and management methodologies. In this context a report is written about breach flow discharge prediction. The formula is the sum of two parts. a rectangular and a triangular weir:

$$Q = 0,55\sqrt{g}B_eH^{3/2} + 0,585 * \tan\left(\frac{\Omega}{2}\right)\sqrt{g}H^{\frac{5}{2}} = 3,126 \text{ m}^3/\text{s}$$

With:  $\Omega$  is equal to two times the angle of the sides =  $28^\circ$

### Formulas for overflow dikes

The flow over an overflow dike is comparable to the flow in the breach. The resulting value however will be too small because there is a lot of friction taken into account in these formulas. It is expected that the friction in the breach in Wichelen will be lower.

This formula is derived for a revetment with artificial grass. (Elskens, 1995)

$$Q = 1,54B_eH^{3/2} = 2,79 \text{ m}^3/\text{s}$$

This formula is used by Flanders Hydraulics Research for overflow dikes with a grass coverage: (Personal communication with P. Peeters)

$$Q = 1,36B_eH^{3/2} = 2,46 \text{ m}^3/\text{s}$$

### Zhao, Visser, Ren and Uijtewaal (Zhao, Visser, Ren, & Uijtewaal, 2015)

$$Q = C_d\left(\frac{2}{3}\right)^{3/2}\sqrt{g}B_eH^{3/2} = 2,69 \text{ m}^3/\text{s}$$

With:  $C_d$  experimentally determined 0,85

### Kamrath, Disse, Hammer and Königether (Kamrath, Disse, Hammer, & Königether, 2006)

$$Q = \frac{2}{3}0,577U^*B_eH^{\frac{3}{2}} = 3,09 \text{ m}^3/\text{s}$$

With:  $U^*$  The parameters to estimate  $U^*$  are unknown in this case an estimation of 1 can be used.

### Bos (Bos, 1985)

$$Q = C_vC_d\frac{2}{3}\sqrt{\frac{2}{3}g}B_eH^{3/2} = 2,89 \text{ m}^3/\text{s}$$

With:  $C_v$  Taken equal to 1

$$C_d = 0,93 + 0,1\frac{H}{L_c} = 0,935$$

## Conclusion

Source of the Formula	Q [m <sup>3</sup> /s]
Cippoletti weir	5,32
(Horton, 1907)	3,27
(Flinn & Dyer, 1894)	3,22
(Singh & Scarlatos, 1988)	3,08
(Visser P. , 1998)	3,09
(Singh & Quiroga, 1987)	3,065
(Fritz & Hager, Hydraulics of embankment weir, 1998)	2,97
(Tracy, 1957)	2,78
(Govinda Rao & Muralidhar, 1963)	<u>2,81</u>
(Néelz, 2008)	3,126
(Elskens, 1995)	2,79
Flanders Hydraulics Research	2,46
(Zhao, Visser, Ren, & Uijtewaal, 2015)	2,69
(Kamrath, Disse, Hammer, & Köngether, 2006)	3,09
(Bos, 1985)	2,89

*Table 3-2 Discharges calculated with different formulas*

It was found that the differences between the different formulas are significant. Some formulas require more input parameters than others. Higher discharges are obtained when the friction along the crest of the dike is neglected. Because the length of the dike crest is rather large in comparison to the side of the dike, these formulas will give a too large discharge. The formulas to calculate the discharge of overflow dikes will give a flow that will be too small. It is assumed that the friction in the breach will be smaller because the sides are made of excavated earth which has a smaller friction compared to grass.

In reality it is expected that the solution will be in between these results. The formula proposed to use in the calculation is the one suggested by Govinda Rao and Muralidhar. In this formula also the length of the crest is considered and it is expected that this will have an influence on the flow.

### *3.2.5.3 Boundary conditions*

To calculate the hydraulic grade lines a starting point is needed. This point is the transition between the crest and landward slope of the dike. Because the slope of the talweg goes from mildly to strong, the critical water height is assumed there. The critical water height can be calculated by equalizing Froude's number to one in this point. Using this downstream boundary condition the hydraulic grade line over the crest can be calculated.

The cross section of the flow changes from a trapezium in the pilot channel to a rectangle at the side of the dike. The width of the rectangular flow is calculated by equalizing the specific energy from the two hydraulic grade lines in the transition point. Then the hydraulic grade

line on the side of the dike can be calculated using the upstream boundary condition. In Figure 3-5 an example of a possible hydraulic grade line is given. Where x=0 m is the transition crest-riverside slope.

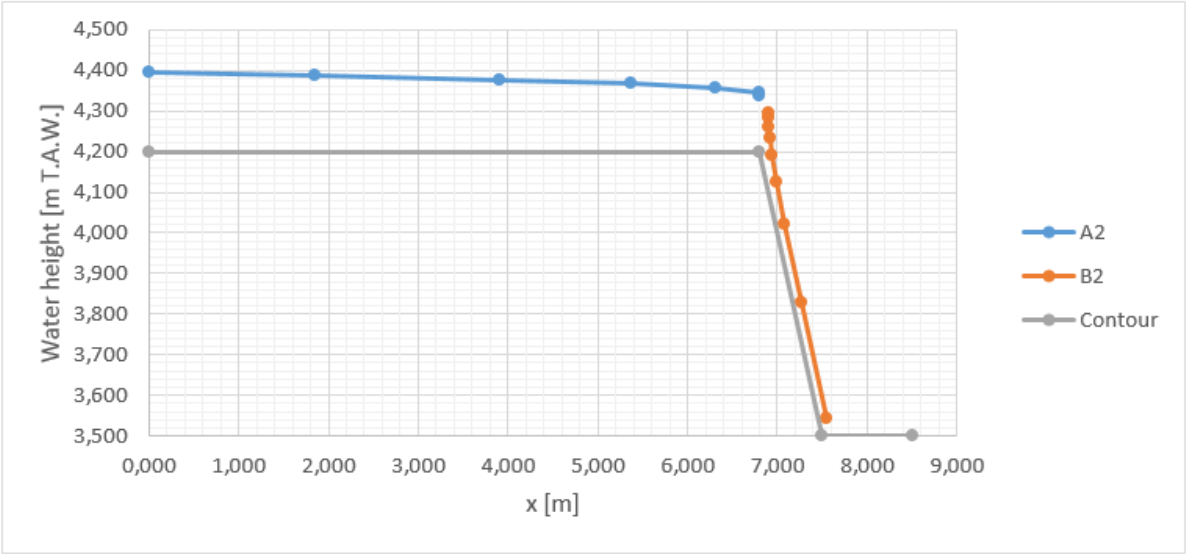


Figure 3-5 Hydraulic grade line example

3.2.5.4 Results

The hydraulic grade lines are calculated with an interval of five minutes during the tide in the morning of 16/11/2015 for different pilot channel depths. The shear force and water velocity at the toe of the dike is calculated for each pilot channel depth, this gives a result as displayed in Figure 3-6. The maximum values are recorded for each pilot channel depth and given in Figure 3-7. The formula used to calculate the shear force is: (De Mulder, 2015)

$$\tau = \frac{\rho_w g n^2 U^2}{R^{1/3}}$$

- With:  $\rho_w$  Density of water
- $g$  Gravitational constant
- $n$  Mannings roughness coefficient this depends on the surface
- $U$  Mean water velocity, in reality this is the water velocity at the contact point between water and soil but this is estimated to be equal to the mean velocity
- $R$  Hydraulic radius

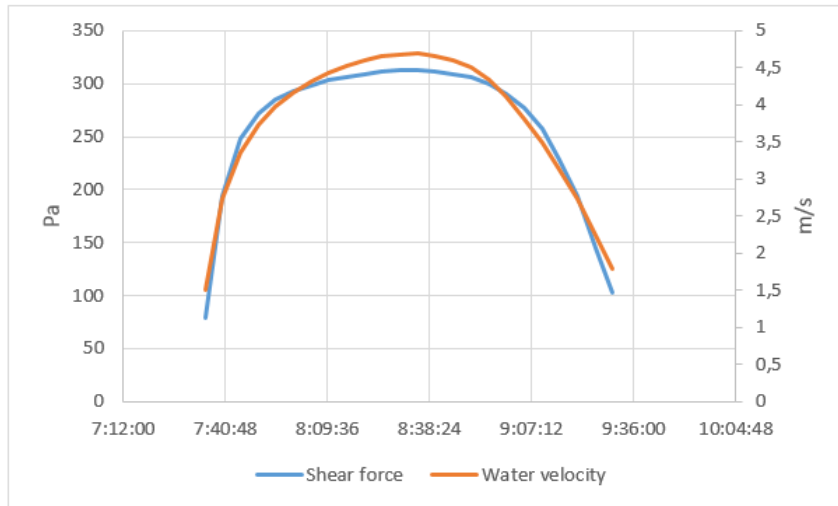


Figure 3-6 Example calculation channel depth 4,5 m T.A.W.

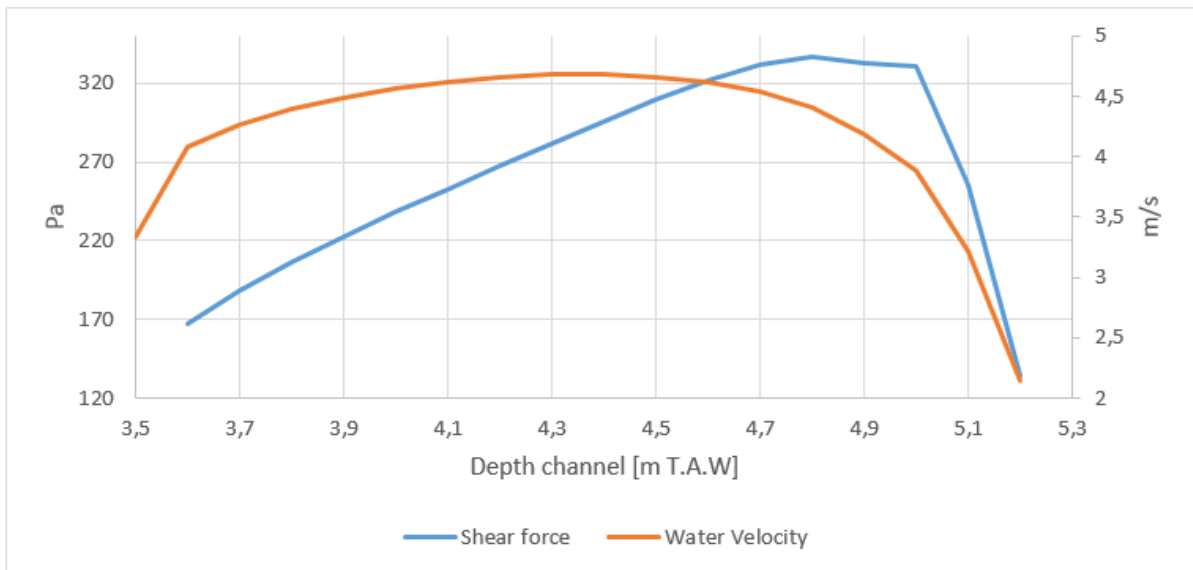


Figure 3-7 Shear force and water velocity at the toe for different channel depths

The shear force and water velocity both have a maximum, this maximum can be explained like this: when the depth of the pilot channel is small, the flow will be limited. The pilot channel is trapezoidal so the hydraulic radius will be large, causing a lot of friction slowing down the flow. When the depth is increased the flow will increase also, but the height difference between the pilot channel and the polder will decrease so the water will gain less energy. For the shear force the optimum is at 4,8 m T.A.W, for the water velocity this is at 4,3 m T.A.W. These values are different because in the formula of the shear force the hydraulic radius occurs. This radius is also function of the water depth.

A pilot channel depth of 4,5 m T.A.W. proposed to be optimum. This is approximately in the middle of the two optima. If the maximum water level on the test day is lower than expected (5,31 m T.A.W) there will be still some room for margin.

It has to be noted that the program doesn't take into account erosion of the pilot channel.

### 3.2.6 Conclusion

The proposed pilot channel is drawn in Figure 3-8.

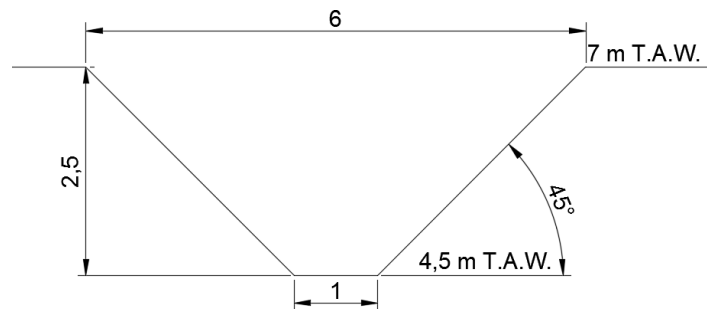


Figure 3-8 Pilot channel

## 3.3 Discharge measurement

The discharge through the breach will be estimated using a volume to height relation of the polder made FHR. To increase the accuracy in the beginning of the experiment it is suggested to construct an extra dike in the polder.

### 3.3.1 Height to volume relation

By executing height measurements of the polder, as shown in Figure 3-9, a volume to height relationship is derived by FHR as shown in Figure 3-10. Only a global image of the height of the polder can be given, small local irregularities like ditches and vegetation aren't taken into account. If the water height of the polder is known, the volume of water can be derived. Therefore in time, the change in volume can be derived, so the flow through the breach can be calculated.



Figure 3-9 Topography of the polder anno 2015



In reality the polder won't fill up evenly. If there is a lower part of the polder surrounded by a higher part the water won't be able to fill it until the higher level is reached. In Figure 3-9 such an area can be seen in the upper left corner. These areas will have an effect on the measurements. Also the water level in the polder won't be flat, if water starts to flow in the polder, close to the breach the water level will rise but further from the breach there will be no influence noticed. Therefore the water level in the polder can't be measured at only one location. At several locations spread in the polder the water height will be measured and the mean water height will be used to have the most accurate result.

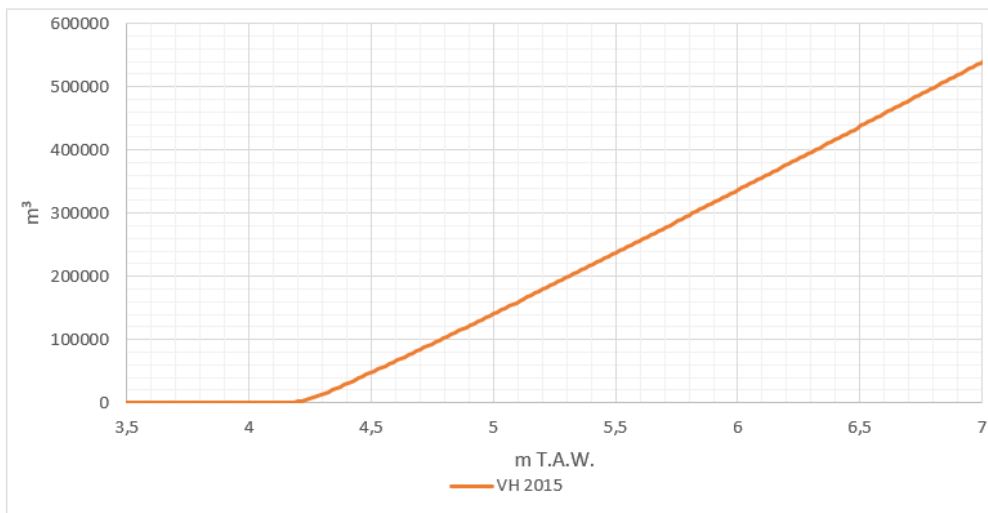


Figure 3-10 Volume to height relationship

### 3.3.2 Extra dike

To avoid distortions due to lower situated areas in the polder, it is suggested to place an extra dike in the polder. This dike will have a small height to minimize the influence on the flow and will surround a smaller, more level part of the polder adjacent to the breach. This will have a positive influence on the accuracy of the flow measurement in the beginning of the breach experiment.

To estimate the dimensions of the extra dike, the expected total flow in the polder has to be known. The hydraulic grade line program as discussed in 3.2.5 is used. The flow through a pilot channel with the following dimensions: 3 m width, sides of 45° and a depth of 4,5 m T.A.W. is calculated for the high tide in the morning of 16/11/2015 using the astronomical water height. In this case the volume of water entering the polder is approximately 15000 m³. It has to be noted that in reality the volume will be higher due to erosion of the breach.

When a dike with a height of 0,5 meter is placed around an area of 2 hectares. it should be possible to store 10000 m³. If the surface inside the extra dike is made flat this should give a considerable increase of the accuracy.

## 3.4 Piezometers

During the dike breach test, piezometers recorded the water pressure inside the dike. Two types of piezometers are used: BAT sensors and MEMS sensors. These sensors are provided

by the geotechnics division of the Flemish government (GEO). Prior to the breach test they were tested on their responsiveness and possibility to measure suction pressures. The installation procedure is explained and the position in the dike where the sensors will be installed is investigated.

### 3.4.1 Saturation

In order to measure pore pressures accurately, the sensor needs to be saturated. Prior to installation, the sensors were tested to investigate to know how long in advance they have to be installed. Also it is tested if it is possible to measure negative, so-called suction pressures, i.e. when the pressure is lower than the air pressure.

#### 3.4.1.1 MEMS

The MEMS sensor consists of a filter element with underneath the actual sensor. The filter element is made of hydrophilic porous polyethylene material which has the property that it completely saturates itself when brought in contact with water, even after repeated drought. Therefore the sensor is suitable for use in a non-continuously saturated zone. It is recommended that prior to installation the filter element is saturated with water or silicone oil. (Alert Solutions, 2011)



Figure 3-11 MEMS sensor (Soil instruments)

The logger of the MEMS sensor is able to measure the air pressure. This pressure is used to calculate the relative pressure.

A unsaturated MEMS sensor was tested to have an indication of the saturation time when placed in water. This was done by placing the sensor in a bucket filled with water ( $\approx 20$  cm). During the test, the sensor was placed at two different water heights, approximately 10 and 20 cm. Every 30 seconds, the actual air and water pressure were logged. The results are displayed in Figure 3-12. There is an overpressure at the beginning of the test which gradually decreases. During the test the alternation of the water height can be seen as the pressure jumps.

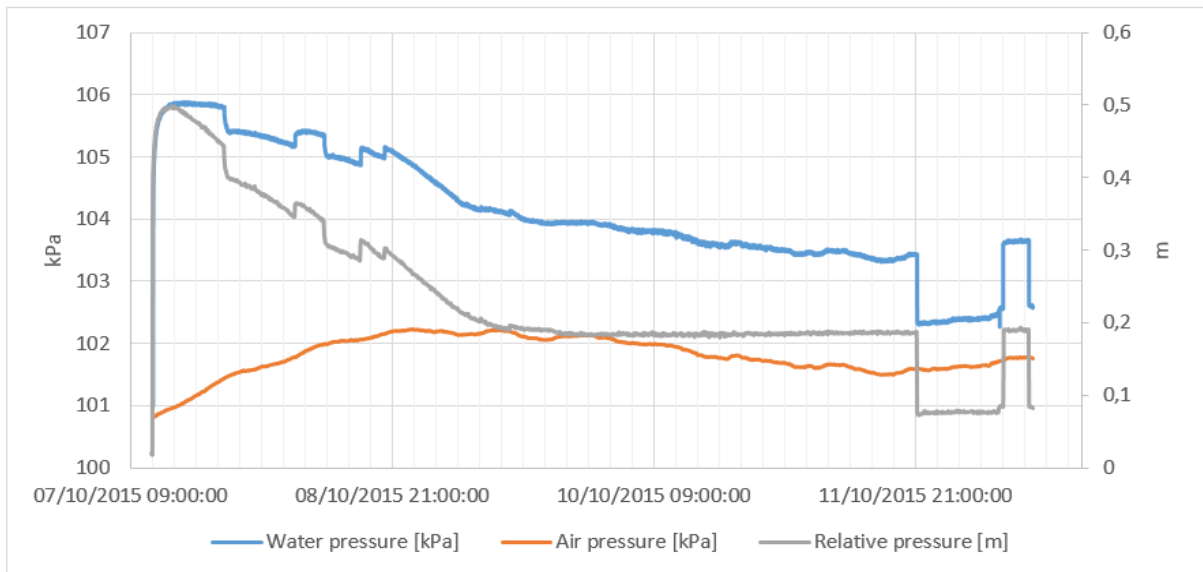


Figure 3-12 Saturation test of MEMS sensor

At the moment the sensor is placed in water, the dry porous filter element attracts water, which explains the overpressure. When the filter element is becoming saturated, the pressure will evolve to a constant value. After two days the sensors reach a constant value. It is also only after this period that the sensor measures the correct water level difference. Therefore it can be concluded that it will be necessary to install the MEMS sensors at least two days in advance before the breach experiment.

The reaction speed of the sensor is also tested, this was done by decreasing the log time to 10 seconds and alternating the water level. The results of this test is shown in Figure 3-13. The jumps occur where the water level was changed, at two moments in time there is an under pressure measured. It is possible that during the transfer between the two water containers the sensor logged the pressure when it was exposed to air, this can explain the under pressure. It is found that the measurements are instantaneous in water, there is no delay on the measurements. This can be different when installed in soil due to the permeability. When installed in a soil with a low permeability it is possible that there is a delay. The effect of hindered erosion will be measured in the sand core of the dike. Sand has the property to have a good permeability so it is assumed that the measurements will be instantaneous.

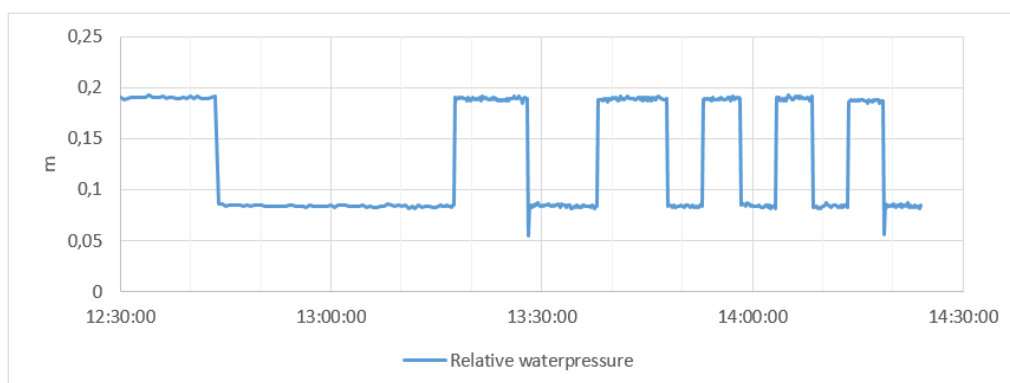


Figure 3-13 Reaction speed test MEMS sensor

### 3.4.1.2 BAT

The BAT sensors are saturated manually before placement by the installer. They don't need to be hung in water or be vacuum saturated. This is because there is no hydrophilic filter element. The filter tip of the bat can be saturated by means of an injection needle. The sensor itself is saturated by turning the top end until there comes a drop of water out of the measuring needle.

A test was done at GEO in Ghent with two BAT sensors. They were placed in a water tube at a depth of 5 meters and this depth was then increased to 10 m. One was saturated following the guidelines and one was directly installed. The results are shown in Figure 3-14. The sensors don't need any time to saturate, in contrary to the MEMS sensor there is no filter element, only a filter membrane and the influence of this is negligible.

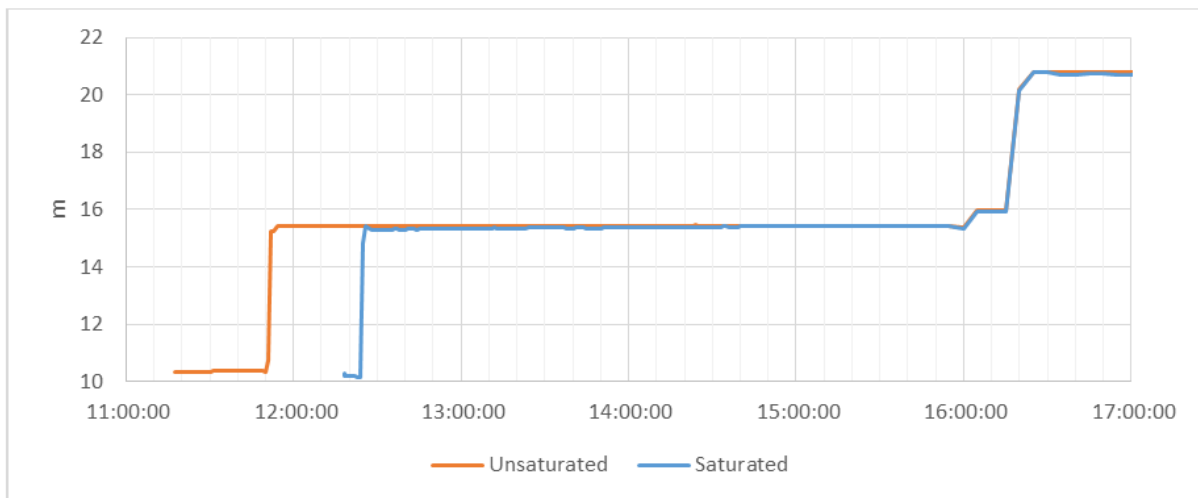


Figure 3-14 Saturation test BAT sensors

The BAT sensor only measures the total pressure therefore during the experiment the air pressure has to be measured.

### 3.4.2 Suction tests of BAT and MEMS sensors

To be sure the sensors can register suction pressures some tests were done in the lab of Geotechnics in Ghent. Suction pressures are pressures smaller than the air pressure. The same effect was simulated that can be noticed when walking on a muddy trail. It is sometimes hard to pull your feet out of the ground. This is because the mud isn't permeable enough and therefore a suction is created.

This effect was created by installing the sensor inside a metal tube filled with wet sand. During the installation the sand was compacted manually in layers of approximately 5 cm. This was done until the sensor was fully surrounded by sand. The sensor was then pulled out of the sand, this should create some suction around it.

#### 3.4.2.1 MEMS

Several successive tests were performed, after each test the sensor was placed in water to remain saturated. The log time of the sensor was set at one second. The results of the tests are shown in Figure 3-15. During the first and the third test the sensor was pulled fast out of

the sand. The second and last test were performed by pulling the sensor more gently out of the ground.

When the sensor is installed it immediately measures a suction pressure. This is the capillary suction of the ground. The pressure rises when the sensor is installed deeper in the sand. After the installation the pressure becomes constant and then the sensor is pulled out. The largest suction pressure is measured during the fast tests.

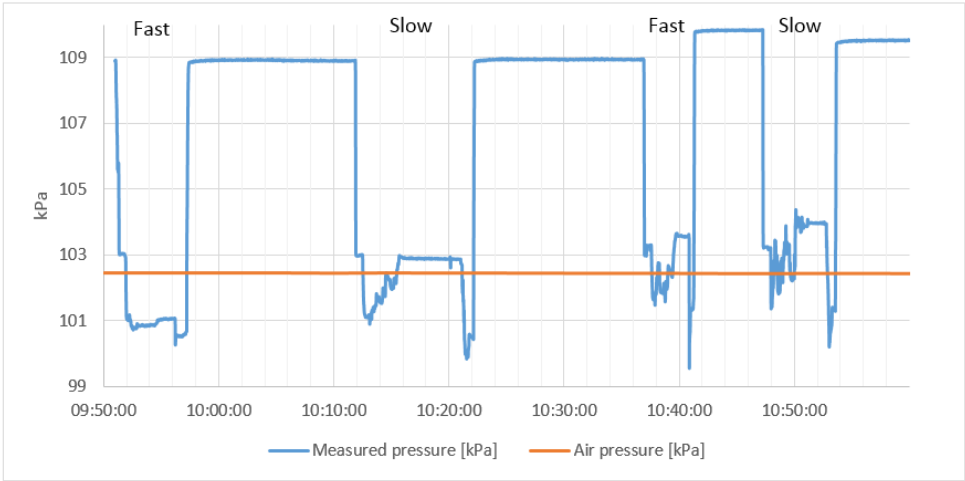


Figure 3-15 Suction test MEMS sensor

The tests show that a suction pressure can be measured with the MEMS sensors even when it is only at a small instance.

3.4.2.2 BAT

The same tests were done as with the MEMS sensor, also at different speeds. The minimal log time for the BAT sensors is one minute. The first three tests are done on the same moment at which the logging takes place. The last test is done in between two loggings.

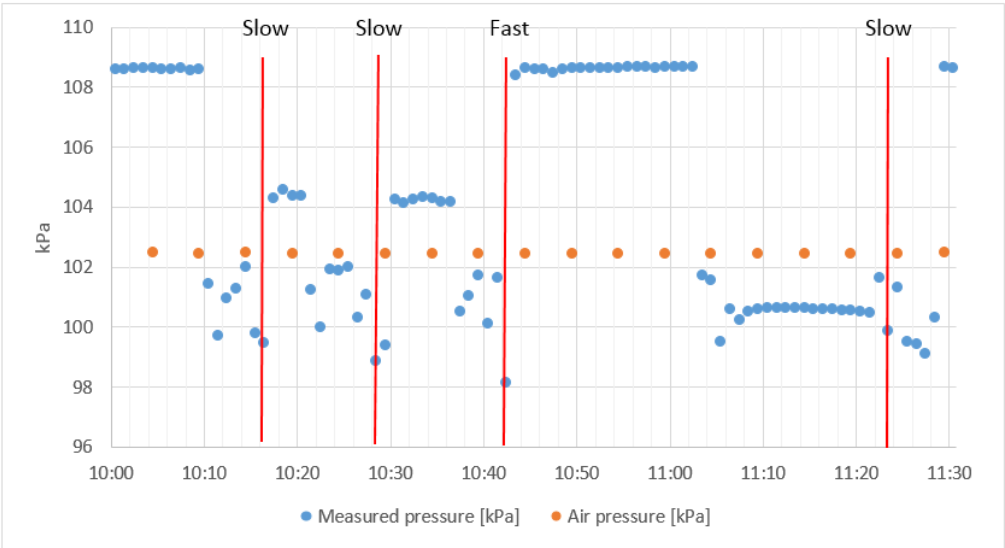


Figure 3-16 Suction test BAT sensor

The tests show that the BAT sensors can only measure suction pressures when they occur at the moment of logging. The largest suction is measured when the sensor is pulled out at the highest velocity.

### 3.4.3 Installation

#### 3.4.3.1 MEMS

For the installation of the MEMS sensors first a vertical borehole is made to the desired depth. A mark is made on the cable to have an indication if the sensor is at the predefined depth. Because the limited weight of the sensor a weight is attached to it for a more vertical descend. Then the MEMS is let down in the borehole. There is no direct contact between the MEMS sensor and the ground. This can have an influence on the measurements.

When the sensor is at the correct depth. The borehole is filled up with fine graded sand (sand of Mol). The upper part is filled with bentonite clay. This is done to eliminate the influence of rainwater intrusion in the borehole.

#### 3.4.3.2 BAT

The BAT sensor is installed inside an iron tube. The end of the tube has thread in it so the filter tip can be screwed on it. This tube can be pushed in the ground using a CPT machine or by making a borehole. The sensors are installed by making a borehole with the diameter a bit smaller than the iron tube. The last 20 cm above the installation depth are done with a smaller drill and the cone is hammered into the ground using a hammer. This is done to obtain a good connection between the filter tip and the surrounding ground. This imposes fast response of the sensor to the pore pressures.

After installation of the sensor, the top of the borehole is filled with bentonite clay to eliminate the influence of rainwater intrusion in the borehole.

### 3.4.4 Location of sensors in the dike

The location of the sensors in the dike is vital for a good measurement. The sensors have to be placed deep enough to be saturated and in a position where hindered erosion takes place. This to measure a possible suction pressure due to hindered erosion.

#### 3.4.4.1 Position

It is expected that most erosion will take place landward in the dike because the largest flow velocities occur here. Due to the influence of the clay lining on the dike it is possible that the breach will become more O-shaped. So, in the middle of the dike, some additional sensors were placed. This gives also an indication of the saturation of the dike during the test. One sensor is placed further away from the breach, this is done to have a reference. It is suggested to place a sensor in advance of the test near the river side to measure possible influences of the tide on the level of the groundwater table in the dike.

The suction pressures linked to hindered erosion can only be measured in a very small zone during a small time interval. High water velocities are needed close to the sand. Therefore it

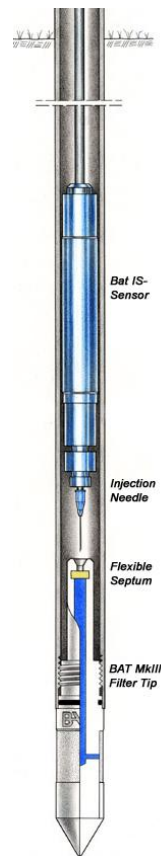


Figure 3-17 BAT sensor (BAT, 2015)

is suggested to place most sensors at the landward side of the dike. If the sensors are installed at the side of the dike this allows also more easy access of the breach before the experiment.

The best results are expected from the MEMS sensors because they have the smallest log time and reaction time, therefore it is suggested to place the MEMS sensors closest to the breach. In Figure 3-18 a proposal of the placement of the sensors is given. The ML XXX\* sensors are the MEMS sensors. The BAT XXXX\* sensors are the BAT sensors. The distance between the sensors is to be defined on site in consultation with FHR and GEO.

\*XXX is the number of the sensor

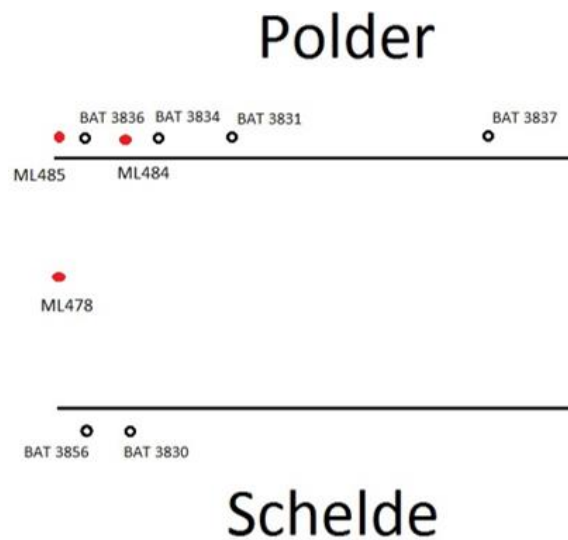


Figure 3-18 Positioning of sensors

#### 3.4.4.2 Depth

The depth of the sensors is determined based on the CPT-diagrams (DOV, 2016). The dike consists of a sand core surrounded by clay. Sand is the most permeable and erodible soil material so the sensors have to be placed in this core. If the sensor is placed too deep it will be situated in clay so it will be difficult to have a good measurement. The more saturated the soil, the more easily the sensor will measure differences, so the sensor has to be placed as deep as possible. A choice has to be made between these two options, the sensor has to be placed deep enough in the sand core but not too deep to prevent the installation in clay. A depth of 2,6 m under the dike crest (approx. 4,5 m T.A.W.) was applied. This depth is just above the lower clay layer.

The installation of the sensors is done using a small auger. The soil is removed from the borehole so it can be seen if there is clay at a depth of 4,5 m T.A.W. If this is the case some fine sand is inserted in the hole and the sensor is installed just above the clay layer.

### 3.5 Other measurements/tests

In this thesis special attention is given to the flow, pore water pressure measurements in the dike and the breach growth. The breach experiment was performed in association with TU Delft and Flanders Hydraulics Research who also made other measurements/tests. In the following the different tests executed on the dike are listed.

### 3.5.1 Before the breach test

- Erosion tests (JET,HET) done by l'Institut national de recherche en sciences et technologies pour l'environnement et l'agriculture commissioned by FHR
- Wave overtopping tests done by INFRAM commissioned by FHR
- Overflow tests done by Technical University of Delft (TUD) commissioned by FHR
- Geophysical research of the dike done by G-tec commissioned by FHR
- Infiltration tests done by GEO
- Soil sampling done by GEO
- Installation of pore water sensors done by GEO
- Installation of divers in the river Scheldt and in the polder done by the Hydrological information centre (HIC)
- Making of volume to height relation of the polder done by FHR

### 3.5.2 During breach test

- Laser scanning done by TUD commissioned by FHR
- Water velocity measurements using floats and cameras done by HIC
- The breach was photographed and 3D models were made using photogrammetry done by the general technical support division from the Flemish government (ATO) commissioned by FHR

### 3.5.3 After breach test

- At regular intervals the breach was photographed and 3D models were made using photogrammetry done by ATO
- Pictures were taken of the breach on a daily basis done by Lode De Vriese
- ADCP measurement of the flow in the breach done by HIC



# 4 Preparations test

The decision was made to organise the breach test on 16/11/2015. Before the actual test, some on-site preparations had to be done. The piezometers need to be installed. Some ground samples were taken and infiltration tests were performed. The pilot channel is dug and a grid is painted on the dike to have a better visualization of the breach growth.

## 4.1 Installation sensors

The BAT sensors were installed four days before the test. The MEMS sensors were first saturated and then installed one day before the test. The placement of the sensors is shown in Figure 4-1. The MEMS sensors are indicated with ML XXX and the BAT sensors are indicated with BAT XXXX. The BAT sensors are placed near the sides of the dike, because after installation an iron tube sticks out. This placement will allow easy access to the dike before the test.

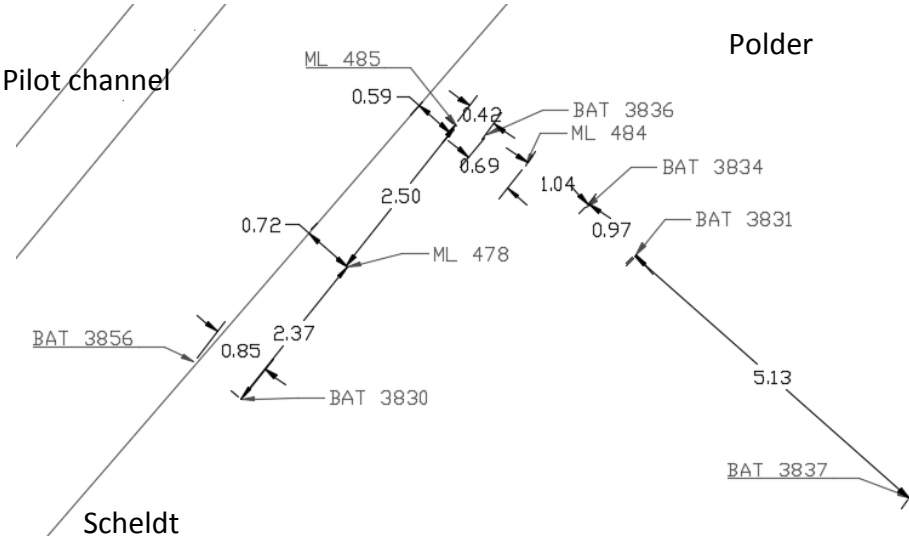


Figure 4-1 Top view of placement of sensors

The log time of the BAT and MEMS sensors was set respectively on 1 minute and 1 second. This was done just before the test.

The actual depth of the measuring sensor was at 2,57 m from the dike crest. The sensor was placed by drilling a hole. This has the advantage that the ground in which the sensor is placed can be examined. A picture of the installation is shown in Figure 4-2. If clay was found at the installation depth the sensor is installed a bit higher in the sand layer. Due to this reason BAT 3837 is installed 10 cm higher.



Figure 4-2 Installation of sensors using an auger

## 4.2 Soil tests

Before the breach experiment a single ring infiltration test is executed on the slope of the dike and a double ring infiltration test is done on the bottom of the pilot channel. This last test is displayed in Figure 4-3. Several ground monsters, disturbed and undisturbed were taken for further testing. The results of these tests can be found in annex A. The positioning of the tests is displayed in annex B.



Figure 4-3 Double ring infiltration test in pilot channel

## 4.3 Pilot channel

The pilot channel was dug a day before the test. The part of the dike near the river is left in place this was dug out just before the test and had the dimensions as described in 3.2. During this excavation, the sand core of the dike was exposed. The clay layer on the sand is approximately 30 cm. Just before the breach test at low tide, the remaining part of the dike is dug out and a small dike is made in the middle. This to have a sudden and clear start of the test.

## 4.4 Grid

To have an indication of the breach growth, a grid of 1mx1m was drawn on the dike and on the crest every one meter a picket is placed. This can be seen in Figure 5-1.



Figure 4-4 Pilot channel before test

# 5 Observations during the breach test

The breaching of the dike was done on two consecutive days. During the first test on 16/11/2015, due to a low water level, the dike did not breach. After this first test the breach was deepened and a small dike was placed in the gap to prevent flow in the breach during the high tide in the evening. The next day, the test was more successful and afterwards the breach was left open to observe the breach growth in time. Some observations are given based on photos and daily on-site visits.

## 5.1 Breach test I on 16/11/2015

During the first test, the water level reached only 5,02 m T.A.W, this was 0,3 m lower than expected from the astronomical data. There was water flowing through the breach for approximately an hour and a half. The pilot channel was deepened but no real headcut was formed during the test.



*Figure 5-1 Breach test on 16/11/2015 (Janssens, 2016)*

At the base of the breach the erosion stopped due to the presence of a clay layer. This clay layer consisted out of very dense clay at a depth of approximately 4,20 m T.A.W. This was expected from the CPT-tests. This clay layer gave the impression to be the ancient dike around the river which was naturally formed.

There was some erosion of the dike laterally but this was only very minor as can be seen in Figure 5-2. The water didn't have enough energy to undermine the sides of the dike causing failure. The pilot channel was widened only approximately 1 meter. It was impossible to determine the different breach phases.

Another test was organized the next day. To have a more successful test, FHR decided to deepen the pilot channel half a meter to 4 m T.A.W, in order to have a larger flow and hopefully more erosion of the sides. The influence of this decision will be positive, but a higher water level is still needed to have a more successful test because the higher situated sand core needs to erode. Due to the deepening of the pilot channel, mainly a lateral growth of the breach will happen so it is expected that only phase IV and V of the breach growth as described by Visser will occur.

A temporary dike was placed inside the pilot channel to prevent the water from entering the pilot channel during the high tide in the evening as shown in Figure 5-2.



Figure 5-2 Breach after breach test I 16/11/2015

## 5.2 Breach test II on 17/11/2015

During the second breach test the water level was approximately 15 cm higher. This higher water level together with a deeper pilot channel caused a faster growth of the breach. Because the pilot channel was dug in the clay layer, the deepening of the breach was negligible. Only breach stages IV and V occurred as described in 2.1.1.

During the test the water eroded the lower part of the sides of the dike, until the moment that slope failure occurred and a chunk of soil fell into the breach. It could be noticed that the shape of the breach was more an O-shape. This can be seen in Figure 5-3 and Figure 5-5. The inner sand core easily eroded and caused a decrease in support for the outer clay layer, but even with the decrease in support the outer layer stayed in place due to the roots that were present. The roots reinforced the outer clay lining so it could hang over the sand core.



Figure 5-3 Breach during test II 17/11/2015

During the test the irregularity of the sand core could be seen. The core was layered but the layering wasn't equal on the both sides of the dike. This supports the assumption that the dike was manmade out of different batches of ground. A lot of rocks and stones were present in the dike. Normally these would be only expected at the river side of the dike but they were found throughout the whole dike.

For larger periods, the outer layer was only supported by roots in the dike as can be seen in Figure 5-4. Pieces of this outer layer only fell into the water when enough sand was eroded, leading to too high forces in the roots. The outer layer eroded also by washing out of the clay particles from the dense root network, but this phenomenon happened more slowly.



Figure 5-4 Roots at the riverside 17/11/2015

The outer clay layer on the river side was thicker compared to the polder side. This can be due to sedimentation between the riprap. The clay layer at the river side was very hard to erode due to a larger thickness, reed, tree roots and the riprap revetment. After the test the shape of the dug pilot channel could still be seen clearly at the river side (Figure 5-5). The width of the breach after the first tide was approximately 7 à 8 meters at the top.



Figure 5-5 Breach after day II photographed from the polder 17/11/2015

After this breach test part of the riprap revetment at the side of Schellebelle (upstream) was removed to see if this had an influence on the breach growth. The breaching process continued the following days and months and is discussed in the next paragraph.

### 5.3 Further progress of the breach

The breach was followed up daily until the breach growth stagnated. The breach growth wasn't linear, It was mainly influenced by the high tide level. The largest growth was recorded between 25/11/2015 and 26/11/2015, corresponding to a spring tide period. The water level at high tide was then around 6 m T.A.W. From Figure 5-6 until Figure 5-10 photos from the polder side are shown at different time instances. The most observed failure mechanism in time was slope failure. The erosion of the sand in the breach due to the water flow was small.



Figure 5-6 Breach 18/11/2015



Figure 5-7 Breach 25/11/2015



Figure 5-8 Breach 27/11/2015



Figure 5-9 Breach 12/12/2015



*Figure 5-10 Breach 8/02/2016*

The width at the end of the observations was approximately 20 meters. The final shape of the breach was more V-shaped with the widest side at the polder side. In Figure 5-11 the inside of the breach is shown. It is remarkable how many rocks were found in the breach. It is assumed that these rocks came from the riprap revetment that was present at the riverside of the dike. These rocks protect the sand core from further erosion. Also the stiff clay layer at the base of the breach can be noticed. There was nearly no erosion of this layer even after 5 months of flow over it. It is noticed that the side of Schellebelle eroded more than the Uitbergen side. An explanation can be that after the breach test on 17/11/2015 the riprap revetment was removed from the Schellebelle side.



*Figure 5-11 Inside of the breach 8/02/2016*

# 6 Flow rate through the breach

The water velocity measured by floats that were thrown in the breach during the test. The discharge through the breach is estimated using divers positioned in the polder together with a volume to height relation. The formulas given in 3.2.5.2 are evaluated. A new coefficient of discharge is suggested for the inflow and the outflow and evaluated using an ADCP-measurement.

## 6.1 Surface floats

The execution of these test is done by HIC.

### 6.1.1 Water velocity using GPS floats

Two floats equipped with a GPS sensor (Garmin 60 Cx) were used during the test. The floats were thrown alternately in the breach at the riverside as can be seen in Figure 6-1. The flow dragged them through the breach. When the floats reached the polder they were retrieved using a rope. During the time in the breach care is taken that the rope didn't slow down the float, to have the most accurate measurement possible.

The measurements are performed on both of the breach days: on 16/11/2015 and on 17/11/2015. During the test on 17/11/2015 one of the GPS devices showed a technical defect so these results aren't used.



*Figure 6-1 Floats in breach*

The GPS sensors have an accuracy of +/- 5 m when used stationary with a good signal reception. The water velocity in the breach is small (<5m/s) and the length of the breach is small (15 meter), therefore the accuracy of the measured velocity will be small. The mean value of each measured series is taken. A series consists out of the location measurement between the two rest moments at the river and polder side of the breach.

Not all data obtained is acceptable, so a filtering is applied. Only measurements when the floats are heading in approximately the right direction (20 to 60°) are used. When this heading is kept on for more than 4 seconds it is assumed to be a good measurement. Rest moments



at the polder sides (speed approximately 0 m/s) are neglected as well as the retrieval of the floats. If there is a bad signal, this is seen by a constant varying heading, the data is neglected.

6.1.1.1 Breach test 16/11/2015

During the measurement the GPS reception on float 2 was poor, so a lot of this data is neglected. The mean velocity of each series is displayed in Figure 6-2. Some of the velocities have a low value <0,5 m/s, this can be the case when the float is stuck in the breach or hindered due to roots or soil in the breach. A correct value of the flow velocity is difficult to derive but it can be concluded that the surface velocity in the breach will be between 0,8 and 1,4 m/s. When assuming a logarithmic speed profile the mean water velocity is 0,7 to 1,2 m/s

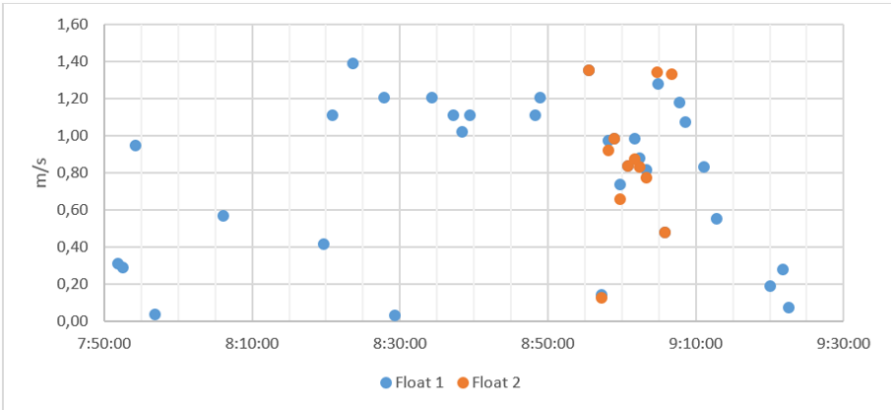


Figure 6-2 Measured velocities 16/11/2015

6.1.1.2 Breach test 17/11/2015

The mean velocity of each series is displayed in Figure 6-3. Some of the velocities have a low value <0,5 m/s, this can be the case when the float is stuck in the breach or hindered due to roots or soil in the breach. It can be seen that the values are all in the range of 1,2 to 2,3 m/s. The flow velocity increases during the breach growth. A reason for this is the increase in water level from the river. When assuming logarithmic speed profile the mean water velocity is 1 to 2 m/s.

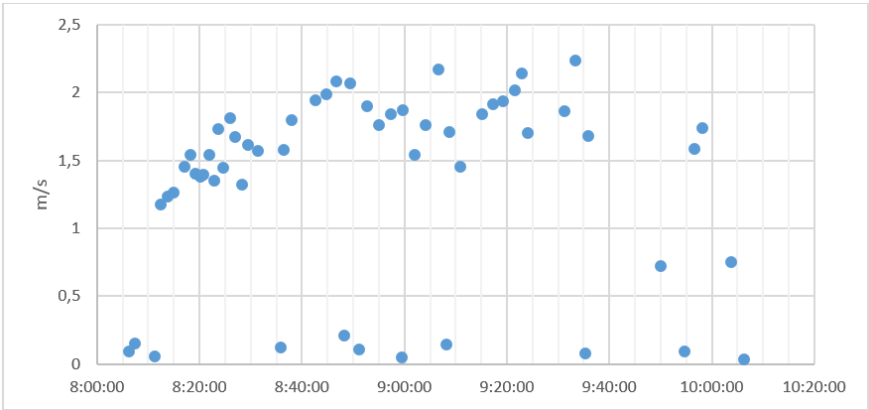


Figure 6-3 Measured velocities 17/11/2015

6.1.1.3 Conclusion

The measurements on 17/11/2015 give a more constant result and less scatter. It can be seen that the velocity increases during the test. On the test of 16/11/2015 this can't be seen, there

is a lot of scatter on the results. When the results of the different days are compared, it can be seen that the velocity is larger the second day. This could be expected because the breach depth during the second day was deeper and the water level was higher. The accuracy of the measured velocities is low. Bearing this in mind the results can be used to confirm other measurements.

### 6.1.2 Water velocity using camera images

An estimation of the water velocity is done using camera images of the floats. The length of the breach is measured before the test (11-12m). On the camera images the time needed for the floats to pass through the breach can be estimated. The time needed to pass through the breach is approximately 8 seconds. So the surface velocity is approximately 1,36 – 1,5 m/s. When assuming logarithmic speed profile the mean water velocity is 1,16 to 1,28 m/s. The accuracy of this method is low because the length of the breach is estimated.

### 6.1.3 Conclusion

The measurements using the GPS floats give a range of mean water velocities from 0,7 to 2 m/s. The camera images give a mean water velocity in the range of 1,16- 1,28 m/s. Both the measurements are in accordance with each other. The accuracy of these measurements is however low therefore it is suggested to only use them as verification.

## 6.2 Divers

The extra dike as suggested in 3.3.2 wasn't constructed so the discharge is calculated using the VH-relationship of the whole polder.

### 6.2.1 Discharge calculation

The mean value of the water heights from the measurements of the divers is used to estimate the flow through the breach. In Figure 6-4 the used diver measurements, mean and water level in the river is shown. The data of two divers was neglected because their measurements seemed to be inaccurate. To know the volume of water in the polder, an interpolation is done on the graph of Figure 3-10. The time step chosen to calculate the discharge is 300 seconds. A smaller time step gave too irregular results.

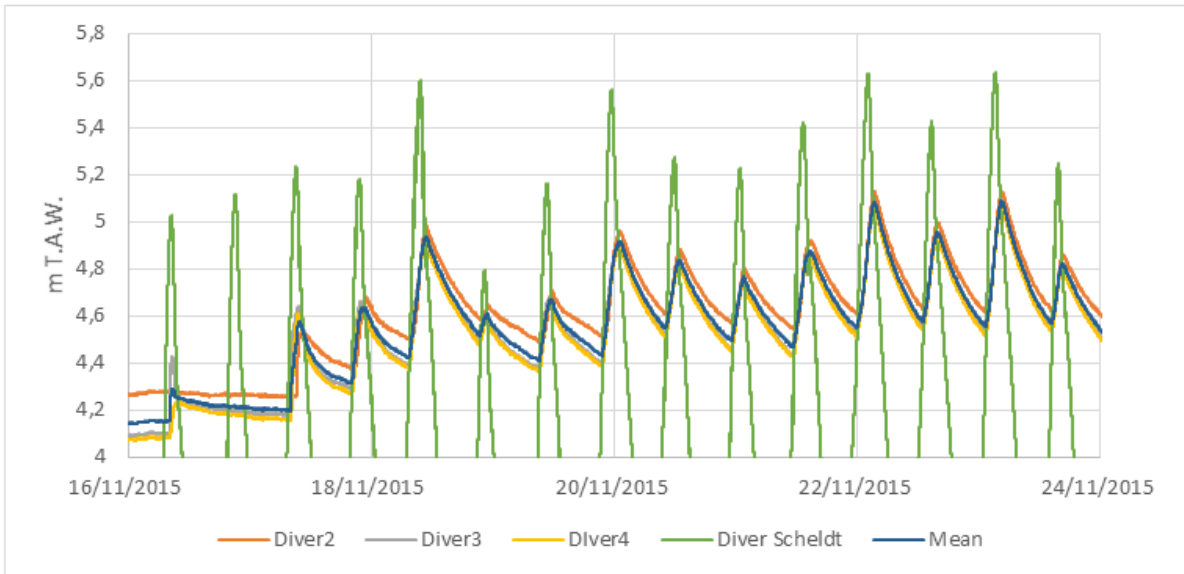


Figure 6-4 Diver measurements

The discharge is shown in Figure 6-5, a positive discharge is inflow into the polder a negative discharge is a flow to the river. The first peak is the flow during the first breach experiment on 16/11/2015. The second larger peak is the discharge during the second breach test on 17/11/2015.

The second peak gives impossible high values for the discharge. An possible explanation is: when the water reaches to a diver for the first time, it is possible that the diver is placed in a lower part of the polder or ditch. In this case the increase in water height will be more than proportional. The influence of this is only important during the first tide, during the tides afterwards the height difference will be more accurate.

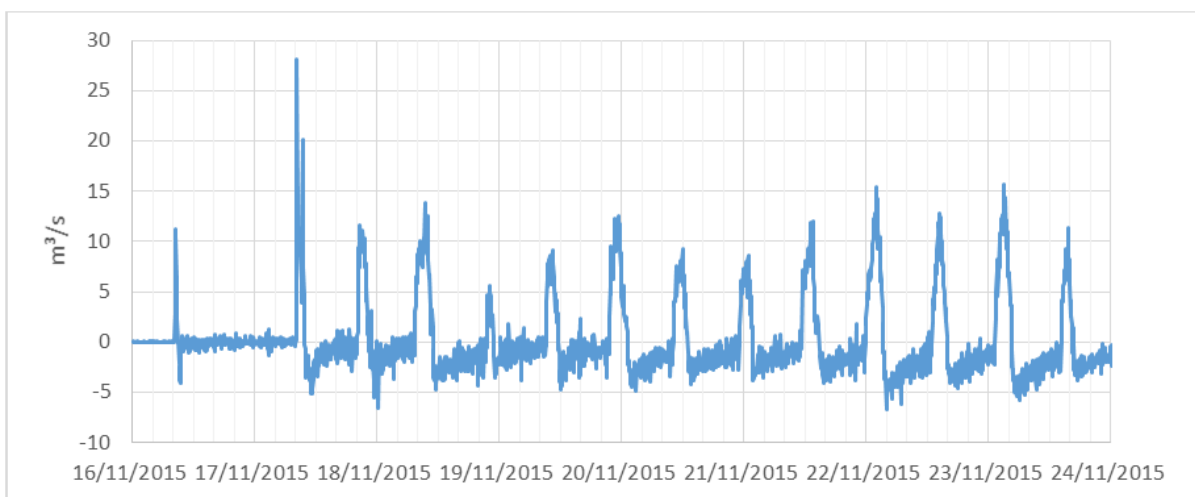


Figure 6-5 Discharge through breach

In Chapter 3 the formula of Govinda and Muralidhar is suggested to be the most accurate to calculate the discharge. The results of this formula are compared to the discharge indirectly calculated by the diver height.

The same formula is used for incoming and outgoing flow. The water level in the river and the mean water height measured by the divers is used in the formula. The weir length is assumed to be 10 meter. In some points in time the flow will be submerged in (Nikolov, Minkov, Dimitrov, Mincheva, & Mirchev, 1978) it is stated that a broad crested weir is submerged when the ratio of the water level downstream on the water level on the weir is larger than 0,75-0,85. The water level in the river change fast therefore the flow in the breach will only be a short time submerged. Therefore the effect of submergence of the flow is neglected.

In time the base width and depth change, they have to be estimated.

The base width of the breach is approximated in time from 1,9 meter, at the beginning of the second breach day, to 6 meter at 24/11/2015. These widths are extracted from the 3D models made of the breach during this period. It is assumed that the breach growth is fast during the first test on 17/11/2015 and then is linearly afterwards. The slope of the sides of the breach are taken at an angle of 18° in correspondence of the 3D models. The inserted base width of the breach and comparison to the measurements is shown in Figure 6-6 and Figure 6-7. It can be seen that at the start a lot of erosion occurs and afterward a constant erosion speed is assumed. The length of the breach is estimated to be 10 meter.

Due to the presence of a clay layer the downward erosion was limited. An estimation of the depth of the breach is done by varying the depth and calculating the lowest root mean square error (RMSE) of the formula compared to the discharge. An optimum is found at 4,1 m T.A.W.

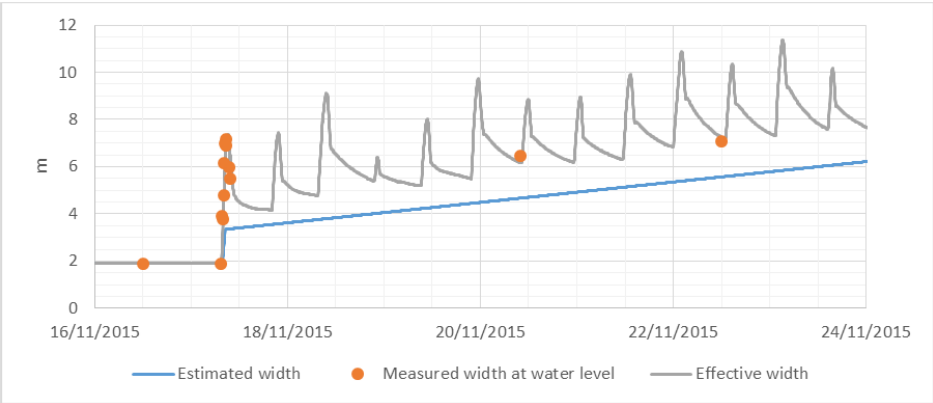


Figure 6-6 Base width breach

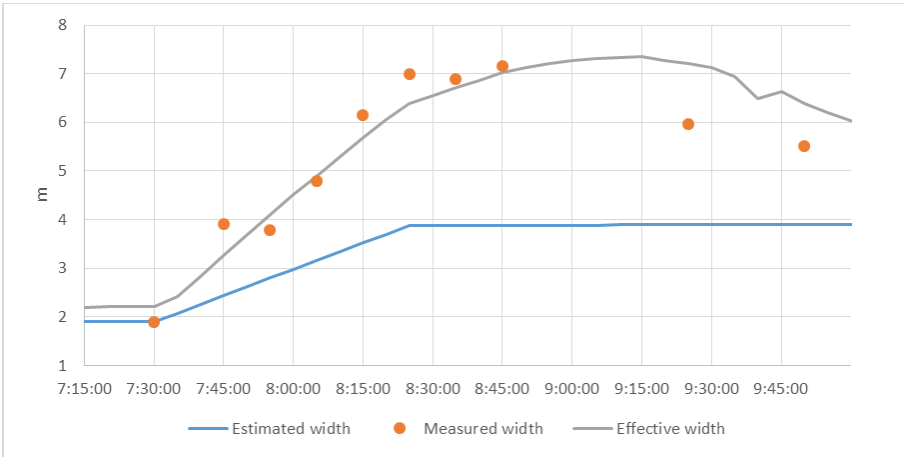


Figure 6-7 Detail base width of the breach

The calculated discharge is given in Figure 6-8. There is a large difference between the calculated values and the measurements. The reason for this difference will be mainly the friction that the water encounters in the breach. From the observations given in chapter 5 it can be concluded that the surface inside the breach is very rough. This roughness will slow down the water causing a smaller flow in the breach. This effect is studied by (Pařilková, Říha, & Zachoval, 2012) and (Jalil, Ibrahim, & Jafer, 2014) and can have an influence on the discharge up to 50%. The coefficient of discharge is influenced by the ratio water height to roughness height and the ratio of water height to breach length. Therefore it will be necessary to split the flow up into two parts the incoming flow and outgoing. The curvature of the streamlines has also an influence on the discharge, if the curvature is large there is a decrease in discharge, due to the highly irregular base of the breach the influence of the curvature of the streamlines can't be neglected. (Zerihun & Fenton, 2006)

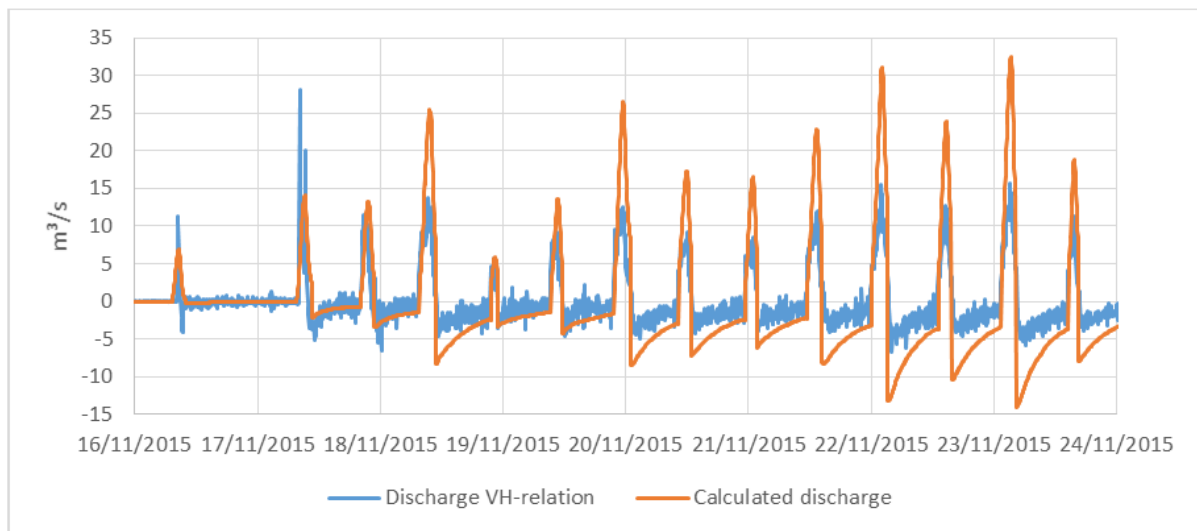


Figure 6-8 Calculated discharge through breach

A better approximation of the discharge is made by adjusting the value of coefficient of discharge for the incoming and outgoing flow and the depth of the breach. This is done by minimalizing the RMSE of the new formula compared to the discharge and water volume in the polder measured by the divers. This is done for a constant value of  $C_d$  in following formula:

$$Q = C_d \sqrt{g} B H^{3/2}$$

and by adjusting the constant X in the formula of Govinda and Muralidhar:

$$C_d = X \sqrt{8/27} \left( \frac{H}{L_c} \right)^{0.022}$$

The comparison of the formulas with the measured values is only done starting from 19/11/2015. This is done to decrease errors due to the placement of the sensors as explained previously. In Table 6-1 these adjusted coefficients are given and in Table 6-2 the corresponding values of the RMSE are given. It is found that the difference between an optimisation according to the flow or volume is small. If the RMSE values are compared, a constant coefficient of discharge gives a better result.

The breach depth is optimised by the same principle. Different breach depths were obtained. In reality this isn't possible the breach depth is constant for the different formulas. The

calculated values all where situated around 4,1 m T.A.W so this depth is used to compare the different formulas. This depth is the same as in the original calculation.

	C <sub>d</sub> Govinda and Muralidhar	Constant C <sub>d</sub>	C <sub>d</sub> Govinda and Muralidhar	Constant C <sub>d</sub>
Optimized using	Discharge		Volume	
Incoming	$0,444\sqrt{8/27}\left(\frac{H}{L_c}\right)^{0.022}$	0,231	$0,409\sqrt{8/27}\left(\frac{H}{L_c}\right)^{0.022}$	0,213
Outgoing	$0,325\sqrt{8/27}\left(\frac{H}{L_c}\right)^{0.022}$	0,167	$0,295\sqrt{8/27}\left(\frac{H}{L_c}\right)^{0.022}$	0,151

Table 6-1 Adjusted values of Cd

	RMSE C <sub>d</sub> Govinda and Muralidhar	RMSE Constant C <sub>d</sub>	RMSE C <sub>d</sub> Govinda and Muralidhar	RMSE Constant C <sub>d</sub>
Optimized using	Discharge		Volume	
Incoming	2,4142	2,4009	4068,60	4037,33
Outgoing	1,3044	1,3021		

Table 6-2 RMSE of adjusted values of Cd compared to the measured discharge or water volume

The graphs with the discharge and volume calculation are given in Figure 6-9 and Figure 6-10. There is a much better correlation between the formulas compared to the initially used formula of Govinda and Muralidhar. The graphs show that the difference in the discharge between the different formulas is negligible. In the volume calculation the difference is more visible.

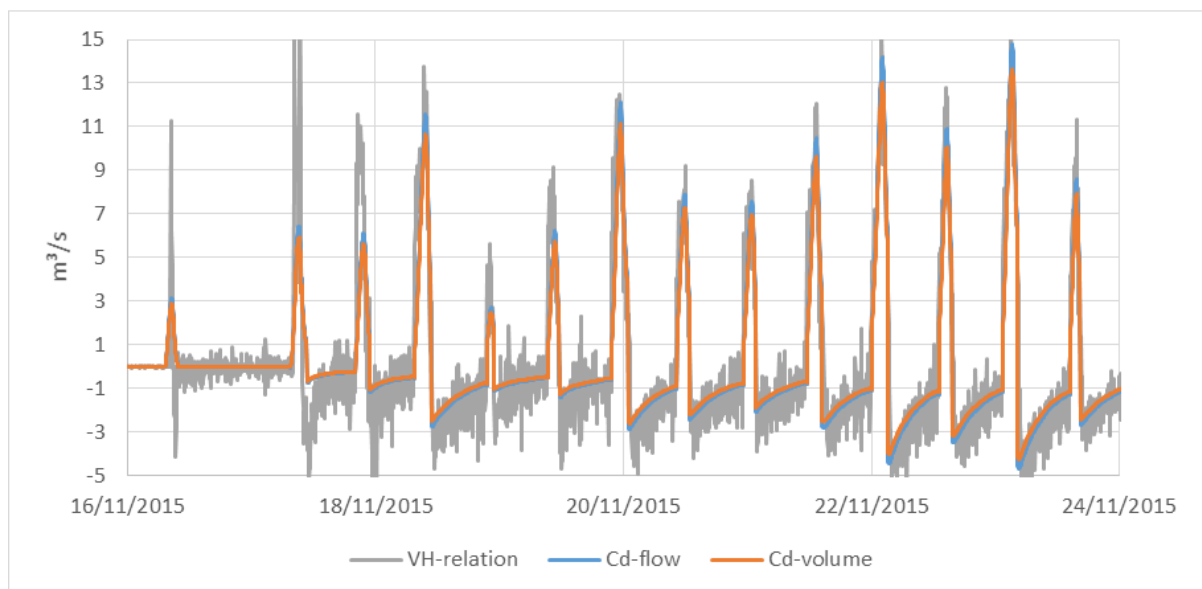


Figure 6-9 Discharge with adjusted coefficients

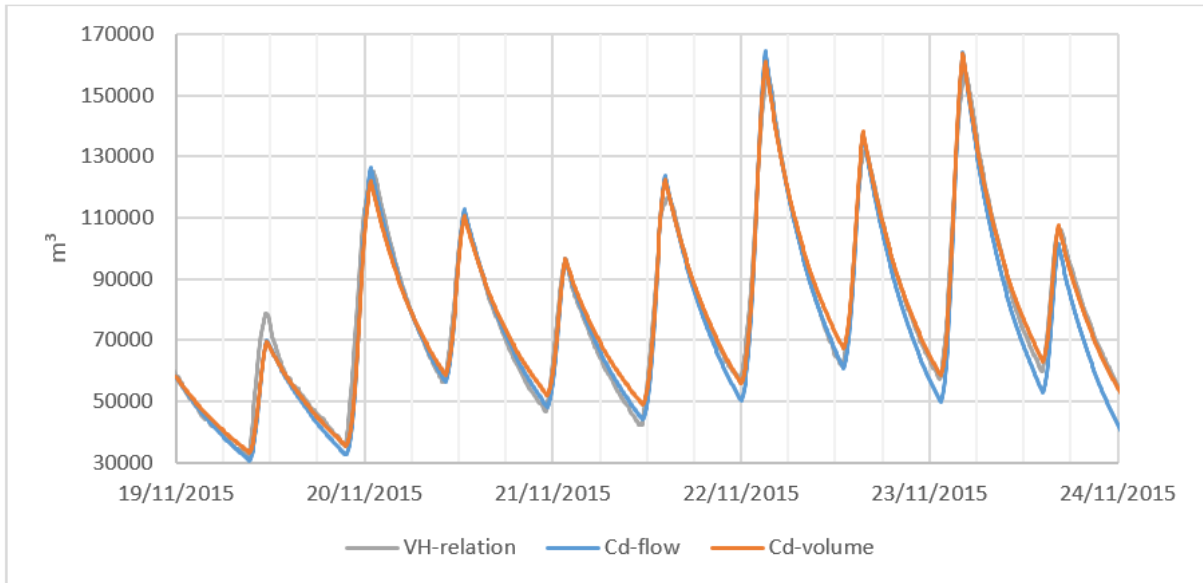


Figure 6-10 Volume with adjusted coefficients

In Figure 6-11 a detail of the discharge is given during one tide. It can be noticed that there is a good agreement with the incoming and the outgoing discharge. It is found that: when the flow changes in direction there is some difference. This can be explained by the fact that the volume of water in the polder is calculated using the mean water height measured by the different divers in the polder. During the transition between inflow and outflow it is possible that the water level is still raising far from the breach but the outflow has already started at the breach. This gives a more smooth transition and a different point in time when the direction changes. This effect can be seen in Figure 6-12. Diver 3 is closest to the breach (53 m) and reacts almost instant, diver 2 (359 m) is furthest from the breach and reacts with a delay.

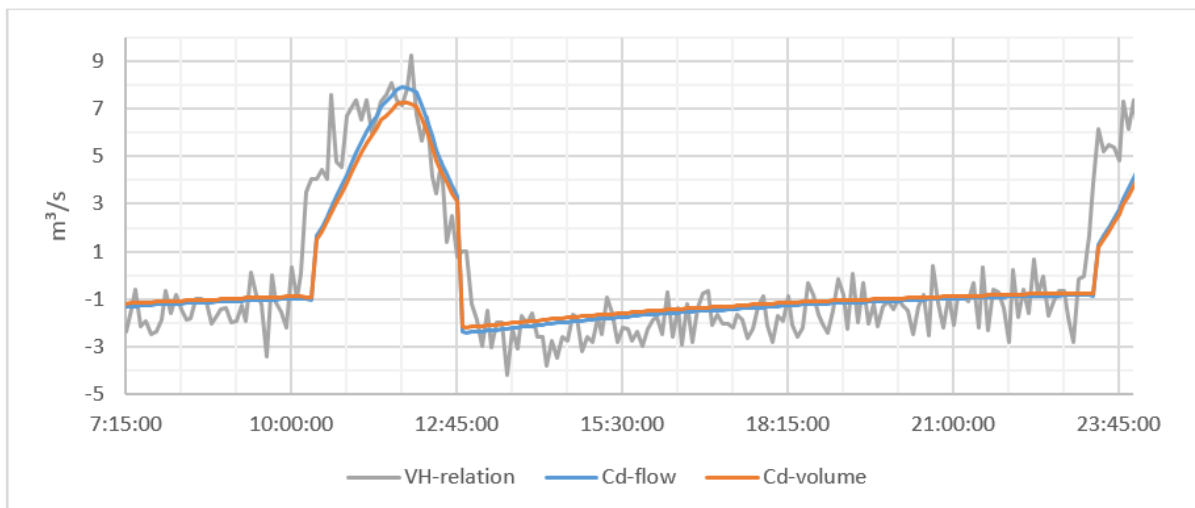


Figure 6-11 Detail of discharge during one tide 20/11/15

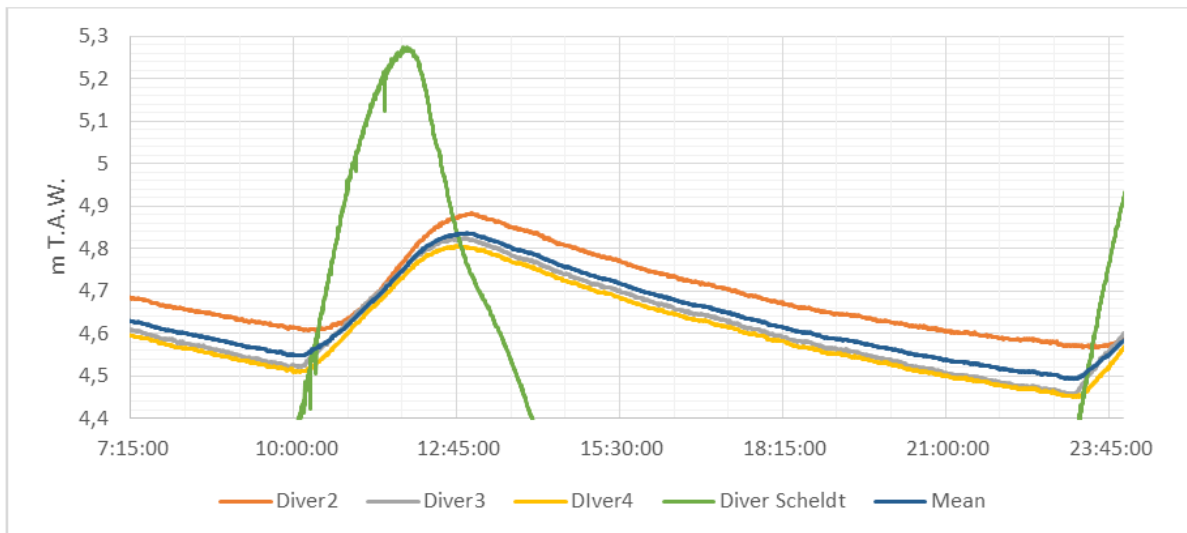


Figure 6-12 Detail diver measurement 20/11/15

## 6.2.2 Conclusion

A large difference is noticed between the suggested formula for the discharge through the breach and the measurements. This difference can be explained by the large roughness in the breach, the curvature of the streamlines, by the occurrence of drowned flow conditions and by the linear assumption of the breach width. The large roughness is because of the presence of rocks in the breach, these rocks come from the riprap revetment at the river side. In other experiments the dike was made out of more homogenous soil. The formula with the most roughness incorporated is proposed by FHR but even this formula gives a too large discharge (+50%). This lower breach discharge is beneficial for the safety of the dike, during an extreme event when dike breaching should occur, the discharge will be smaller than expected so there is more time for evacuation.

The discharge formula derived is different for inflow compared to outflow. A reason for this is the water level. During inflow the water level is much higher. This increase in water height decreases the influence of the friction causing a larger discharge. It is found that a constant coefficient of discharge is more accurate compared to the formula of Govinda and Muralidhar. An exact similarity between the measurements and the calculations isn't possible because the relation of the flow to  $H^{3/2}$  is only an approximation and it isn't sure that the measurements are 100% correct. Further evaluation of the suggested parameters has to be done.

Further research is needed to examine the influence of the riprap revetment on the breach discharge. It is expected that the lower discharge has also an influence on the breach growth.

## 6.3 Water velocity calculation

### 6.3.1 Estimation

From the discharge calculation and the estimated cross section of the breach, a water velocity can be calculated. The cross section is taken equal to the one used in the flow calculation. Two estimations are done: the water level in the breach is taken equal to the maximum of the



water level in the polder and the water level in the Scheldt. This gives an lower estimation of the mean flow velocity, when the minimum of the water levels is taken an upper estimation can be found. The discharge used to calculate the velocity in the breach is taken from the VH-relation and from the calculation using the constant coefficient of discharge adjusted to the volume and flow.

The results are shown in Figure 6-13 and Figure 6-14, a positive water velocity is during filling of the polder, a negative velocity is during drainage of the polder. The upper estimation is only relevant during inflow because during outflow the water level of the river is below the breach depth so no minimum or maximum estimation can be done.

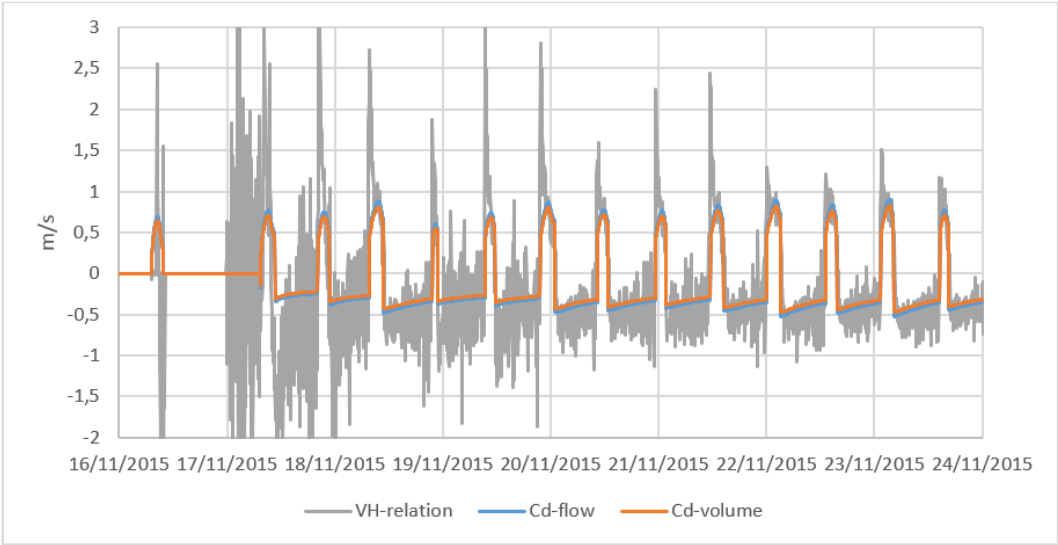


Figure 6-13 Lower estimation of mean water velocities in the breach

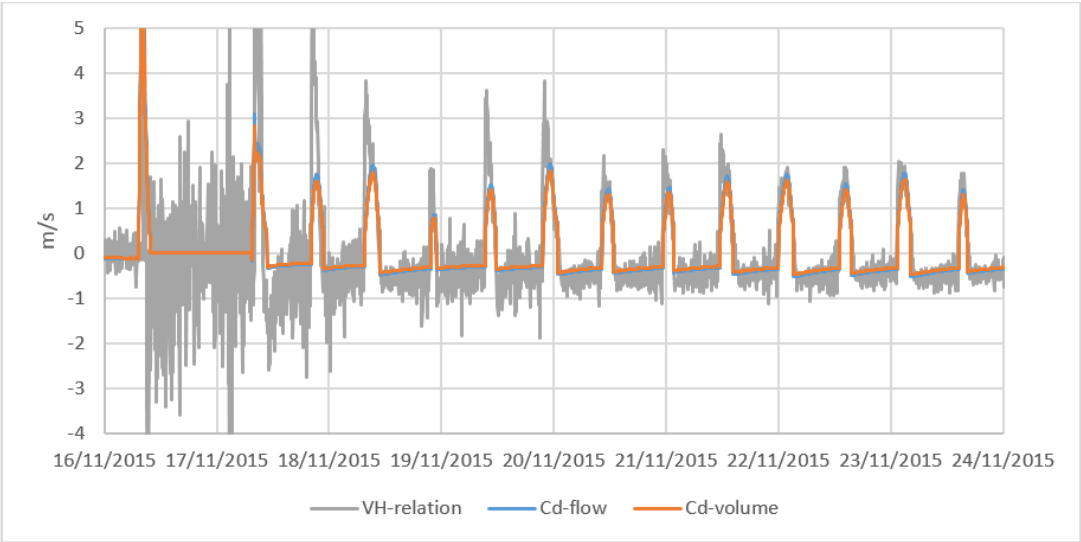


Figure 6-14 Upper estimation of mean water velocities in the breach

### 6.3.2 Conclusion

The maximum outflow calculated using the VH-relation is mostly larger than what is calculated by using the formulas. It is expected that the real flow velocities will be in-between the upper

and lower limit. The interval of the water velocities will be mostly around 1 to 3 m/s for inflow and around 0,5 m/s for outflow. The calculated values are comparable to the measured values using the surface floats and to the Zwin '94 breach experiment (Visser, Kraak, Bakker, & Smit, 1995).

## 6.4 ADCP measurement

An ADCP measurement is done by HIC on 15/03/2016 in the breach. An acoustic beam is sent through the water measuring the depth and the water velocity every meter in the cross section of the breach. This gives an indication of the water velocity in different sections of the breach. The duration of one series of measurements is approximately 15 minutes, the flow will change during this period so the measurement is only an estimation. The maximum water level during the ADCP measurement was 4,84 m T.A.W. An ADCP measurement measures the water velocity using an acoustic beam, this is done for every 10 centimetre of depth. The lateral distance between two measurements is one meter. When the depth and velocity is known, the discharge can be calculated. In Figure 6-15 the ADCP measurement is shown.



*Figure 6-15 ADCP measurement Scheldt side*

The measurements are divided in three parts.

- The incoming tide measured at the Scheldt side.
- The outgoing tide measured at the Scheldt side
- The outgoing tide measured at the polder side

In Figure 6-16 the minimum, maximum and mean water velocity are given. The incoming velocities have approximately the same values as the outgoing. All the velocities lie under 2 m/s. The minimum velocities measured at the side of the breach where approximately constant.

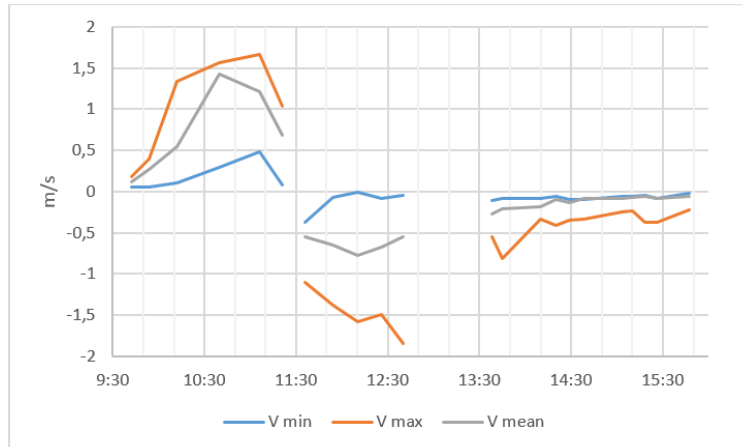


Figure 6-16 Measured velocities

In Figure 6-17 the measured discharge is shown. The shape of the discharge curve has a large incoming peak and a more smooth outgoing curve. The incoming discharge is approximately twice as large compared to the outgoing.

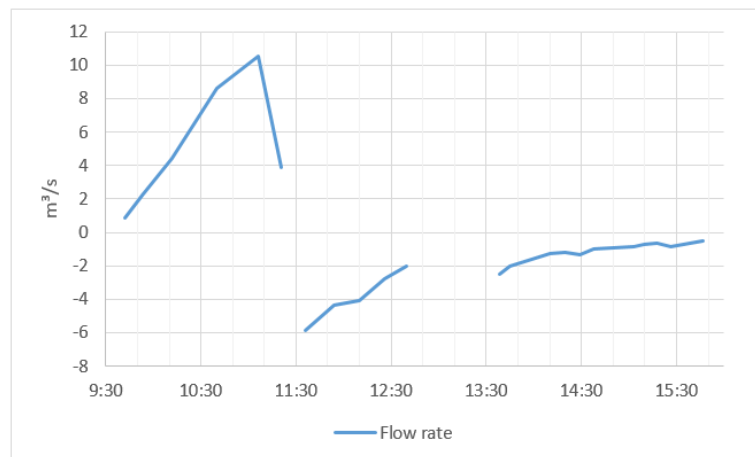


Figure 6-17 Measured discharge

## 6.5 Evaluation of coefficient of discharge

Using the ADCP measurement, the formulas elaborated to calculate the discharge are evaluated. This can only be done for the inflow of the breach because no diver measurements in the polder were available. The formula used is:

$$Q = C_d \sqrt{g} B H^{3/2}$$

For the coefficient of discharge two values are proposed: 0,231 and 0,213. The first one is optimised using the discharge measurements and the second one is optimised using the volume measurements.

The water height is assumed to be the mean value of a gauge station situated in Schoonaarde and Wetteren. These measurements can be consulted on Waterinfo.be (Flemish government, 2016). These gauge stations are situated respectively 7 km upstream and 5 kilometre

downstream of the breach. Comparison between this mean water height and the water height measured at the breach location gave good results.

During the ADCP measurements the water depth is also measured. The ADCP measurements were done at the river side of the breach so the water level is assumed to be the same as in the river. When this water level is decreased by the depth of the breach an estimation can be done of the bottom level. The timing of each series is given in Table 6-3. In Figure 6-18 the measured depths for each series are given. The depth measurements all coincide except series 1 and 2: these are neglected for the depth calculation. The mean value of the depth measurements was taken, this resulted in a value of 3,75 m T.A.W.

Series	Start time [h]	End time [h]
1	9:39	9:44
2	9:46	10:02
3	10:04	10:20
4	10:28	10:51
5	10:59	11:14
6	11:16	11:26

Table 6-3 Timing of each series

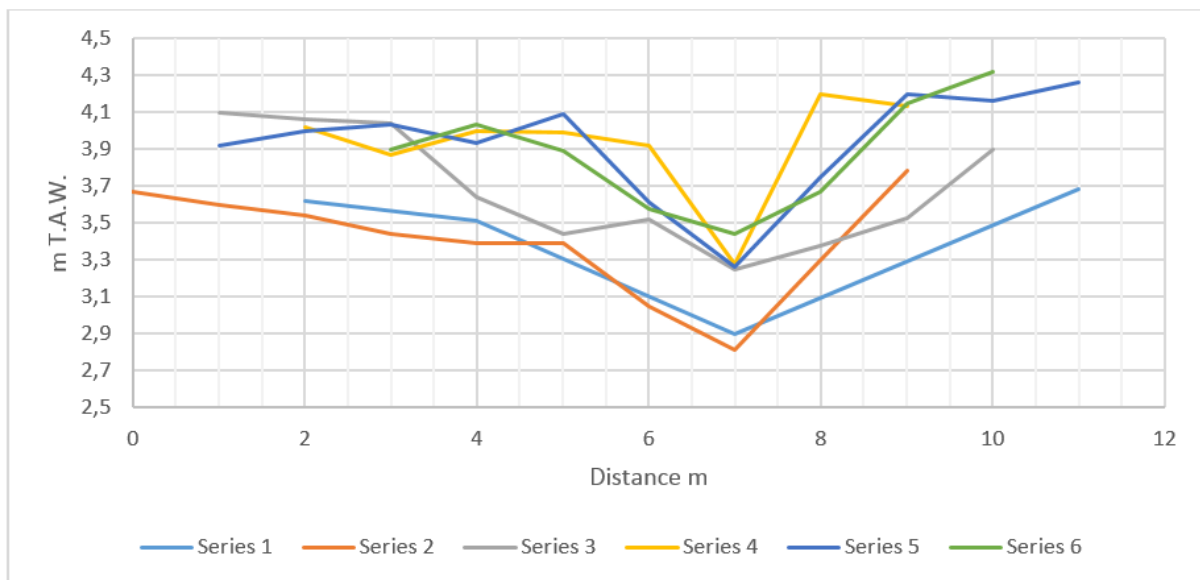


Figure 6-18 Measured breach depth

The base width of the breach is estimated to be 9,5 meters with sides of an angle of 30°. This gives a maximum breach width at the water line of 11,4 meters. This is in accordance with the observations. The comparison is given in Figure 6-19. In total 6 ADCP measurements were done. As the measured discharge is shifted in time, it is assumed that the clocks in the diver and the ADCP weren't synchronized. The shifted value is also depicted. The shape of the proposed functions is approximately equal to the measured one. There is one deviating measurement, the cause of this can be the duration of the test. The discharge is calculated by combining discharge measurements each meter in the cross section of the breach when the flow changes a lot this can give a distorted value. To have a better indication of the discharge,

it is proposed to perform the ADCP measurement as fast as possible. When using multiple devices the measurement should be better.

From the comparison it is noted that the coefficient of discharge optimised using the volume gives too small values for the maximum and the one optimised using the discharge has a good similarity with the measurements.

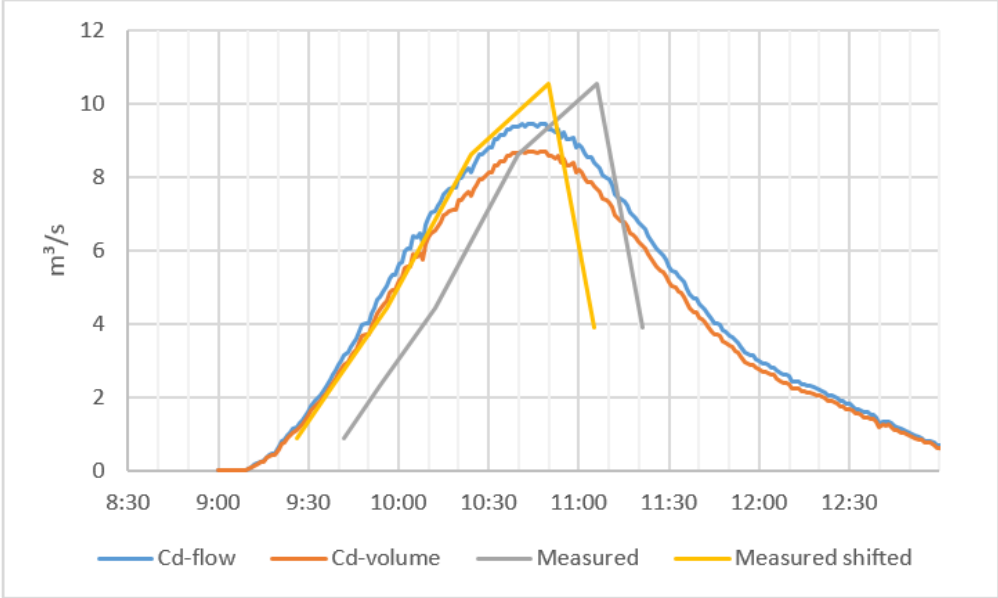


Figure 6-19 Comparison ADCP measurement and calculations

## 6.6 Conclusion

It was noticed that formulas in literature for the discharge through a breach gave a too large discharge. This was mainly the case because friction is neglected, the streamlines that are strongly curved in the breach and submerged flow. The riprap revetment on the river side of the dike flowed into the breach causing more friction and therefore a smaller discharge in the breach. Further research is needed to investigate this mechanism. A smaller breach discharge during an extreme event gives more time for evacuation.

A proposal is made for a new coefficient of discharge to estimate the breach discharge. The best solution was obtained when a optimisation is made using the discharge. The proposed formula is evaluated using an ADCP measurement in the breach. There was a good similarity.

# 7 Water pressures in the dike

During the breach test, the water pressure in the dike is measured. The pressure represented in the graphs is already corrected for the air pressure. The goal is to measure a suction pore water pressure due to hindered erosion and to evaluate how the dike is saturated due to water which is in direct contact with the sand core.

## 7.1 Breach test I on 16/11/2015

It can be noticed that the sensors at the polder side, BAT sensors 3837, 3831 and 3834, have the lowest pressures. This can be explained by the fact that the water line in the dike declines towards the polder. The MEMS sensors don't log a negative or suction pressure. This is because they are placed in a bore hole and afterwards fine sand is deposited around them. This sand was dry so doesn't have any matric suction therefore only the air pressure is measured. The BAT sensors have a more direct contact with the ground because they are hammered into the ground so measure directly the unsaturated pressure. During the first breach experiment no significant changes could be noticed.

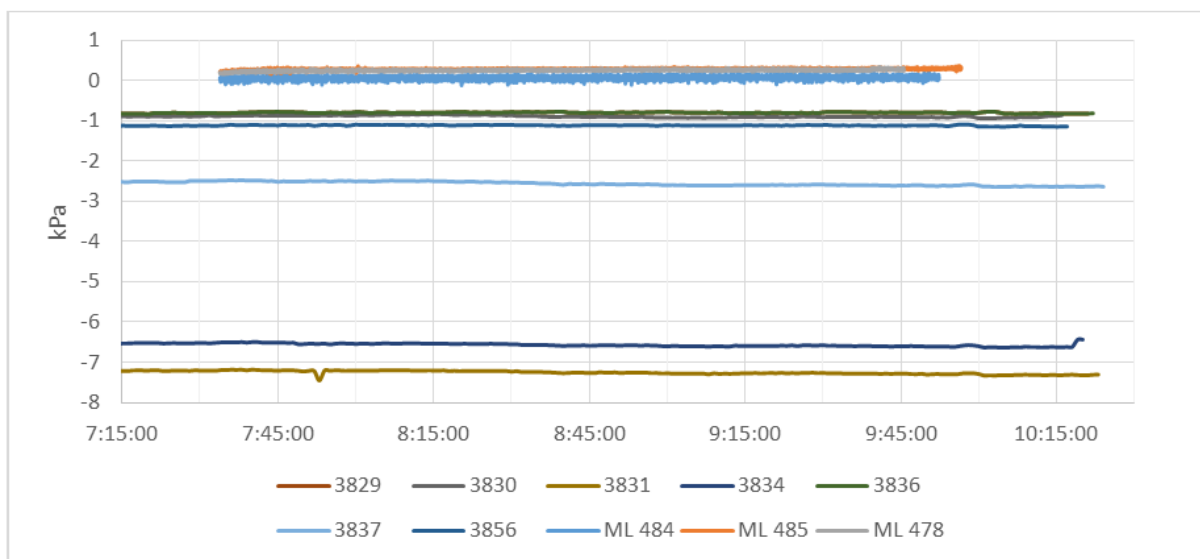


Figure 7-1 Water pressure at breach day I

In Figure 7-2 the results are given of BAT sensor 3856 and the tide. This sensor is placed closest to the river. If there is an influence of the tide on the water level in the dike, at this place has the highest potential to measure it. It is found that influence of the tide in the river to the ground water level is negligible. There are only very small differences, which can be due to atmospheric conditions. However the time span of the measurements was very small, a longer time span is needed to obtain a more accurate result. Also the breach test can have an influence. A longer measurement is needed to have a better result.

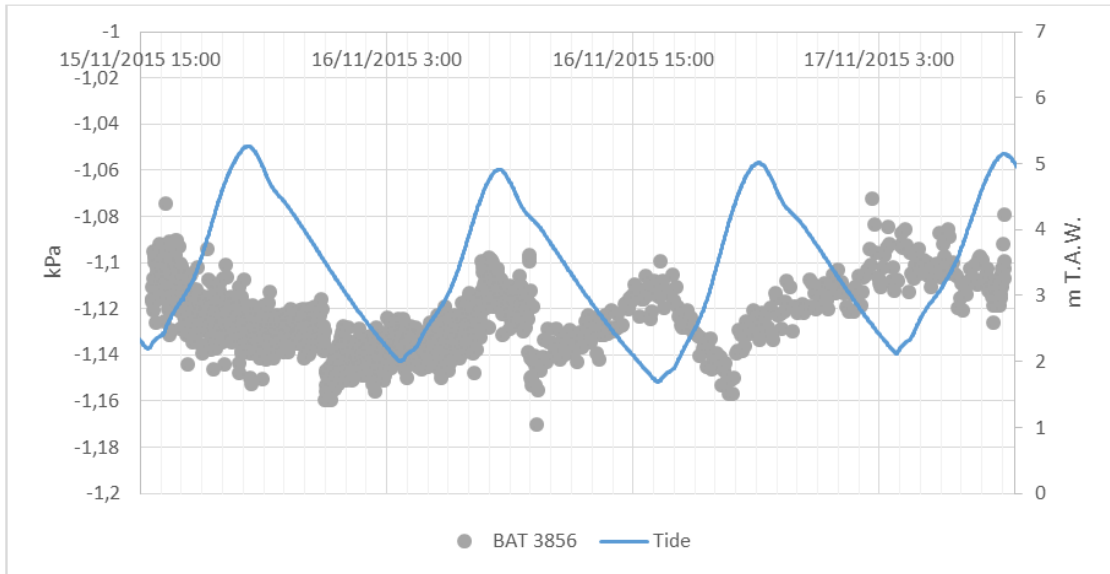


Figure 7-2 Pressure BAT sensor 3856 and tide [0,1 kPa=0,01 m]

## 7.2 Breach test II on 17/11/2015

The second breach experiment was more successful, resulting in large differences in the water pressure measurements. BAT sensor 3856 and MEMS sensor ML 478 felt the influence of the water in the breach. The MEMS sensor recorded two jumps in the pressure. These jumps are recorded when the soil near the sensor collapsed in the breach. BAT sensor 3856 gets saturated by the water flowing through the breach and then a piece of the sides fell in to the breach. This causes a decrease in pressure because the dry ground of this piece will suck the water towards it. From 9:17 h the water level in the breach decreases causing a decrease in the measured pore water pressure.

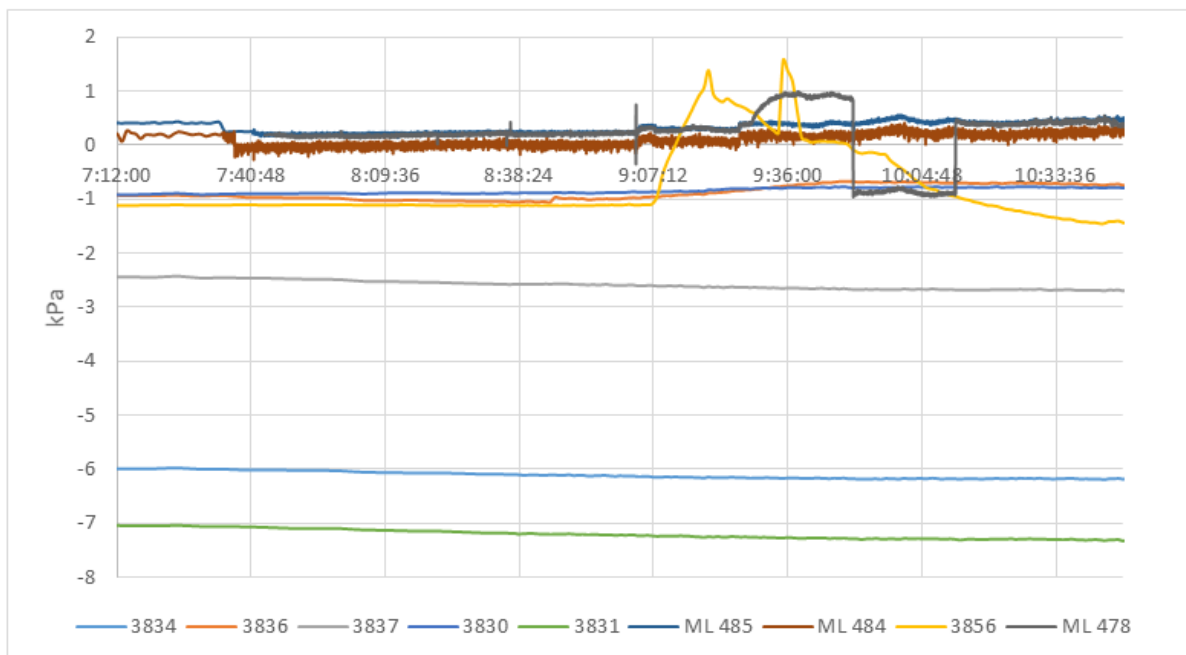


Figure 7-3 Water pressure at breach day II 17/11/2015

The measured values of sensor ML 478 are examined in detail.

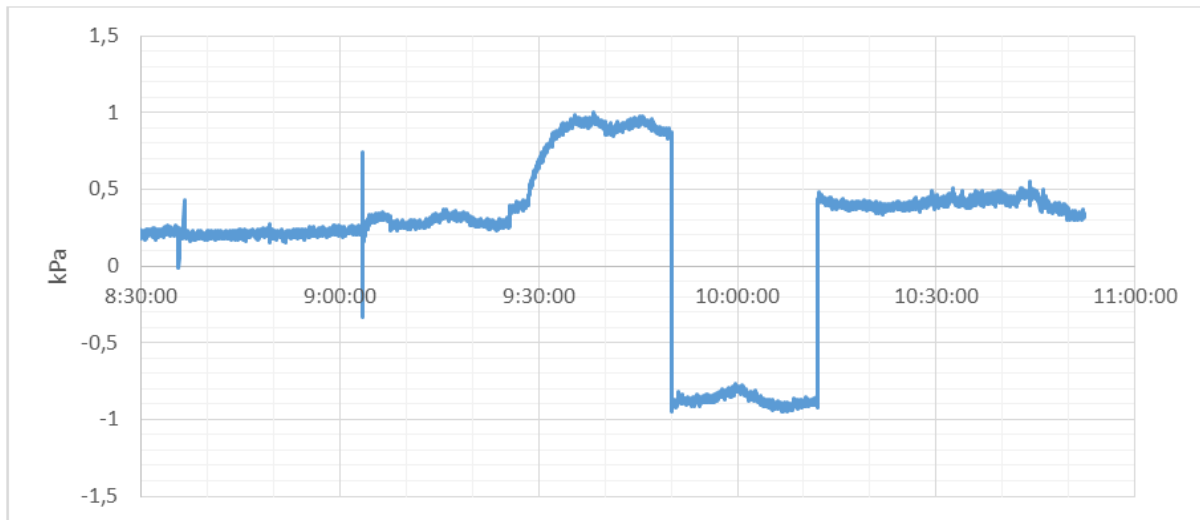


Figure 7-4 sensor ML478

The sensor was installed in the middle of the dike. At this location most erosion took place during the experiment. The water flow into the polder caused the sensor to saturate from approximately 9:25 h. At 9:35 h the pressure becomes constant. This is due to a decrease in water level in the breach. High tide is at 9:17 h. Therefore the water level is dropping when the sensor gets saturated so the increase in pressure will become smaller and smaller. This can be seen in the graph: first a fast increase and then a more constant value.

At 9:50 h a jump occurs this is when a chunk of soil collapses into the breach. A tension crack is formed close to the sensor. This causes a sudden decrease in pore water pressure. The falling soil “sucks” out the water near the sensor. This suction is maintained for approximately 12 minutes.

At 10:12 h a new jump is recorded. This is when a new chunk collapses in the breach. The sensor is then dragged away in the breach.

### 7.3 Further progress of the breach

In Annex C the full measurements are given. It can be observed that the sensors first saturate and then measure the influence of the tide.

### 7.4 Calculation with SEEP/W

The measured water pressures are simulated using SEEP/W. This is a finite element software for the analysis of groundwater flow. SEEP/W can both model saturated and unsaturated groundwater flow, both in a transient or steady state model. The ground water flow is modelled for 7 days. The modelling of the ground water is done for a vertical plane close to the polder side where 6 sensors were placed. The calculation is done from 8:07 h 17/11/2015 until 8:00 h 24/11/2015



### 7.4.1 Model

The schematisation of the breach inserted in SEEP/W is an approximation of the real breach. Only the side wherein the sensors were installed is modelled. There are 3D models of the breach made at different time intervals by ATO. A vertical cut of these models is made at the line of the sensors parallel to the river at the polder side.

An approximation is made of the breach geometry in SEEP/W. It is chosen to split the model in SEEP/W in three different geometries because from the cross section it is obtained that there are three major shapes of the breach sides. The start geometry is the shape of the pilot channel. In Figure 7-5 the model is shown, the thick red lines are used as input in SEEP/W. The crosses represent the sensors placed in the dike. The time interval of each geometry is: 0-1200 sec, 1200-100380 sec, 100380 sec-end. The choice of 100380 sec is done because it is assumed from the daily photos taken of the breach that the erosion causing the shape measured at 20/11/2015 happened on 18/11/2015. The geometry is changed at 12:00 18/11/2015.

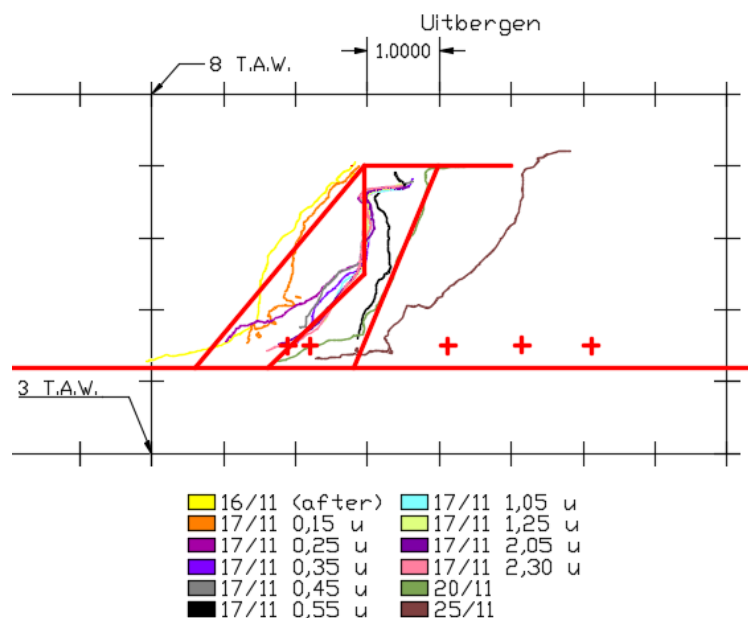


Figure 7-5 SEEP/W model compared to sections

In the model, two different types of soils are inserted: sand and clay. The depth of the breach is set at 4,2 m T.A.W. The soil underneath this level is clay. The dike body above is modelled as a sand core with a layer of 25 cm clay on top of it. In Figure 7-6 this is displayed. The brown sections are clay and yellow is sand. The black dots show the locations where the sensors were installed. The mesh size of the model is set to 0,3 m.

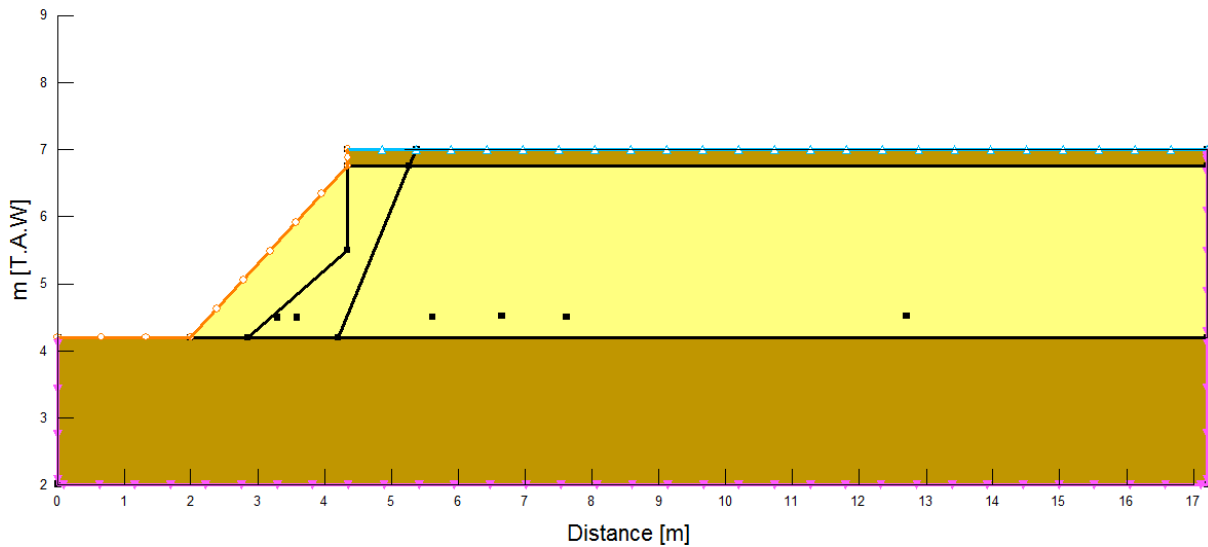


Figure 7-6 model in SEEP/W

#### 7.4.2 Boundary conditions

In Figure 7-7 the different boundary conditions are depicted as can be seen in Figure 7-6. It was decided to have a varying water level inside the pilot channel with the maximum value of the water level in the river and in the polder as can be seen in Figure 7-8. This is as approximation, but it is a reasonable assumption. The water level in the polder was taken equal to the height of the diver closest to the breach. The other sides are inserted as no flow conditions. The start time for the calculations is 8:07 h 17/11/2015.




Name	Category	Color
Potential Seepage Face	Hydraulic	
No flow	Hydraulic	
Tide	Hydraulic	

Figure 7-7 Boundary conditions

As initial condition a constant water level is applied in the model. All the sensors give different measurements before the test. This can be due to different soil conditions or an incorrect measurement of the negative pressures. It is assumed that the best measurement of negative pressure is to be done with the BAT sensors, as they are in direct contact with the soil. The BAT sensors measure a pore water pressure in the range of -2 to -7 kPa. The decision is made to use -6 kPa as the initial pore water pressure in the sensors. The initial value in the calculation is less important. Choosing a low value has the advantage that it gives a clear indication when the sensors start to become saturated.

A calculation in the transient phase is performed every 60 seconds for the first 1200 seconds, afterward the calculation interval was lengthened to 300 seconds.

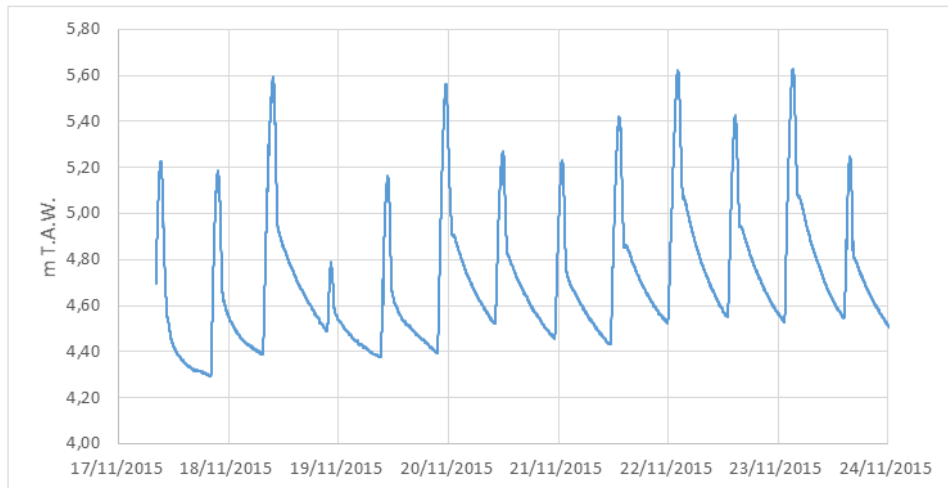


Figure 7-8 Estimated water level in breach

### 7.4.3 Soil properties

The soil properties for the SEEP/W analysis consists of two main aspects: the volumetric water content function and the hydraulic conductivity function. The volumetric water content curve gives the relation between the water content and the matric suction. In SEEP/W there is a possibility to estimate this function. The estimation method using grain-size data is used. The parameters required for this estimation method are: the saturated water content,  $D_{10}$ ,  $D_{60}$ , the liquid limit and compressibility. A value for these parameters is given by GEO based on laboratory tests.

The hydraulic conductivity function gives the relation between the hydraulic conductivity and the matric suction. This function is estimated from the predicted volumetric water content function using the Van Genuchten method. The parameters needed are: hydraulic conductivity at saturation, residual water content and the volumetric water content curve.

The parameters needed for the different curves are estimated from the soil investigation.

#### 7.4.3.1 Sand

Saturated Water content	0,4 m <sup>3</sup> /m <sup>3</sup>
$D_{10}$	0,09 mm
$D_{60}$	0,17 mm
Liquid limit	0 %
Compressibility	2e-5 kPa <sup>-1</sup>
Hydraulic conductivity	1,4e <sup>-5</sup> m/s
Residual water content	0,02 m <sup>3</sup> /m <sup>3</sup>

Table 7-1 Properties of sand

#### 7.4.3.2 Clay

The hydraulic conductivity has to be estimated. The flow through the clay will be negligible so a value of the hydraulic conductivity of  $e^{-10}$  m/s is used.

Saturated Water content	0,4 m <sup>3</sup> /m <sup>3</sup>
D <sub>10</sub>	5e-5 mm
D <sub>60</sub>	0,06 mm
Liquid limit	62 %
Compressibility	8e-4 kPa <sup>-1</sup>
Hydraulic conductivity	e <sup>-10</sup> m/s
Residual water content	0,09 m <sup>3</sup> /m <sup>3</sup>

Table 7-2 Properties of clay

#### 7.4.4 Results

The results of the sensors are listed from the breach outward. The positioning of the sensors is given in Figure 4-1.

##### 7.4.4.1 ML 485 and BAT 3836

These sensors are installed closest to the breach. Two results are shown in Figure 7-9 and Figure 7-10, in the model with erosion a piece of the toe is removed after 1200 sec. In the model without erosion, the model stays the same. The measurement differs a lot from the calculated values with erosion because the soil stays in place at this location (polder side) while in the model the soil is removed. The results of the non-eroded model are much better. The measured values show a good similarity with the calculation. The reason of the better result with the non-eroded model is that in reality there was more sand at the toe at this location, as can be seen in Figure 7-5. The model inserted is only an estimation of the geometry at the side of the breach during this period.

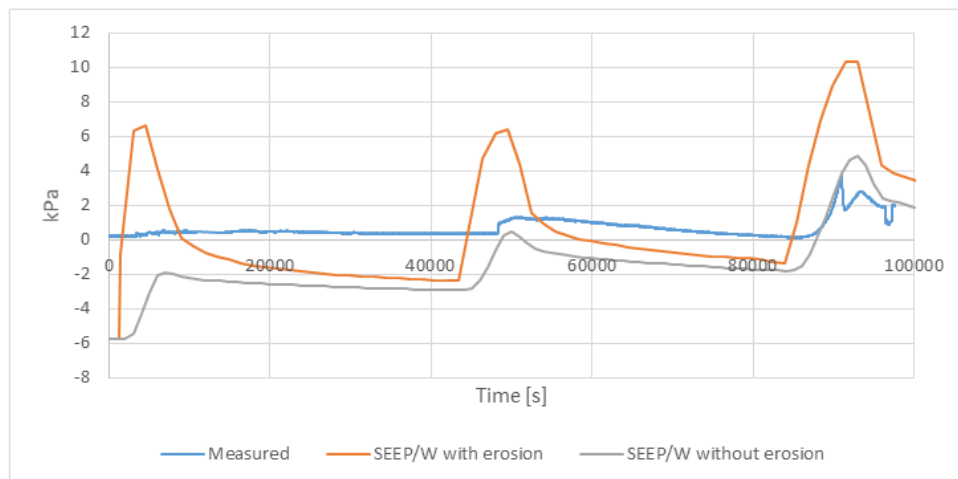


Figure 7-9 ML 485

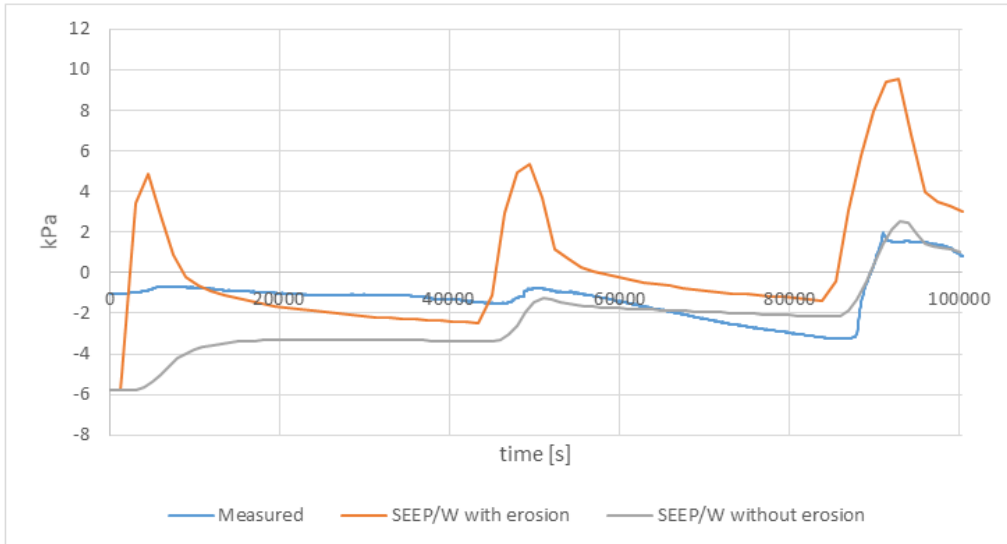


Figure 7-10 BAT 3836

#### 7.4.4.2 ML 484

There is a good similarity between the measurements and the SEEP/W calculation. The saturation of the sensor begins at approximately the same moment, 100000 seconds. The peak values and the shape of the function are approximately the same but it can be noticed that the outflow in the model is too slow.

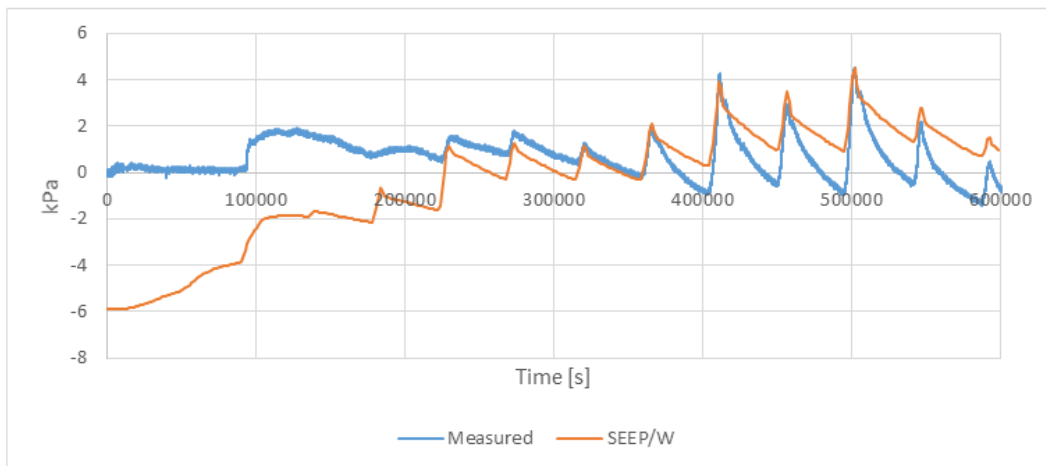


Figure 7-11 ML 484

#### 7.4.4.3 BAT 3834

There is a good similarity between the measurements and the SEEP/W calculation. The saturation starts at the same moment and the values are approximately the same. The calculated value is slightly too large.

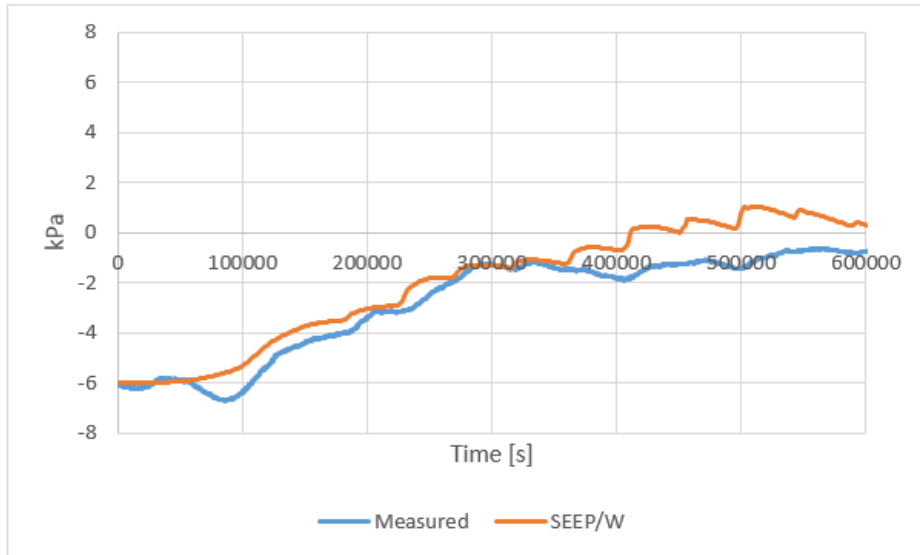


Figure 7-12 BAT 3834

#### 7.4.4.4 BAT 3831

There is a good similarity between the measurements and the SEEP/W calculation. The measurement isn't continuous due to an empty sensor battery.

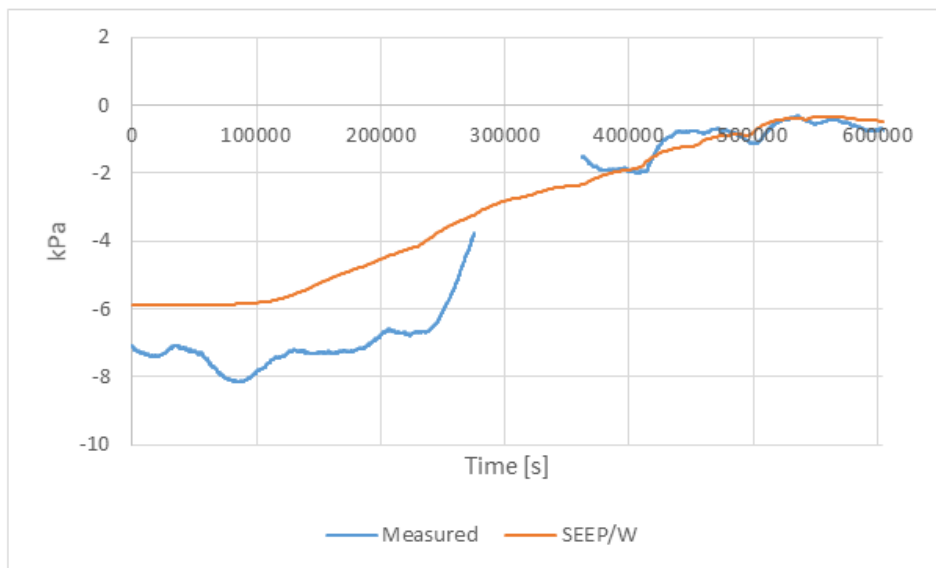


Figure 7-13 BAT 3831

#### 7.4.4.5 BAT 3837

This is the reference sensor. This sensor is placed at a large distance from the breach so in the SEEP/W there is no difference in measurement. In reality the water table isn't constant and precipitation or sunshine can wet or dry the ground causing a different outcome of the measured value.

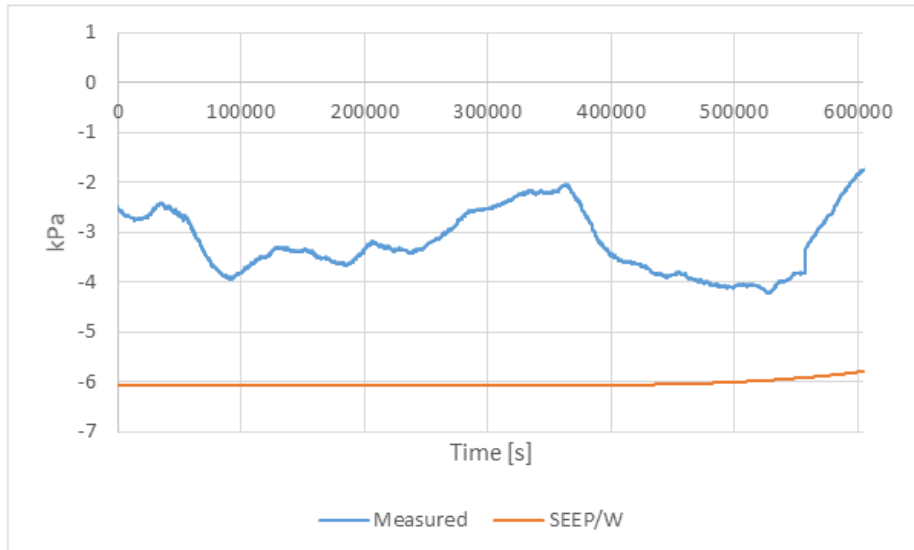


Figure 7-14 BAT 3837

#### 7.4.5 Sensitivity analysis

In general, it can be seen that the outflow is too slow, hence a sensitivity analysis is performed on different inserted parameters to see if this is due to an incorrectly estimated parameter. The comparison is made for sensor ML 484 where the difference is the most distinct. Graphs are given for the hydraulic conductivity, level of the clay layer, the saturated water content and the water level in the breach. Influence of the different parameters in the clay will be negligible because the flow in the clay will be very small hence only the parameters of the sand are changed. A negligible influence was found for the residual water content and when adjusting the default suction range of the soil. (0,01-1000 kPa)

##### 7.4.5.1 Level of the clay layer

In the model, the clay layer was set at 4,2 m T.A.W. It is possible that the clay layer is situated lower in reality hence a model is made with a clay layer situated at 4 m T.A.W. The influence can be seen in Figure 7-15. When the clay layer is situated lower, there is more sand exposed to the water in the breach. More water intrusion can be noticed due to higher peaks. A larger outflow is also expected, which could result in lower minima. This can't be noticed in the calculation: the outflow is larger but the minima aren't smaller. It seems that this is more dependent on the minimum water level in the breach. The level of the clay layer is assumed to be a good estimation.

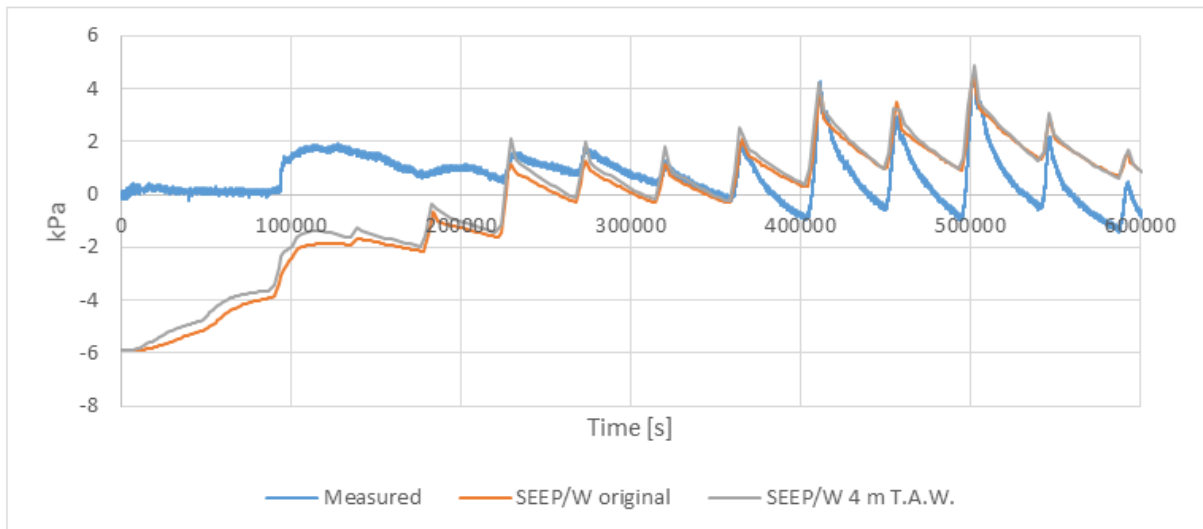


Figure 7-15 Influence of level clay layer

#### 7.4.5.2 Hydraulic conductivity

The hydraulic conductivity for sand is set to  $1,4e-5\text{m/s}$  in the model. This value is obtained from soil investigation. Considering the high variability in the dike, it is possible that in reality there is a difference. The hydraulic conductivity is increased and decreased by a factor 10 and the results are given in Figure 7-16. A lower hydraulic conductivity isn't possible because then the influence on the groundwater pressure would be very small. When the hydraulic conductivity is increased, it is noticed that the water intrusion is higher, but also starts earlier. The peak values increase but the minima stay the same. The same reason as in 7.4.5.1 can be given: the minima will be more dependent on the water level in the breach. The chosen hydraulic conductivity gives the best fit to the measured values.

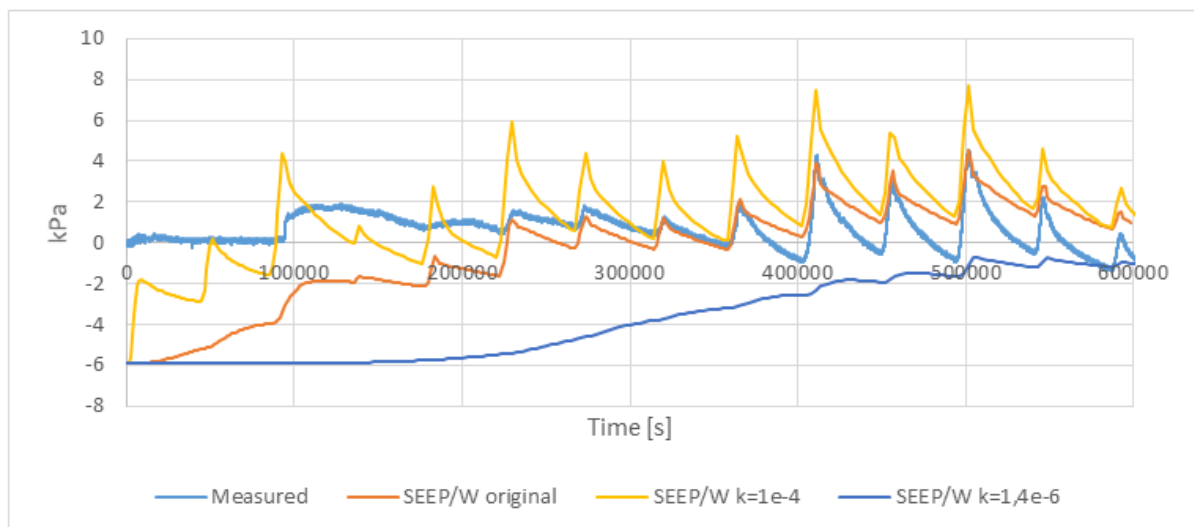


Figure 7-16 Influence of hydraulic conductivity

#### 7.4.5.3 Saturated water content

In the model the saturated water content is estimated to be  $0,4\text{ m}^3/\text{m}^3$ . The solution of the calculation with water contents of 0,3 and 0,5 is shown in Figure 7-17. If the saturated WC is increased, a slower reaction of the groundwater pressure is observed. More water needs to



flow in the dike before saturation occurs. The opposite is observed when decreasing the saturated WC. The chosen value shows the best accordance with the observed values.

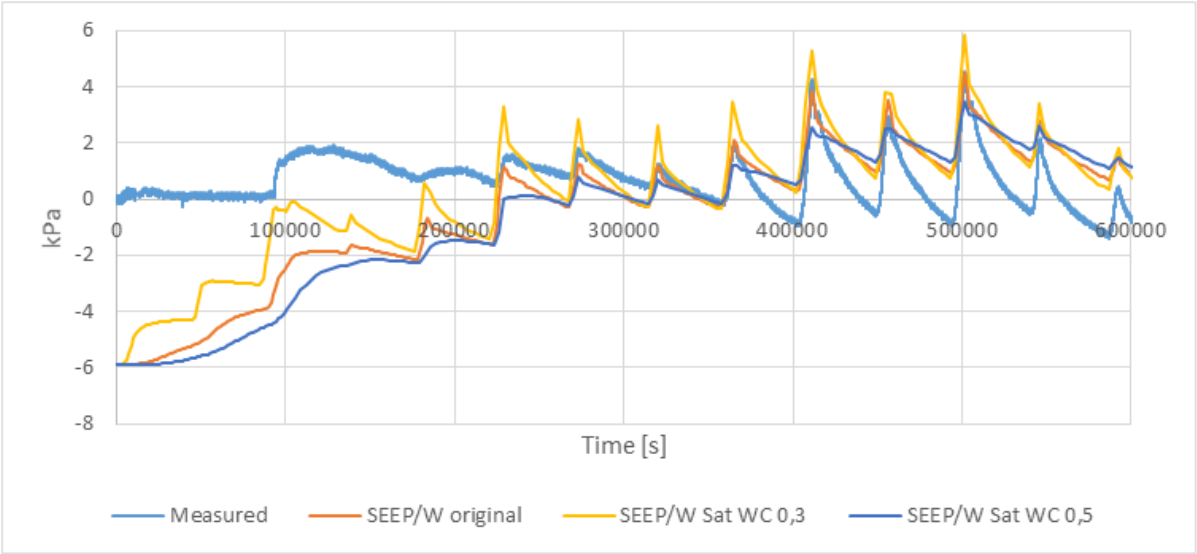


Figure 7-17 Influence of saturated water content

7.4.5.4 Water level

The minimum pressures calculated don't vary much when changing the inserted parameters. It is assumed that the estimated water level in the breach during outflow is too large. The reasons can be: the extra decrease in level due to the water level in the river, a wrong measurement of the height of the diver in the polder or a wrong assumption of the position of the sensor in the breach. The measured values of the diver are decreased, first by 0,15 then by 0,25 meters, the results can be seen in Figure 7-18. It can be seen that when the water level during outflow is decreased, the decrease in pore water pressure is larger. The influence on the maximum pressure is small.

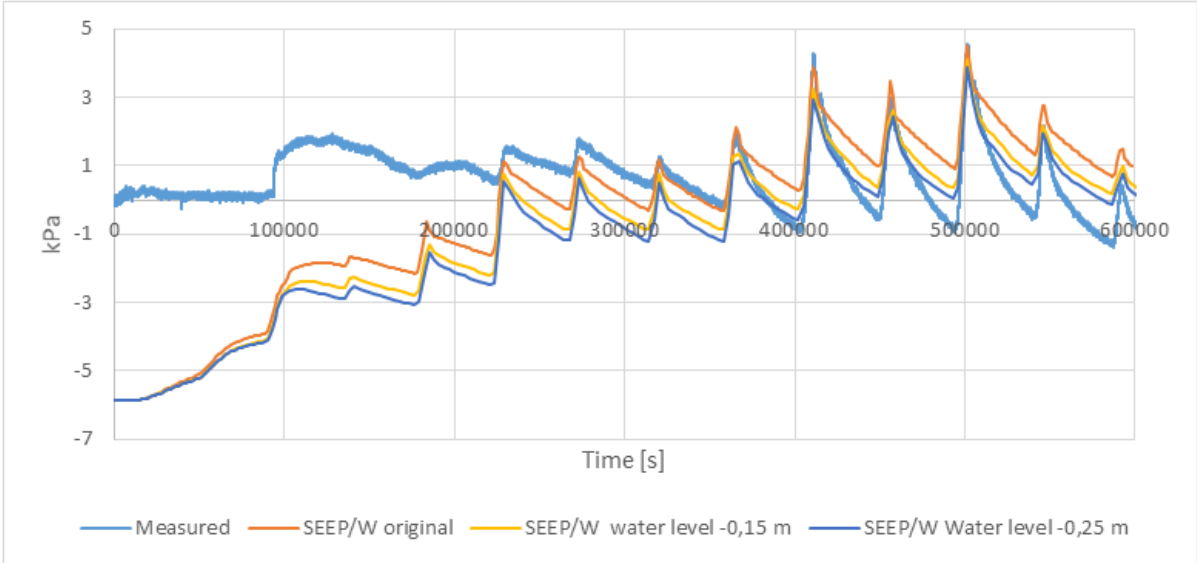


Figure 7-18 Influence of water level in breach

#### 7.4.5.5 Conclusion

From the assessed soil parameters it is found that the initial choices are good assumptions. It is found that when the water level during outflow is decreased, a better similarity is obtained. The differences can also be due to the changing geometry from the photos taken it can be noticed that a piece is eroded in the middle of the dike at 21/11/2015 this is approximately 350000 seconds into the simulation. From this moment on a different pore water pressure is observed. Due to this it is assumed that a change in geometry is also a reason of the too low outflow. When a piece of soil erodes the increase and decrease of pressure will be larger. It is suggested to use the SEEP/W calculation with a decreased water level during outflow of -0,15 m in subsequent calculations. The adjusted calculations are given in Annex D.

## 7.5 Conclusion

In (Bisshop, Visser, Van Rhee, & Verhagen, 2010) is stated that the influence of hindered erosion is noticed from 1 m/s. The flow velocities measured in the breach is around 0,75-4 m/s so this requirement is fulfilled but the expected negative pore water pressures related to hindered erosion weren't measured. This can be due to the packing of soil, the sand in the dike is loosely packed so dilatancy will be very small. The measurement of this phenomena is also very difficult, the sensor has to measure very sudden changes in pore water pressures. The sensor has to be placed at exactly the right position close to the flow in the soil. Further research is needed to really measure this effect.

When a similar experiment would be repeated, the possibility should be examined to place the sensor at the bottom of the landward inclined side of the dike. At this location the flow velocities are largest. Because the small height difference between the pilot channel and the polder, this wasn't possible in this experiment.

There is a good comparison between the measured values of the pore water pressure and the calculated values using SEEP/W. The only difficulties are the erosion in time of the dike and the water level in the breach during outflow. When this experiment is repeated a sensor should be placed in the breach to measure the water level. The results of the SEEP/W model are used in a SLOPE/W calculation.

# 8 Breach growth

Using photogrammetry, 3D models were made of the breach. Using these models the breach growth is discussed. The breach growth is calculated using the method of Van Rijn (Van Rijn, 1993) and using an excess shear strength equation. Finally the breach growth is simulated using limit state equilibrium software.

## 8.1 3D models

The breaching of the dike is split into two parts: the initial phase, during the first tide that went through the breach and the further breach growth afterwards. 3D models of the breach were made using photogrammetry. This was done by the general technical support division from the Flemish government (ATO). An accuracy of +/- 5cm in the models is pursued. From these models, sections of the breach can be drawn. A cut is made at 6,5 meter T.A.W, this is approximately half a meter under the crest, to obtain a top view. A section is made in the middle of the dike to examine the vertical breach growth. The initial phase is only discussed for the second breach test on 17/11/2015.

## 8.2 Initial phase

### 8.2.1 Breach growth in top view

In Figure 8-1 the different sections are shown. The grid has a spacing of one meter. It can be seen that the breach growth is more O-shaped. This is because at the polder side the grass cover and clay layer appeared to be very erosion resistant. In Figure 8-2 the breach width is put into a graph at three different places. There is nearly no erosion at the side of the Scheldt. This is due to the riprap revetment, reed and clay layer there. The erosion on the polder side is also small, due to the rooted clay layer surrounding the sand core. The majority of the erosion takes place in the middle of the dike due to the easily erodible sand core. The breach growth is more or less symmetrical. At the end of breach test II on 17/11/2015, the breach was widened at the top by approximately 3 to 4 meters.

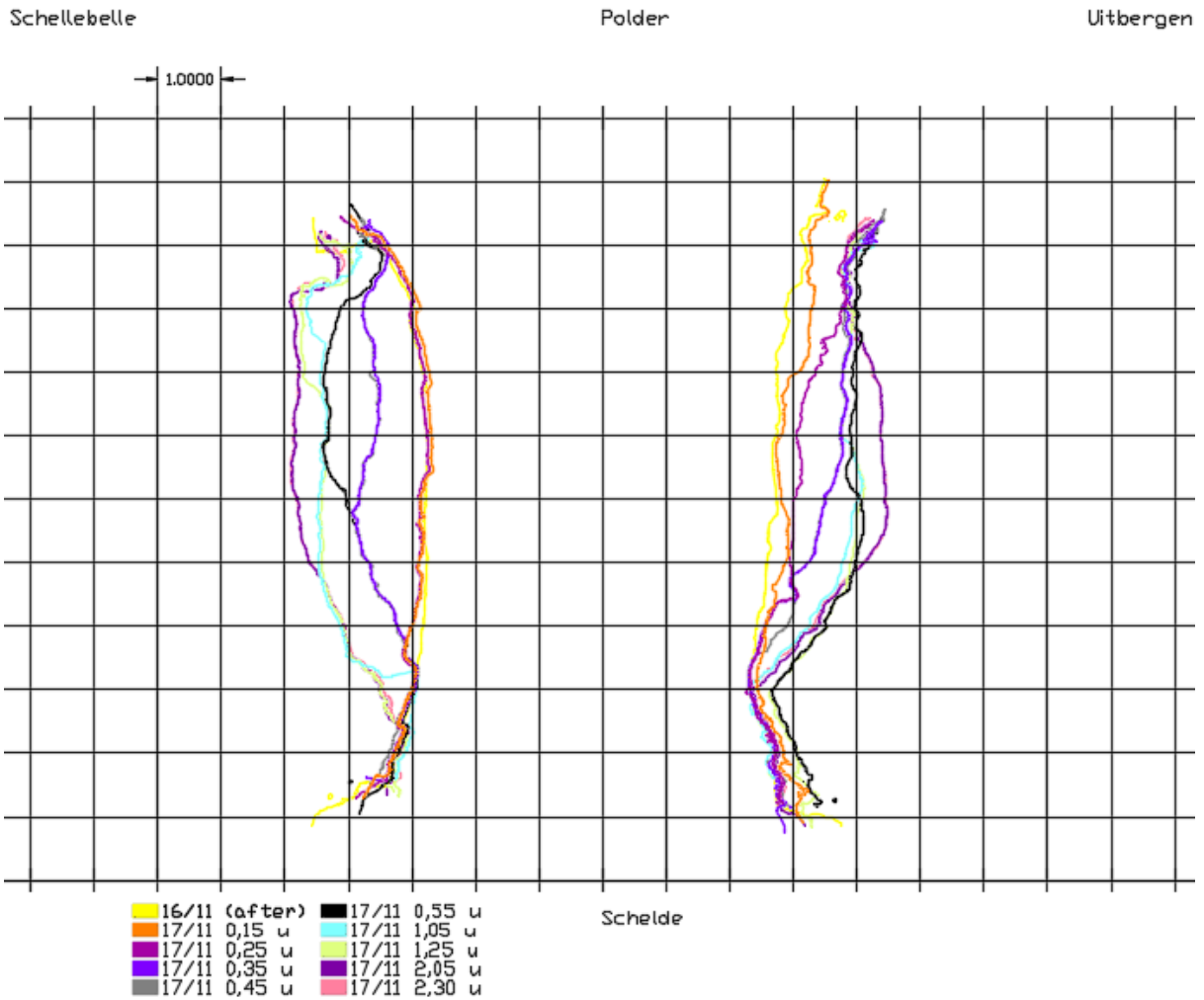


Figure 8-1 Plan view initial phase at 6,5 m T.A.W.

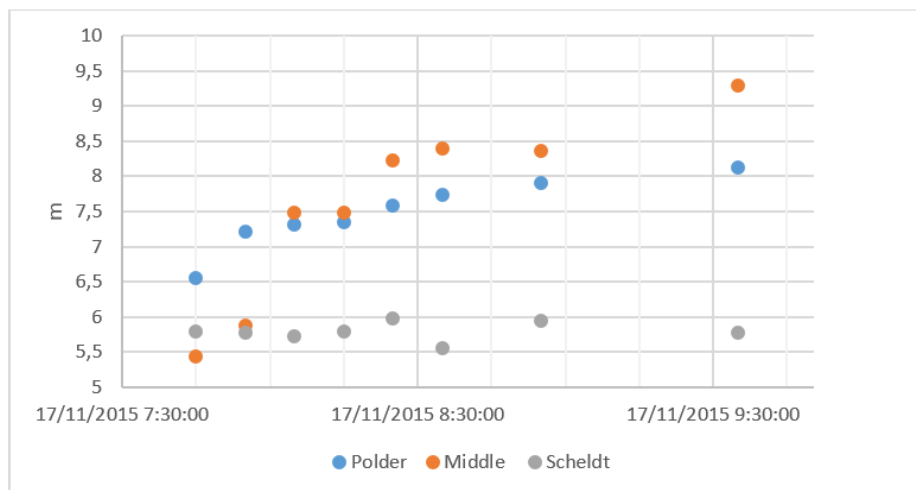


Figure 8-2 Breach growth in top view at 6,5 m T.A.W.

### 8.2.2 Vertical breach growth

The breach growth is also examined in a vertical plane, this is shown in Figure 8-3. The first model is made at the end of the first breach test on 16/11/2015, there was negligible erosion of the dike during this test. At the start of the test the pilot channel is clearly visible. The side

angle was approximately 45°. During the test there is some undermining of the dike. This causes a cavity at the bottom of the dike which decreases the stability until the overhanging sand falls into the breach. The slope angles become more steep at the top +- 90° and at the bottom the slope angle is close to the angle of internal friction +-34°.

A remark has to be made: the photogrammetry can only visualize points above water. At low tide, it could be seen that the bottom of the breach wasn't deepened because of the presence of a very stiff clay layer.

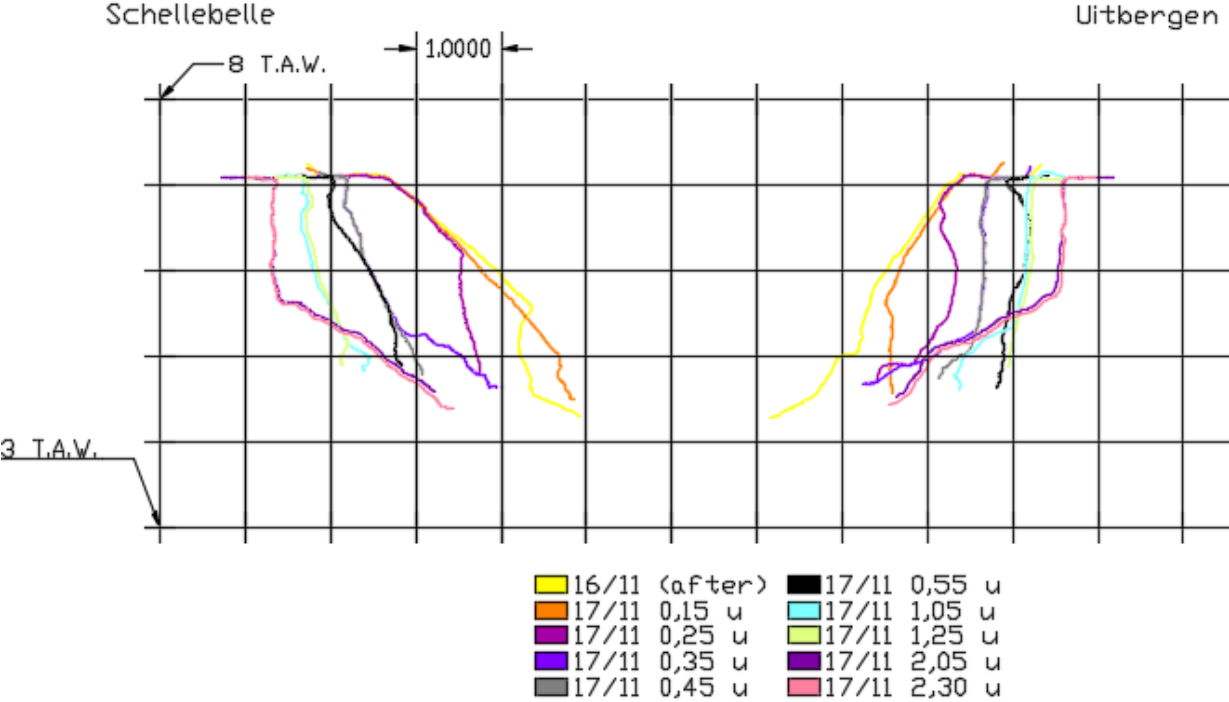


Figure 8-3 Initial phase vertical cross section

8.2.3 Calculation

The calculation will estimate the erosion in the middle of the dike where the sand core is present.

8.2.3.1 Empirical approach

The empirical shear stress approach is used. The formula given in (Van Rijn, 1993) is used.

$$\theta = \frac{\tau_b}{(\rho_s - \rho_w)gD_{50}}$$

- Where:  $\rho_s$  Density of sand 2720 kg/m<sup>3</sup>
- $\rho_w$  Density of water 1000 kg/m<sup>3</sup>
- $D_{50}$  Median particle diameter 1,5 10<sup>-4</sup> m
- $\tau_b$  Near bed shear stress

The mean near bed shear stress is approximated.

$$\tau_b = \frac{\rho_w g n^2}{R^{1/3}} U_b^2$$

- Where
- R Hydraulic radius estimated from the 3D models  $\frac{4A}{P} = \frac{4 \cdot 1,2}{6} = 0,8$
  - n Manning coefficient: 0,022 s/m<sup>1/3</sup> excavated earth (Whipple, 2002)
  - U<sub>b</sub> Water velocity at the bed: the water velocity used, is the estimation of the mean velocity calculated with the adjusted Cd-value with volume optimisation, the upper and lower estimation are examined
  - $\rho_w$  Density of water 1000 Kg/m<sup>3</sup>

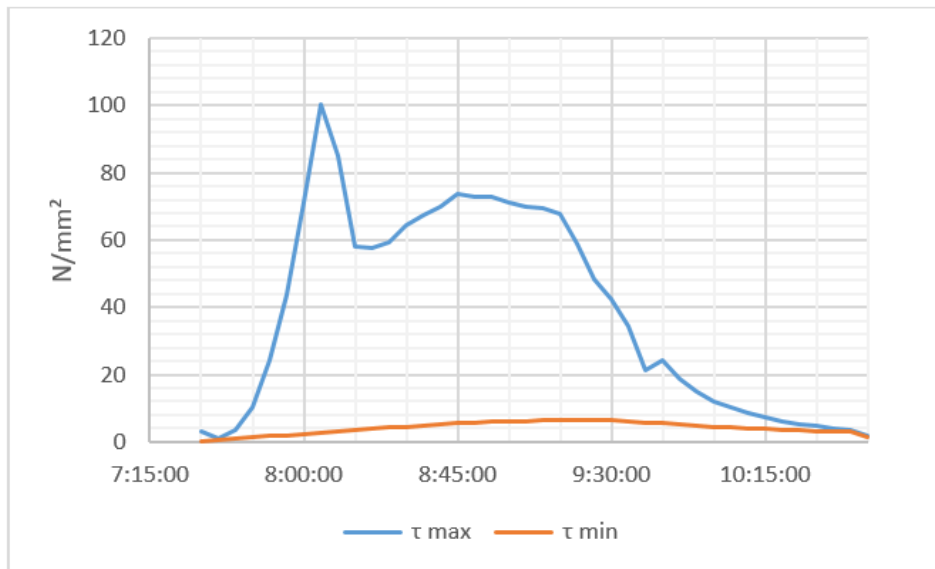


Figure 8-4 Variation of shear force in time for 17/11/2015

From Figure 8-4 it can be seen that the shear force obtained, when using the lower limit of the water velocity, is so small that no erosion will occur. This isn't realistic. Therefore only the upper limit will be taken into account in the following calculations.

For flow velocities in the range of 0,5 – 1 m/s (Van Rijn, 1993) has derived following pick up function:

$$E = 0,00033\rho_s[\Delta g D_{50}]^{0,5} D_*^{0,3} T^{1,5}$$

- Where:
- E Pick-up rate in kg/sm<sup>2</sup>
  - D<sub>\*</sub> Dimensionless particle diameter  $D_* = [\Delta g / v^2]^{1/3} D_{50} = 3,85$
  - $\Delta$  Relative density  $(\rho_s - \rho_w) / \rho_w = 1,72$
  - T  $(\tau_b - \tau_{b,cr}) / \tau_{b,cr}$
  - $\tau_{b,cr}$  Critical shear stress 8,2-14 N/m<sup>2</sup> (Irstea, 2015)
  - $\tau_b$  Acting shear stress: Figure 8-4

The erosion rate v<sub>e</sub> in m/s is given by:

$$v_e = \frac{E}{\rho_s(1 - n_o)}$$

Where:  $n_o$  In-situ porosity of sand 0,40

An upper and lower value are given using the two measured values for the critical shear strength. If the acting shear strength is lower than the critical one, it is assumed that no erosion occurs. The results are given in Figure 8-5 and the measured breach width at 6,5 m T.A.W. is given. The estimated erosion of the breach will be between 4 and 10 meters.

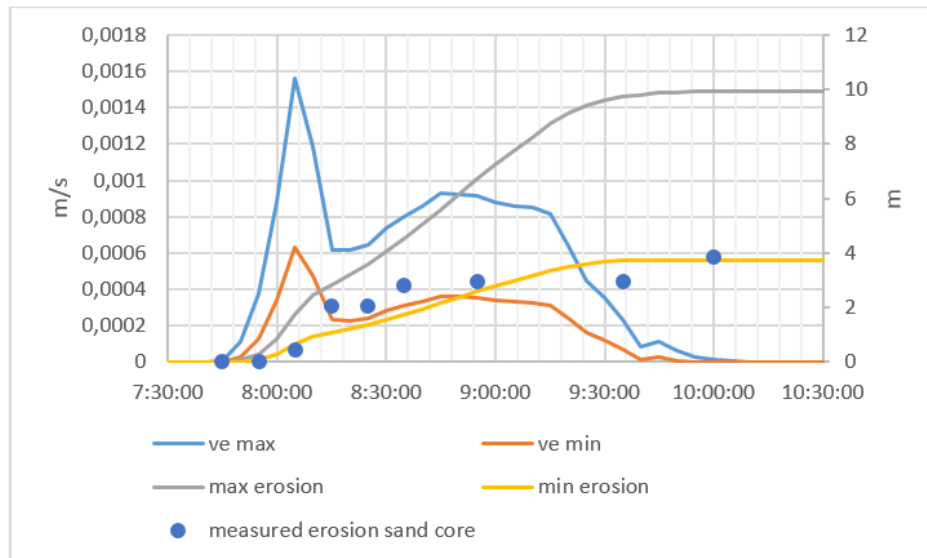


Figure 8-5 Erosion in time using formula of Van Rijn 17/11/2015

### 8.2.3.2 Excess shear stress

The excess shear stress equation used is the following formula: (Hanson & Simon, 2001)

$$v_e = k_d * (\tau_b - \tau_{b,cr}) = 0,0044 - 3,56 * 10^{-4} \text{ m/s}$$

Where:  $k_d$  coefficient of erosion  $55,1 * 10^{-6}$ - $356,8 * 10^{-6} \text{ m}^3/(\text{sN})$  JET-Test

$\tau_{b,cr}$  critical shear stress 8,2-14  $\text{N/m}^2$  (Irstea, 2015)

$\tau_b$  Acting shear stress: Figure 8-4

An upper and lower value are given using the two measured values for the critical shear strength and coefficients of erosion. If the acting shear strength is lower than the critical one, it is assumed that no erosion occurs. The results are given in Figure 8-6. The estimated erosion will be between 36 and 270 meters.

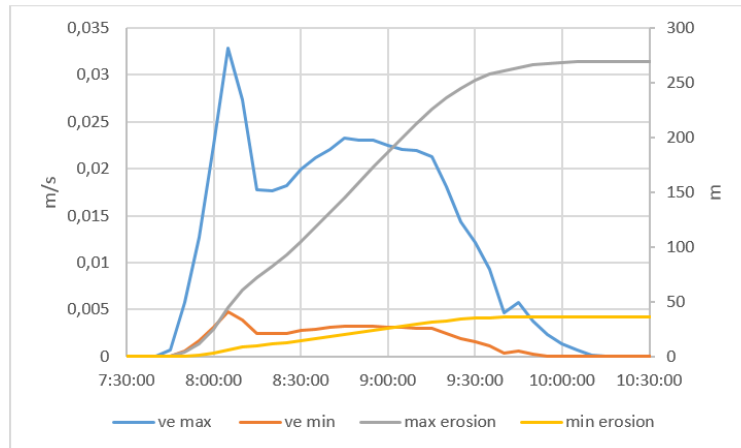


Figure 8-6 Erosion in time using the excess shear stress formula 17/11/2015

### 8.2.4 Conclusion

The initial phase of the breach is mainly laterally. It isn't possible to determine the first three breach phases as described by Visser (Visser P. , 1998). There was no noticeable deepening of the breach so the stages occurring where: stage IV and V. The difference between these phases is the water velocity in the breach: subcritical or critical. This velocity was mainly influenced by the tide in the river.

The outer clay lining had no influence on the breach growth in the middle of the dike but on the erosion close to the polder and river there was a large influence. This difference can be explained by the clay soil, roots, riprap revetment and the continuation of this layer. To erode the outer clay lining there were two erosion processes observed. Undermining of the sides causes rupture of chunks of the layer. This causes some tensile stresses in the roots. In Figure 8-7 this phenomenon can be seen. Another erosion mechanism is washing out of the soil in between the roots. This phenomenon is slower. In reality both phenomena occur at the same time



Figure 8-7 Roots in clay lining



The calculated erosion speed using the Van Rijn formula gives results comparable to the observations. The observed values are in the lower part of the estimated erosion range because the maximum calculated flow velocity is used. It is also possible that hindered erosion will occur in the sand core of the breach. (Bisshop, Visser, Van Rhee, & Verhagen, 2010) suggest that if the water velocity is larger than 1 m/s the model of Van Rhee (2007,2010) should be used however large differences between Van Rijn and Van Rhee are only noticed from 4 m/s. The water velocity in the breach is much smaller this explains the good similarity with Van Rijn.

The excess shear stress equation of Hanson and Simon presents too large values for the erosion and a large estimated range. The reason can be due to measuring errors of the JET-test. The scatter on these measurements is large. This results in a large uncertainty concerning the erosion speed values.

Both formulas used to calculate the erosion speed don't take into account slope failure of the sides of the breach. To have a better understanding of this process and to see if it is possible to predict the breach process better, a limit state equilibrium calculation was performed using the software SLOPE/W in 8.4.

## 8.3 Further breach growth

### 8.3.1 Breach growth in top view

For approximately one month, 3D models were made of the breach at regular time intervals. The top view is shown in Figure 8-8. After some time the O-shape of the breach becomes slightly more V-shaped with the widest part at the side of the polder. At the polder side still some influence of the clay layer surrounding the dike can be noticed. The most eroded point in the breach is always some meters towards the river.

The breach growth isn't symmetrical. At the side of Schellebelle more erosion occurs. During the last week end of the breach geometry measurements no significant changes were noticed in breach shape or size. A reason for this can be that the water levels weren't that high the last week of the measurements.

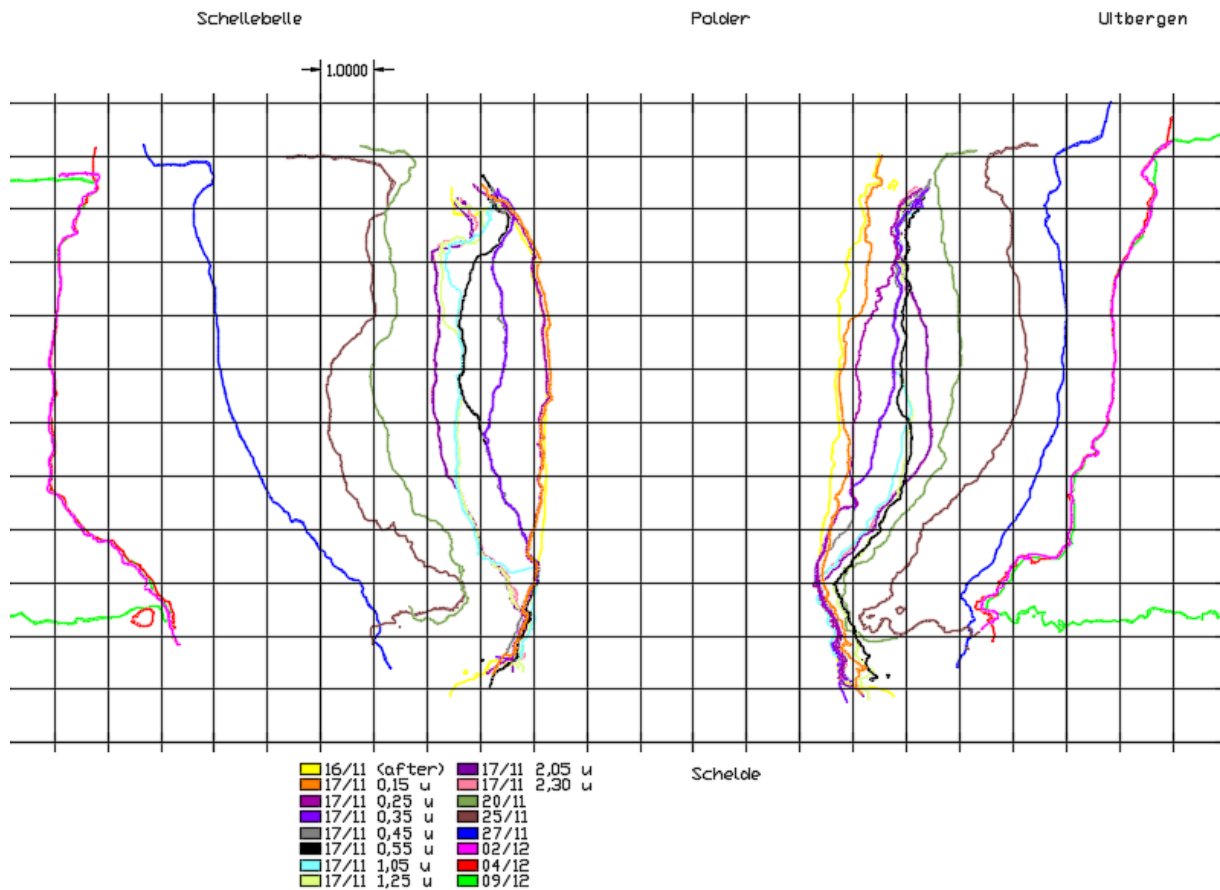


Figure 8-8 Stagnant growth in plan view at 6,5 m T.A.W.

The comparison between the breach growth and the water height at high tide is shown in Figure 8-9, a clear relation can be noticed. When the water height is larger than a previous occurred one, there is a large increase in growth. This can be explained by the fact that the bottom the sand core is protected by the eroded riprap that has flowed into the breach. If the water level is higher, new unprotected sand from the core is subjected to erosion. This combined with the fact that a higher water level increases the water table in the dike thus reducing the stabilizing matric suction pressures and causing a larger outflowing gradient, which in turn will cause a more critical situation. If the same water height is repeated, the influence on the breach growth is rather limited.

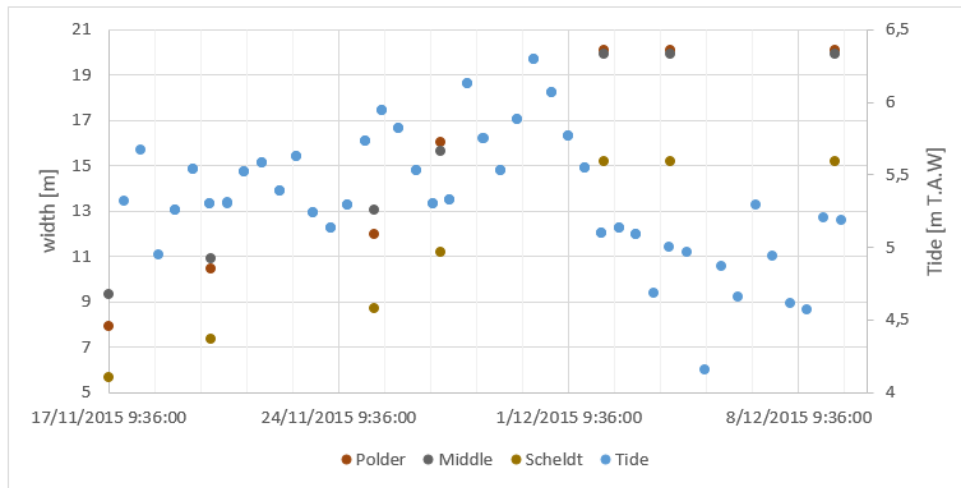


Figure 8-9 Stagnant breach growth

### 8.3.2 Vertical breach growth

The same progress as described in 8.2.2 is noticed. At the bottom of the breach there is a mild slope angle and the angle at the top part is approximately 90°. The sand is supported at the top by the old bicycle path on top of the dike. This path consisted out of asphalt. It is also very clear that the breach growth is asymmetrical: the side of Schellebelle where the riprap revetment was removed has eroded more. This shows the influence of the riprap on to the breach growth.

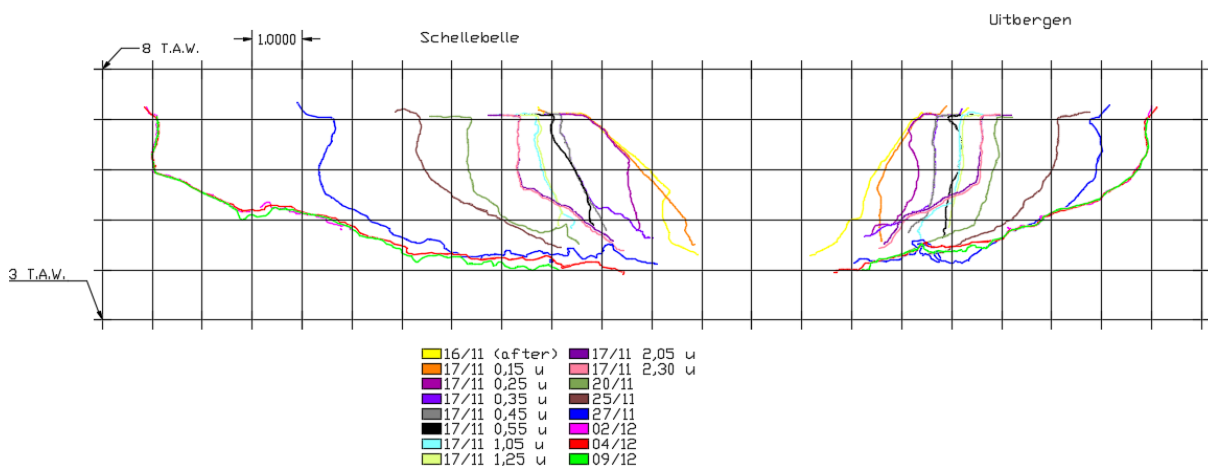


Figure 8-10 Vertical steady breach growth

### 8.3.3 Calculation

The same calculation is done as in 8.2.3. The erosion in time is calculated using the Van Rijn formula. The water velocity is still the maximum calculated using the suggested formula with optimisation of  $C_d$  according to the water volume. The calculation is done for a duration of one week. The results are displayed in Figure 8-11 and the measured breach width at 6,5 m T.A.W. is given.. The estimated erosion is in between 20 and 6 meters. The calculated breach width is too large in comparison to the observations. In the middle the breach growth is 3-5 meters, at the sides it's even less. The high estimation of the flow velocity can be a reason for this overestimation but the main expected cause is the outer clay layer. The breach will be O-

shaped causing a relatively calm zone in the water near the sand core. Also part of the riprap revetment has flowed in the breach causing an erosion protection of the sand. Therefore it is deemed that the solutions of the Van Rijn formula aren't valid. From the daily observations it is noticed that not every tide extra erosion occurs. Most erosion occurs due to slope failure, which appeared to be the main failure mechanism causing further breach growth.

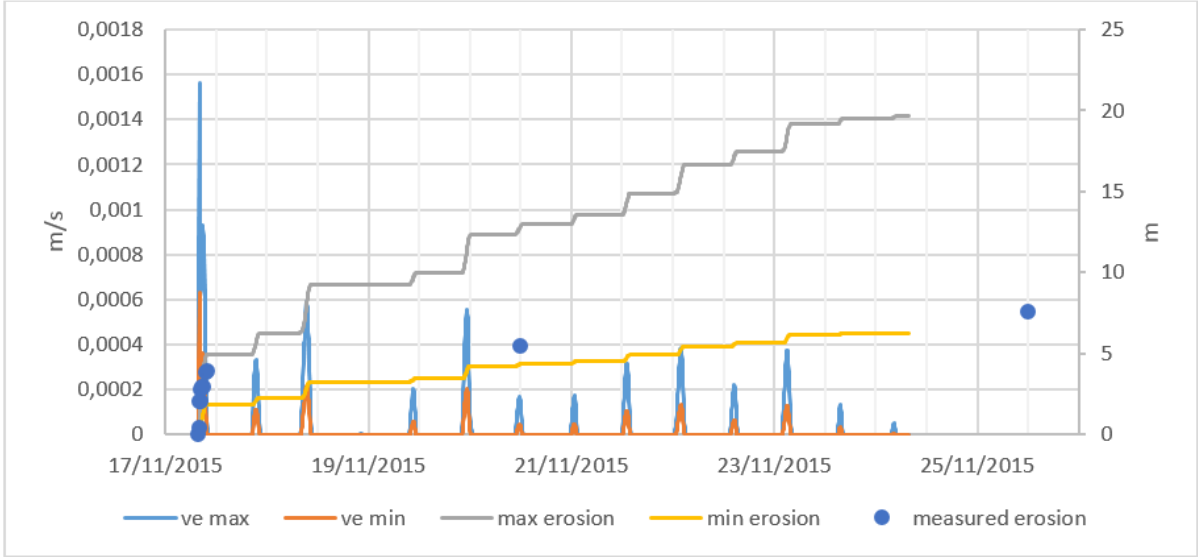


Figure 8-11 Erosion in time using the Van Rijn formula 17-24/11/2015

8.3.4 Conclusion

The calculation using the Van Rijn formula gave too large values for the breach width but it is assumed that this formula isn't valid because no real surface erosion can occur due to the riprap in the breach and the clay layer. These two elements will cause a more O-shaped breach growth causing a calm zone in the breach with lower water velocities. A new model is needed to calculate the further breach growth, this is done using the limit state equilibrium in the following section.

8.4 Calculation of breach growth in SLOPE/W

The slope failure erosion process is modelled using SLOPE/W.

8.4.1 Model

SEEP/W and SLOPE/W are software programs, both part of the same software suite: GEO studio. Hence the SEEP/W model can be imported in the SLOPE/W program. The SEEP/W model consists out of three different steps: 0-1200 sec, 1200-100380 sec and 100380-end sec. Because the geometry in SEEP/W is constant during each step, erosion was incorporated to have more accurate results. This is done by removing a piece of the lower part of the dike in the models. In the first model this is done at the end. An erosion speed of 5e-4 m/s is assumed. This is in accordance with the calculations in section 8.2.3.1. This corresponds to a piece of 0,6 meter that is removed. This can be seen in Figure 8-12.

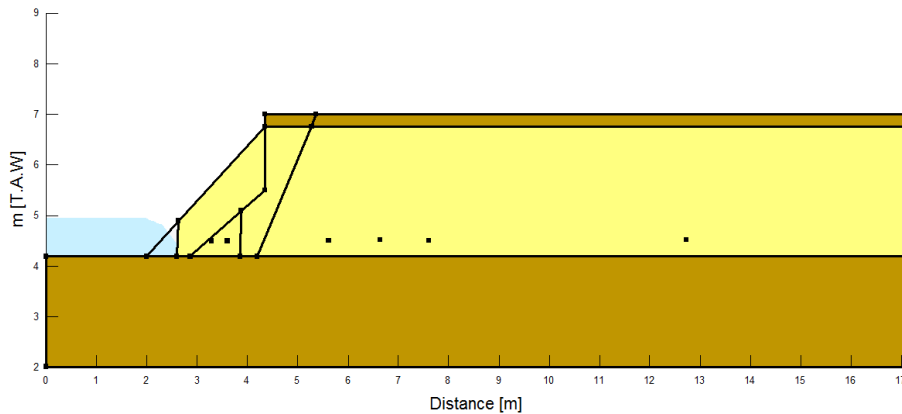


Figure 8-12 Model 0-1200 sec adjusted geometry

In the model from 1200-100380 sec, a piece of the toe is removed on the moment when the lowest safety factor occurs. This is done at the most critical moment in time for the model without erosion, this is calculated and at this time the bottom toe of the model is deleted. An erosion speed of  $2e-5$  m/s is assumed in accordance with the calculations in section 8.3.3. This corresponds to a part of 1 meter that is eroded. This erosion speed is less than in the beginning, because the breach will be more protected from erosion and the flow won't be constant during this period. One tidal cycle will pass, so there will be inflow and outflow. The erosion during the outflow is negligible due to the small flow velocities.

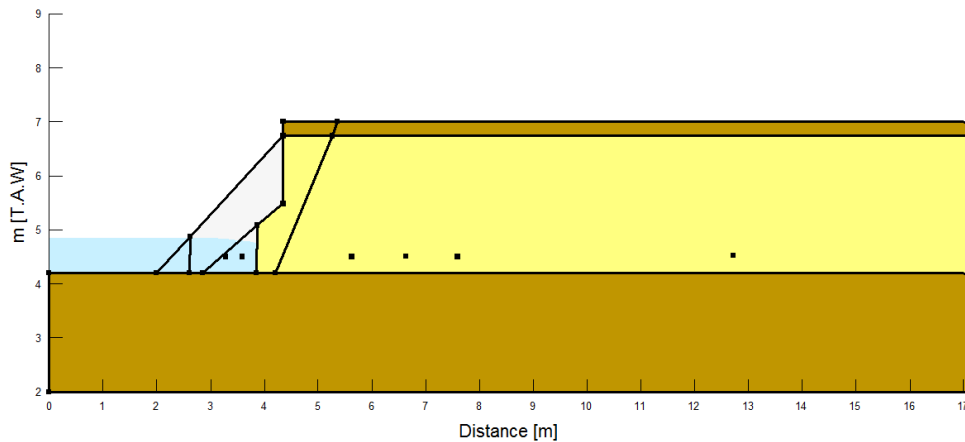


Figure 8-13 Model 1200-100380 min with adjusted geometry

A remark has to be made: overhanging pieces of soil where observed during the breach test. These overhanging pieces of soil can't be modelled in SLOPE/W. Also the roots in the dike aren't modelled.

#### 8.4.2 Soil properties

In the model there are two different types of soil: sand and clay. The different soil parameters are estimated using the soil investigation performed by GEO. Mohr-Coulomb is chosen as material model (Whitlow, 1983):

$$\tau = c' + (\sigma_n - u_w) \tan \varphi'$$

With:  $c'$  Effective cohesion

$\varphi'$	Effective angle of internal friction
$\sigma_n$	Normal stress in soil
$u_w$	Pore water pressure
$\tau$	Shear stress

Soil Parameter	Sand	Clay
Wet unit Weight [kN/m <sup>3</sup> ]	17	17
$\varphi'$ [°]	33,5	20*
Cohesion	0	4*

Table 8-1 Soil parameters

\*Estimated using the national annex of Eurocode 7, moderate stiff clay

The suction forces in the unsaturated zone are also incorporated in the model. These forces have the effect of increasing apparent cohesion of the soil. This is described by (Fredlund & Rahardjo, 1993).

$$\tau = c' + (\sigma_n - u_w)\tan\varphi' + (u_a - u_w)\tan\varphi^b$$

Where:  $u_a$  Soil-air pressure

$\varphi^b$  Angle indicating the rate of increase in shear strength relative to matric suction, this value is calculated in SLOPE/W from the Volumetric water content curve. This curve is already calculated in the SEEP/W model.

#### 8.4.3 Forces on the soil

The stabilizing forces on a slope consist out of three parts: Cohesion, Suction, Friction. The dike consists mostly out of sand so cohesion can be neglected. The suction forces in the dike depend on the water content. This effect can be noticed on the beach when building sand castles. There is an optimum water content where the suction forces are biggest. Too dry sand has no cohesion, neither has too wet sand. The friction will be the same for each equal slip surface in the dike because the materials don't change.

The destabilizing forces are the weight of the soil and an outward water flow.

#### 8.4.4 Calculation

Entry and exit points of possible slip surfaces have to be inserted manually. First they are estimated and a less detailed calculation is performed with a large entry and exit zone. The entry and exit zone is then narrowed to the zones where the entry and exit of the slip surfaces with lowest factor of safety are located to obtain a more detailed calculation.

The slip surfaces are divided into slices and a limit state equilibrium is used to calculate the stability of the slope. The methods of Bishop (Bishop, 1955), Spencer (Spencer, 1967) and Morgenstern Price (Morgenstern & Price, 1965) are compared. Spencer and Morgenstern - Price both satisfy all statically equilibrium conditions: vertical and horizontal force balance and moment balance. The method of Bishop doesn't fulfil the horizontal equilibrium but is more

easy to calculate. The calculation is done for the time step 1200-100380 sec. The results are shown in Figure 8-14. Bishop gives the lowest safety factor because the interslice shear forces are neglected. Spencer and Morgenstern-Price method gives approximately the same result. The irregularities can be explained by the calculation itself if for a slice no horizontal and moment equilibrium is found this slip surface is assumed to be non-critical because it can't exist. At some moments in time a solution is found for these slip surfaces which can give a jump in the results. In further calculations the method of Morgenstern-Price is used because this result is more regular and the values satisfy all statically equilibrium conditions.

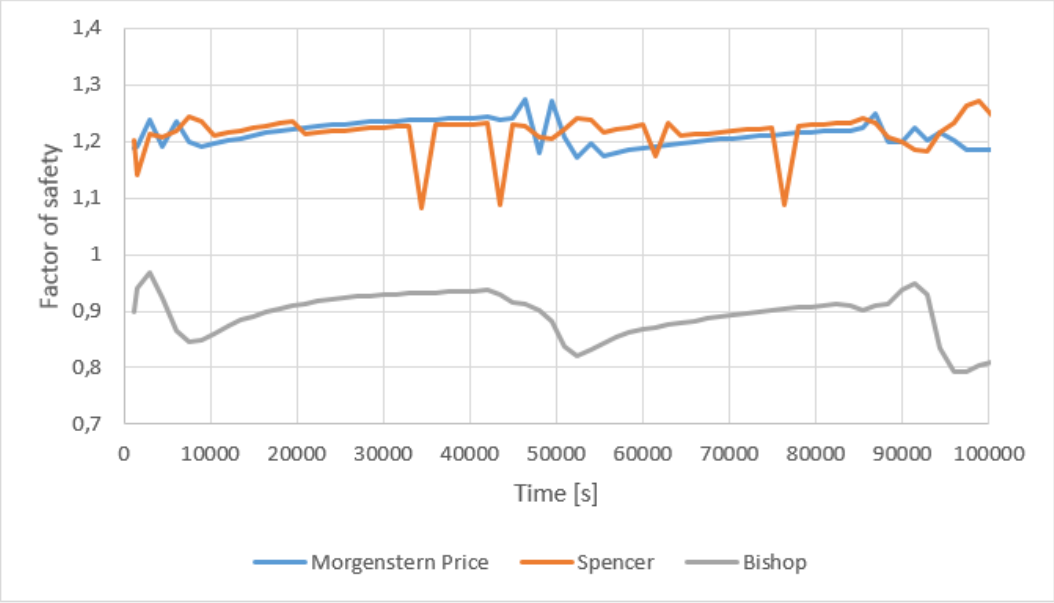


Figure 8-14 Comparison of different calculation methods

Some assumptions are made in the Morgenstern-Price method:

- Dividing planes between blocks are always vertical
- The line of action of the weight of the block passes through the centre of the slip surface of each block
- The normal force  $N$  acts in the centre of the segment
- The inclination of the interslice normal forces  $E$  is different for each block and is at the end points of the slip surface 0.

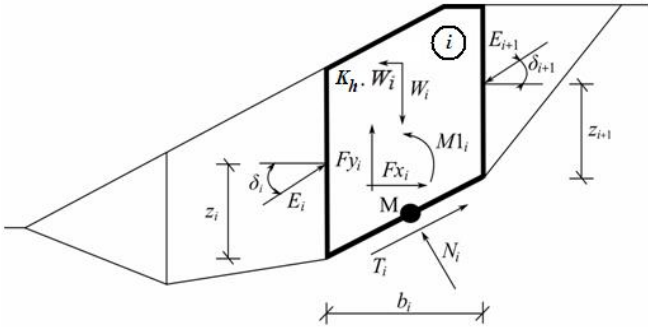


Figure 8-15 Static scheme of Morgenstern-Price method (finesoftware, 2016)

The limit state equilibrium uses following equations of statics to calculate for  $F_s$ :

$X_R$  and  $X_L$  are the interslice shear forces on the right and left side of a slice.

$$X = N_i \lambda f(x)$$

Where:  $\lambda f(x)$  Inclination  $\delta$  of the interslice normal forces,  $\lambda$  is the percentage of a half-sine function

$N_i$  The interslice normal force

$N$  is the normal force at the base of the slice:

$$N = \frac{W + (X_R - X_L) - \frac{c' \beta \sin \alpha' + u_w \beta \sin \alpha' \tan \varphi'}{F}}{\cos \alpha' + \frac{\sin \alpha' \tan \varphi'}{F}}$$

Where:  $W$  Weight of the slice

$\beta$  Geometrical parameter

$c'$  Cohesion

$\alpha'$  Inclination at the base

$\varphi'$  Effective angle of internal friction

$F$  Factor of safety

$u_w$  Pore-water pressure

$F$  can be the moment ( $F_m$ ) or force equilibrium factor of safety ( $F_s$ ). The moment equilibrium around a point in each slice can be rearranged to:

$$F_m = \frac{\sum (c' \beta R + (N - u_w \beta) R \tan \varphi')}{\sum W x - \sum N f}$$

The summation of forces in a horizontal direction for all slices gives rise to a force equilibrium of factor safety:

$$F_s = \frac{\sum (c' \beta \cos \alpha' + (N - u_w \beta) \tan \varphi' \cos \alpha')}{\sum N \sin \alpha'}$$

Where:  $R, \beta, f, d$  Geometrical parameters

$u_w$  Pore-water pressure

$c'$  Cohesion

$\alpha'$  Inclination at the base

$\varphi'$  Effective angle of internal friction

$W$  Weight of the slice

Using previous formulas, the moment and force equilibrium factor of safety can be calculated. By changing the value of lambda it should be possible to obtain a safety factor that is equal



for the moment and force equilibrium. This safety factor is the solution of the stability of the slip surface.

### 8.4.5 Results

The results are given and discussed for each model. The entry and exit zones are shown in the results by the red lines.

#### 8.4.5.1 Model 0-1200 sec

The safety factor is calculated every 300 seconds and is given in Figure 8-16. It can be seen that the factor of safety rises and the height of the critical slip surface becomes higher. This can be explained due to the entry of water in the dike.

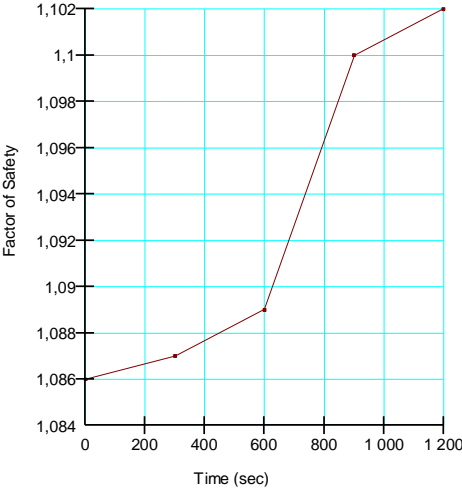


Figure 8-16 Minimum factor off safety 0-20 min

In Figure 8-17 the different forces: friction, suction and cohesion, are given acting on two identical slip surfaces each slice, 300 and 900 seconds into the breach test. The slip surface is shown in .

The friction force is the same, this is logical because the slip surface is the same and the materials don't change. There is no cohesion because the slip surfaces are in the sand core. The suction force increases because the soil in the dike is too dry to have significant stabilizing suction forces. Therefore when the water content increases, the suction forces increase. The water table in the dike increases causing an inward flow. This flow stabilizes even more. In Figure 8-19 this flow is displayed.

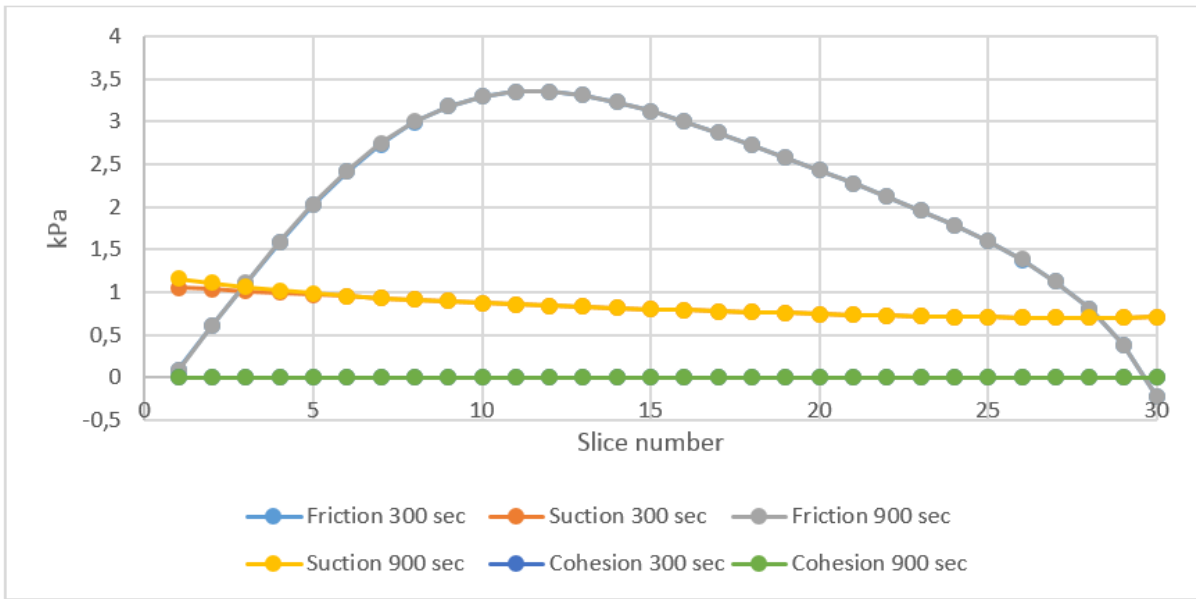


Figure 8-17 Forces 300 and 900 sec

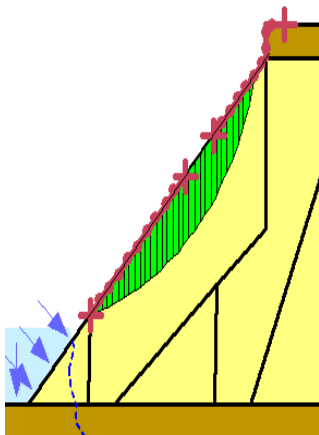


Figure 8-18 Critical slip surface

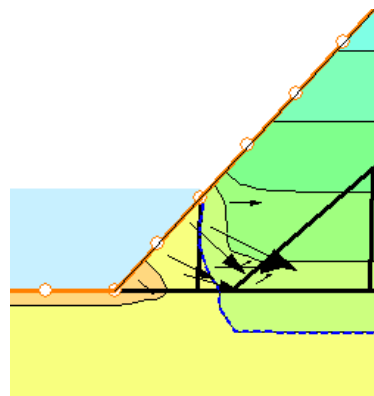


Figure 8-19 Stabilizing flow

At second 1200 of the model, a piece of the toe is removed following breach widening by erosion. This results in the slip surface displayed in Figure 8-20. The slip surface entry and exit zones are the red lines at the bottom and top. The factor of safety is reduced to 0,995 so failure of the dike is most likely. The shape of the slip surface is similar to the observed failure. Only a piece in the sand core fails.

The displaced slip surface is the most critical one but it is possible due to irregularities in the dike that another slip surface occurs. Also the slip surface is generated in a 2D model in reality 3D slip surfaces will occur. The safety factor when performing a 3D calculation will be higher. (Albatineh, 2006)

0.995

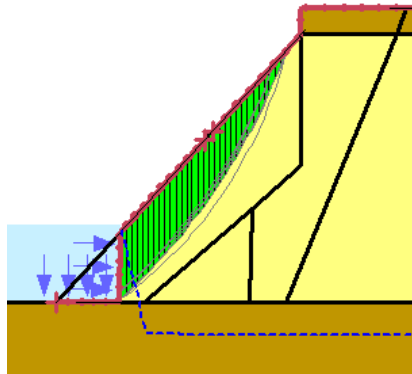


Figure 8-20 slip surface with toe erosion 1200 sec

#### 8.4.5.2 Model 1200-100380 sec

In Figure 8-21 the factor of safety and tide are given. At high tide the factor of safety is maximal. This is because the stabilizing inflow is largest. Hereafter the minimal factor of safety occurs because the outflowing gradient is then largest and a large part of the dike is saturated so no suction forces will occur. Afterwards, the destabilizing outflowing gradient decreases causing an increase in factor of safety.

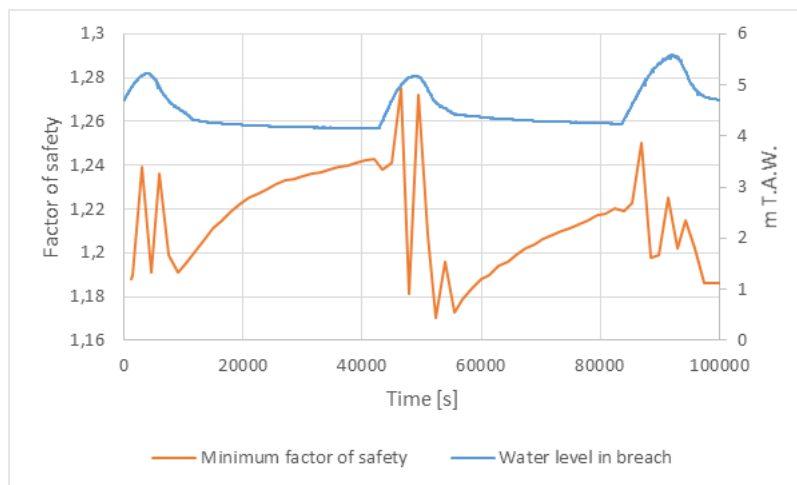


Figure 8-21 Factor of safety 20-1673 min

At 52440 seconds into the test the lowest safety factor occurs. At this moment in time the eroded toe piece is modelled. The result is displayed in Figure 8-22. The safety factor is larger in this model (1,186<->1,170). This is only possible when the stabilizing forces compared to the destabilizing forces on the toe are smaller. The explanation of this result is due to model errors: the flow is modelled for the whole non-eroded dike part. In the eroded SLOPE/W model a part of the toe is deleted but the same flow pattern is used as in the non-eroded model. In reality the flow will penetrate much deeper in the dike causing a larger destabilizing gradient and a lower safety factor. Modelling geometrical changes in time isn't possible in the SLOPE/W and SEEP/W software, they have to be inserted manually.

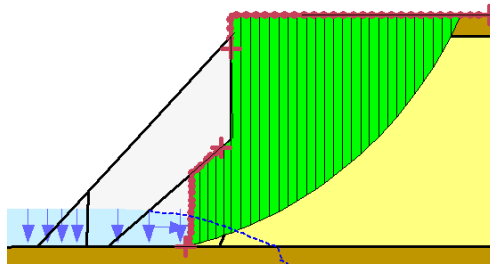


Figure 8-22 Slip surface with toe erosion 52440 sec

#### 8.4.5.3 Model 1673-10071 min

The safety factor and tide are given in Figure 8-23. The stability of the dike is calculated with intervals of 3000 sec. It can be noticed that during the outflow the safety factor increases. After the high tide there is a drop in the safety factor. At this moment, there is a destabilizing outflow in the dike. It can be seen that the safety factor becomes smaller than 1 sometimes so failure will occur. A possible failure slip surface is displayed in Figure 8-24. The occurrence of a shallow slip surface is the same as what is observed.

The further breach growth can be explained using this mechanism. A shallow slip surface occurs and the soil falls into the breach. This soil erodes due to the flow in the breach, under an angle close to the angle of internal friction. When at the toe of the breach enough soil is eroded, a new shallow slip surface will occur. This mechanism will be repeated.

Five times the safety factor is below 1. The slip surfaces that occur have a depth of 0,3 meter so the breach will grow approximately 1-2 meter. In the observations, as can be seen in Figure 8-10, the breach growth during this period is approximately 1-2 meter.

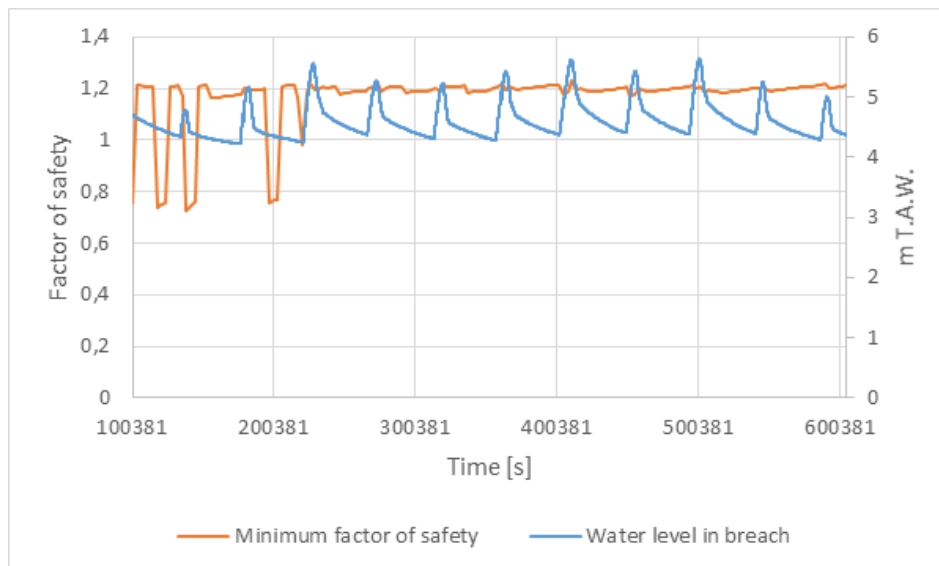


Figure 8-23 Factor of safety with shallow slip surfaces 100380-end sec

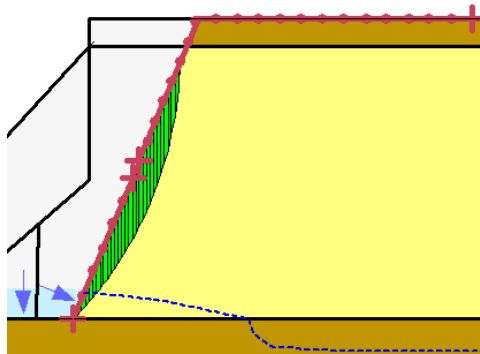


Figure 8-24 Shallow slip surface

#### 8.4.6 Sensitivity analysis

A sensitivity analysis is performed on different parameters. The parameters that are changed are: the suction range, hydraulic conductivity, compression modulus and a calculation is performed without suction forces. The comparison is done for the second model 1200-100380 sec into the simulation.

##### 8.4.6.1 Suction range

In Figure 8-25 the results are shown. The default suction range in SEEP/W is used in the original calculation 0,01-1000 kPa. The maximum is decreased to 100 and 10 kPa. No noticeable influence is seen.

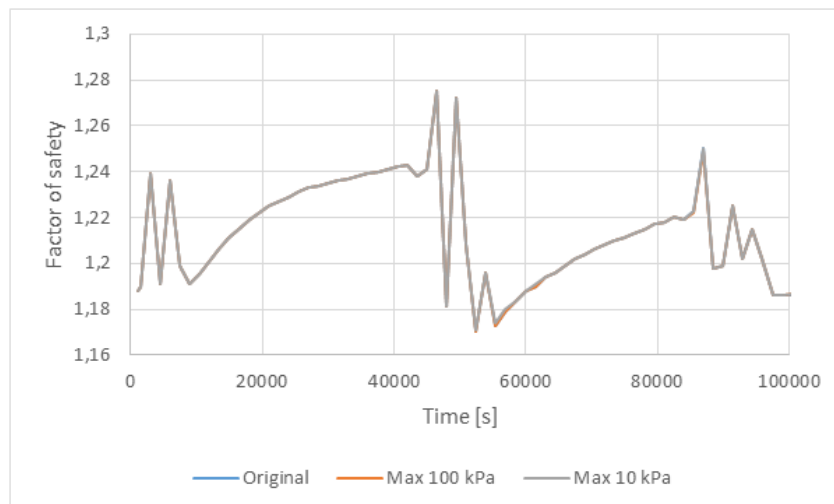


Figure 8-25 Influence of suction range

##### 8.4.6.2 Hydraulic conductivity

In the original model the hydraulic conductivity is  $1,4 \cdot 10^{-5}$  m/s. There was a noticeable influence on the SEEP/W model so an influence on the slope model is expected too. In Figure 8-26 the comparison is made. It can be seen that, as the conductivity raises the reactions are faster. The lowest hydraulic conductivity gives the highest values of the safety factor. It is expected that there is less water penetration in the dike if the conductivity is smaller so a smaller destabilizing gradient will occur. The opposite will occur when the hydraulic

conductivity is increased. In general it can be noticed that the differences in factor of safety between the different values are rather small: 0,02.

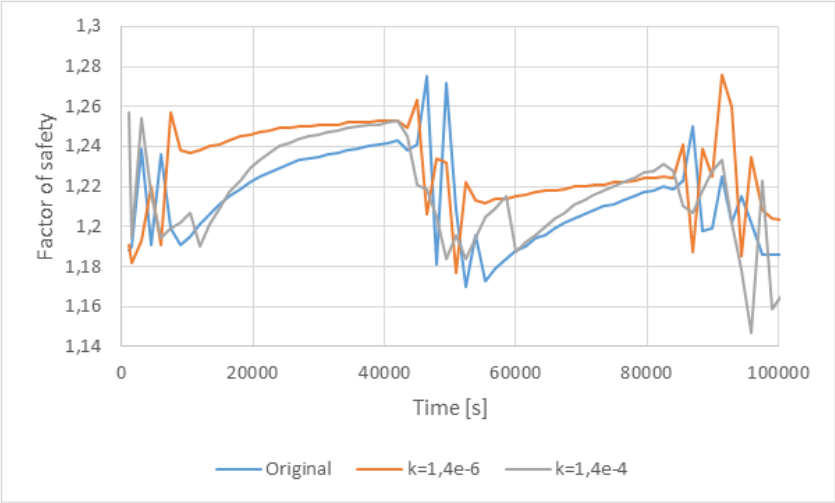


Figure 8-26 Influence of hydraulic conductivity

8.4.6.3 Calculation without suction forces

A calculation is performed without taking into account the suction forces, this is shown in Figure 8-27. When there is no suction taken into account, the slope isn't stable and the factor of safety is always below 1. The function is also more constant so it is assumed that the influence of the water gradient in the breach sides is small. The difference in suction has a large effect.

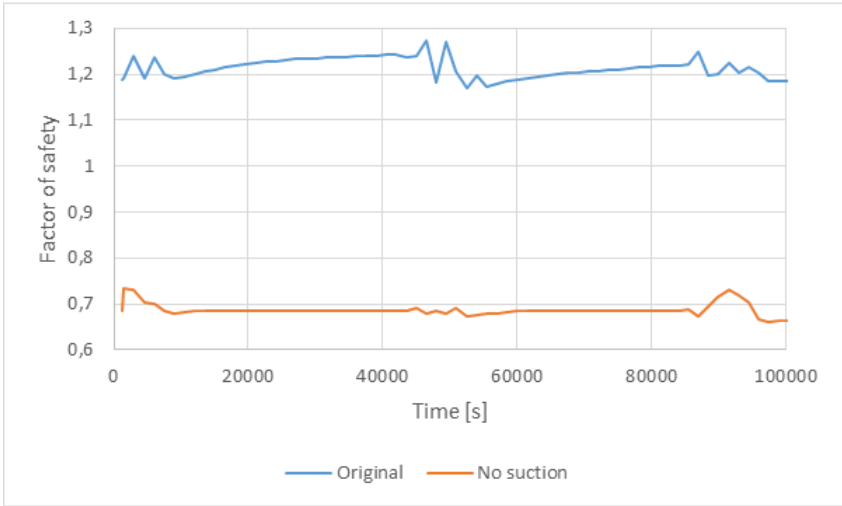


Figure 8-27 Influence of suction

8.4.6.4 Coefficient of volume change

From Figure 8-28 it can be noticed that the influence of this parameter on the breach stability is negligible.

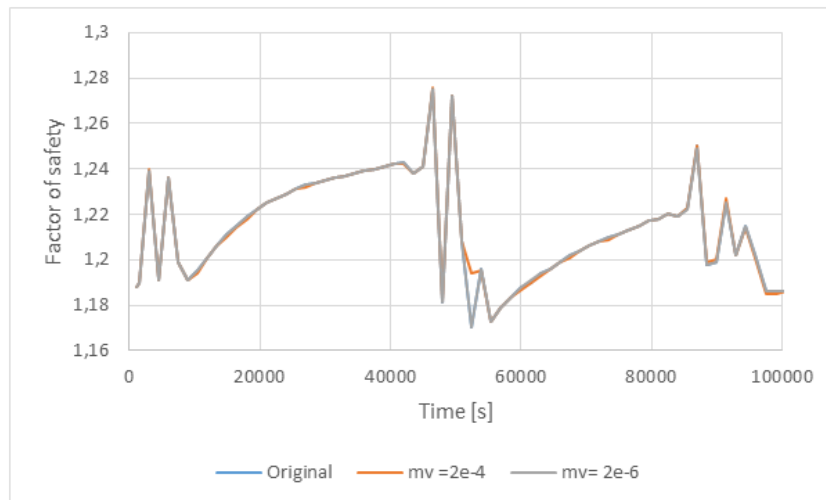


Figure 8-28 Influence of coefficient of volume change

## 8.5 Conclusion

The breach process in the dike is in accordance to other breach experiments that were done on specially made dikes. From the 3D models that were made, it was noticed that the influence of the clay layer on the breach growth in the middle is negligible in the initial phase. In the further breach growth it is noticed that the growth was asymmetric, a reason for this is the removal of part of the riprap revetment at this side. Hence it is assumed that at this side there were less rocks in the breach causing a larger flow causing more erosion. It is clear that the riprap at the river side has an influence on the breach growth. Further research should be done on this subject.

When the breach growth is split-up into two different phases, it is possible to make a prediction of the breach growth in each model. The breach growth during the first hours is best modelled using the formula of Van Rijn (Van Rijn, 1993). The subsequent breach growth is best modelled using a limit state equilibrium. This gave, in comparison to the breach experiment, the best results. In the initial phase actual erosion takes place in the breach and after some time this erosion is reduced due to the occurrence of rocks in the breach and the outer clay layer protecting the weaker inside of the dike. Then the breach growth is more prone to slope instability caused by the outflowing gradient just after high tide.

Further research and evaluation of this concept is needed on other in situ dike breaching experiments.

# 9 Conclusion and recommendations

In this master thesis the flow, pore water pressure and breach growth pertaining to an in situ breach test are investigated.

First other breach tests are discussed and compared to the executed test. This to gain insight into the breaching process. It is expected that the breaching would occur according to the different breach phases as described by Visser (Visser P. , 1998). The pilot channel used to initiate the breach test is designed. The optimal dimensions were: 1 m bottom width with sides of 45° and a depth of 4,5 m T.A.W.

During the first breach test on 16/11/2015 the water level was much lower than expected therefore the breach growth was very limited. The bottom of the pilot channel was deepened to 4 m T.A.W. and a new test was performed the next day. This test was more successful and the breach was left open for a couple of months to perform further measurements and to examine further breach growth.

The discharge through the breach was much smaller than predicted by discharge formulas found in literature. Friction in the breach is assumed to be the main reason for this difference. The bottom of the breach was very rough because of the presence of riprap that came from the river side of the dike. Further research is needed to examine the influence of bank protection on the breach discharge. A smaller discharge means more time for evacuation of the area around the breach.

A new coefficient of discharge is suggested for the inflow and outflow. A constant coefficient optimized using the indirectly measured discharge is found to be the best. The new inflow coefficient of discharge is evaluated using an ADCP measurement and a good agreement was obtained. A more general formula of the coefficient of discharge can be obtained by performing model tests with different geometries simulating a breach and with a very rough surface simulating the riprap protection.

The pore water pressures in the dike were measured. During the breach test no suction pressures related to hindered erosion were measured. Two main reasons can be mentioned why this wasn't measured: the flow velocities were too small and the packing of the sand was too loose. It is very difficult to measure this effect in situ because a sensor has to be placed close to the eroding layer, only there the effects will be measurable, and has to measure very sudden changes in pore water pressure. Further research is needed to measure the effects of hindered erosion.

The pore water pressures were simulated using finite element software (SEEP/W). A good similarity between the measurements and the simulated values was obtained. The only difficulty is the calculation when there is a lot of erosion. It isn't possible to calculate an in time changing model, only piecewise changes can be made. If this was possible a better approximation of the breach growth could be made.



The breach growth is split up into two different phases: the initial phase during the first tide flowing through the breach and the further breach growth. During the initial phase, the breach is more O-shaped, due to the influence of the clay layer surrounding the sand core. The different breach phases as described by Visser weren't noticed because only lateral breach growth occurred. The erosion of the sand core is in good agreement with the erosion calculated using the formula of Van Rijn (Van Rijn, 1993).

During the further breach growth, the outer clay layer and the riprap in the breach will obstruct further erosion due to water flow. Therefore it is assumed that the further breach growth occurs more due to slope instabilities. The slope stability is calculated in time using software calculating a limit state equilibrium in time (SLOPE/W). A good similarity was obtained between this model and the observations. The same shape and size of failure is observed. The most critical moment in time is just after high tide when there is an outflowing destabilizing gradient in the dike.

At the end of the test it is noticed that the breach is asymmetric. More erosion occurred at the side where the riprap revetment was removed. It seemed that the revetment not only decreased the flow but also the breach growth. This mechanism can increase the safety of the dikes considerably. Further research is needed to study the influence of bank protection onto the breach growth.

To calculate breach growth in in situ dikes it is suggested to use the Van Rijn formula to estimate the initial phase and to use the limit state equilibrium to calculate the further breach growth. This method has to be confirmed with other in situ breach tests.

# 10 References

- Albataineh, N. (2006). *Slope stability analysis using 2D and 3D methods*. Master thesis, University of Akron.
- Alert Solutions. (2011, april). *ACE-250 Analoge Waterspanningsmeter, Product specification sheet*.
- Azimi, A. H., & Rajaratnam, N. (2009). Discharge Characteristics of Weirs of Finite Crest. *Journal of hydraulic Engineering, Vol. 135, No 12*, 1081-1085.
- BAT. (2015, 11 23). *BAT Piezometer*. Retrieved from BAT ground water monitoring: <http://www.bat-gms.com/bat-piezometer.asp>
- Bishop, A. W. (1955, march). The use of the slip circle in the stability analysis of slopes, Volume 5 issue 1. *Géotechnique*, 7-17.
- Bisshop, F., Visser, P., Van Rhee, C., & Verhagen, H. (2010). Erosion due to high flow velocities: a description of the relevant processes. *Proceedings of 32nd Conference on Coastal Engineering 2010*. Shanghai, China: ASCE.
- Bos, M. G. (1985). The head discharge relationship. In Bos, M G, *Long-throated flumes and Broad-crested weirs* (pp. 18-63). Dordrecht: Martinus Nijhoff/Dr W. Junk Publishers.
- Bureau voor normalisatie. (2005). *Eurocode 7*.
- Chang, D., & Zang, L. (2010). Simulation of the erosion process of landslide dams due to overtopping considering variations in soil erodibility along depth. *Natural Hazards and earth system sciences 10*, 933-946.
- Claeys, s., Michelsen, S., De Sutter , J., Peeters, p., & Mostaert, F. (2009). *Water- en sedimentbalans voor lippenbroek - periode 2006-2008*. Antwerpen België: Waterbouwkundig Laboratorium.
- Claydon , J. F. (2016, 05 30). *jfccivilengineer*. Retrieved from Broad crested weir: [http://www.jfccivilengineer.com/broad\\_crested\\_weir.htm](http://www.jfccivilengineer.com/broad_crested_weir.htm)
- Coleman, S. E., Jack, R. C., & Melville, B. C. (1997). Overtopping breaching of noncohesive embankment dams. *Proc., 27th Congress of the Int. Association for Hydraulic Research*, (pp. 42-47). San Francisco.
- CROW. (2004). *Handboek zandboek (in Dutch)*. Ede, the Netherlands.
- Daniel, M. (1995). Permeability, porosity , and grain-size distribution of selected pliocene and quaternary sediments in the albuquerque basin. *New Mexico Geology 14(4)*, 79-87.
- Das, B. (2008). *Advanced Soil Mechanics*. London & New York: Taylor & Francis.

- De Baets, S., Poesen, J., Reubens, B., Wemans K, De Baerdemaeker, J., & Muys, B. (2007). Root tensile strength and root distribution of typical mediterranean plant species and their contribution to soil shear strength. *Plant and soil volume 305 issue 1*, 207-226.
- De Mulder, T. (2015). *Hydraulica I*. Course notes, Ghent University, Gent.
- DOV. (2016, februari 15). Retrieved from Databank ondergrond vlaanderen: <https://dov.vlaanderen.be/dov/DOVInternet/startup.jsp>
- Du Boys, D. (1879). Le Rhône et les rivières à lit affouillable annales des ponts et chaussées. *Annales des ponts et chaussées, Série 5,18*, 141-195.
- Elskens, F. (1995). Protecting overflow dikes for controlled flood areas in Belgium. *PIANC, Inland waterways and flood control*, (p. 13). Brussels.
- finesoftware. (2016, 04 30). *Morgenstern price*. Opgehaald van finesoftware: <http://www.finesoftware.eu/help/geo5/en/morgenstern-price-01/>
- Flanders Hydraulics Research; Universiteit Antwerpen; Vrije Universiteit Brussel. (2009). 31<sup>èmes</sup> Journées de l'hydraulique de la SHF: Morphodynamique et gestion des sédiments dans les estuaires, les baies et les deltas. *SEDIMENT BEHAVIOUR WITHIN A FLOOD CONTROL AREA WITH A CONTROLLED REDUCED TIDE – PILOT PROJECT LIPPENBROEK*, (p. 15). Paris.
- Flemish government. (2016, 5 2). *Tides*. Opgehaald van Waterinfo: <https://www.waterinfo.be/>
- Flinn, A. D., & Dyer, C. W. (1894). The cippoletti trapezoidal weir. *Trans. ASCE 32*, 9-32.
- Fox, G. A., & Wilson, G. V. (2007). Erosion of noncohesive sediment by ground water seepage: lysimeter experiments and stability modeling. *Soil Science Society of America J. Volume 71 Issue 6*, 1822-1830.
- Fredlund, D. C., & Rahardjo, H. (1993). *Soil mechanics for unsaturated soils*. New York: John Wiley & sons.
- Fritz, H., & Hager, W. (1998). *Hydraulics of embankment weir*. Georgia.
- Geisenhainer, P., & Kortenhaus, A. (2006). *Hydraulic model tests on breaching with and without waves*.
- Govinda Rao, N. S., & Muralidhar, D. (1963, Aug/Sept). Discharge characteristics of weirs of finite crest width. *La Houille blanche No. 5*, 213-232.
- Hahn, W., Hanson, G. J., & Cook, K. R. (2000). Breach morphology observations of embankment overtopping tests. *Proc. 2000 Joint Conference of Water Resources Eng. Planning and Management*.
- Hanson, G. J., & Simon, A. (2001). *Erodibility of streambeds in the loess area of the midwestern USA*.

- Hanson, G., Cook, K., & Hunt, S. (2005). *Physical modelling of overtopping erosion and breach formation of cohesive embankments*.
- Horton, R. E. (1907). *Weir experiments, coefficients and formulas*. Washington: U.S. Government Printing office.
- Hunt, S. L., Hanson, G. J., Crook, K. R., & Kadavy, K. C. (2005). Breach widening observations from earthen embankment tests. *Transactions of the ASAE Vol 48(3)*, 1115-1120.
- Hunt, S., Hanson, G., & Temple, D. (2005). Breach widening observations related to clay core earthen embankment tests. *Annual conference proceedings-association of state dam safety officials incorporated*; 2 (pp. 810-819). New York: ASDSO.
- Irstea. (2015). *Digues de l'escaut- Belgique Etude des propriétés des sols constitutifs des digues, Rapport d'etape n°3 in commision of FHR*.
- Jalil, S. A., Ibrahim, S. S., & Jafer, R. A. (2014). Surface roughness effects on discharge coefficient of broad crested weir. *Research Journal of Applied Sciences, Engineering and Technology 7(24)*, 5227-5233.
- Janssens, G. (2016). *Scheldedijk wordt doorgestoken*. Retrieved from inshore.yachtweb: <http://inshore.yachtweb.be/wp-content/uploads/2015/11/bresproef.jpg>
- Kamrath, P., Disse, M., Hammer, M., & Köngether, J. (2006). Assessment of discharge through a dike breach and simulation of flood wave propagation. *Natural hazards, Volume 38, Issue 1*, 63-78.
- Morgenstern, N. R., & Price, V. E. (1965). The analysis of the stability of general slip surfaces. *Geotechnique 15*, 79-93.
- Morris, M. W., Kortenhaus, A., & Visser, P. J. (2009). Modelling breach initiation and growth. *FLOODSITE Report*.
- Néelz, S. (2008). Breach flow discharge prediction: analysis of USDA breach flow dataset. *Floodsite report number T06-08-03*, (p. 35).
- Nikolov, N. A., Minkov, I. N., Dimitrov, D. K., Mincheva, S. K., & Mirchev, M. A. (1978). Hydraulic calculation of a submerged broad-crested weir. *Hydrotechnical Construction, Volume 12, Issue 6*, 631-634.
- Oumeraci, H., Kortenhaus, A., & Visser, P. J. (2005). Breaching of coastal dikes: state of the art. *Floodsite Report*.
- Pařilková, J., Říha, J., & Zachoval, Z. (2012). The influence of roughness on the discharge coefficient of a broad crested weir. *Journal of Hydrology and Hydrodynamics, Volume 60, no 2*, 101-114.
- Peeters, P., Visser, P., & Mostaert, F. (2012). Organisation of in situ dike breaching experiments in Belgium: Monitoring program. Version 2\_0. WL Rapporten, 706\_08e. Flanders Hydraulics Research & Delft Unifersity of Technology. Antwerp, Belgium.

- Peeters, P., Zhao, G., Visser, P., & De Vos, L. (2012). Large-scale Dike Breaching Experiments at Lillo in Belgium. *Proceedings of the 7th international conference on Scour and Erosion, Chapter 32* (pp. 289-297). Perth, Australie: CRC Press.
- Rinaldi, M., Casagli, N., Dapporto, S., & Gargini, A. (2004). Monitoring and modelling of pore water pressure changes and riverbank stability during flow events. *Earth Surface Processes and Landforms volume 29*, 237-254.
- Singh, V. P., & Scarlatos, P. D. (1988). Analysis of gradual earth-dam failure. *Journal of hydraulic engineering* , 10.1061/(ASCE)0733-9429(1988)114:1(21), 21-42.
- Singh, V., & Quiroga, C. (1987). A dam-breach erosion model: I. Formulation. *Water Resources Management Volume 1, Issue 3*, 177-197.
- Skogerboe, G. V., & Hyatt, L. (1967). *Analysis of submergence in flow measuring flumes. Reports. Paper 94*. Retrieved from [http://digitalcommons.usu.edu/water\\_rep/94](http://digitalcommons.usu.edu/water_rep/94).
- Soil instruments. (sd). Datasheet W15 MEMS piezometer modem logger; .
- Spencer, E. (1967). A method analysis of the stability of embankments. *Geotechnique vol 17 issue 1*, 11-26.
- Temple, D. M., Hanson, G. J., Neilsen, M. L., & Cook, K. R. (1993). Simplified Breach Analysis Model for Homogeneous Embankments: Part 1, Background and Model Components. *Proceedings USSD, Salt Lake City*.
- Thant, S., Claeys, S., & Peeters, P. (2016). *Bresproeven Wijmeers*. Report Flanders Hydraulics Research, WL2016.
- Tracy, H. (1957). *Discharge characteristics of broadcrested weirs*. Washington D.C.: U.S. Departement of the interior.
- Van Rhee, C. (2007). Erosion of granular sediments at high flow velocity. *Hydrotransporte 17, The 17th international conference on hydraulic transport of solids*. Cape town, South Africa.
- Van Rhee, C. (sd). Sediment entrainment at high flow velocity. *Journal of hydraulic engineering, ASCE, vol. 136 no. 9*, (pp. 572-582).
- Van Rijn, L. (1993). *Principles of Sediment Transport in Rivers, Estuaries and Coastal Seas*. Amsterdam: Aqua publications.
- Visser, p. (1994). A model for breach growth in sand-dikes. Proc. 24th Int. Conf. coastal Eng., (pp. 2755-2769). Kobe, Japen.
- Visser, P. (1998). *Breach growth in sand-dikes, Doctoral thesis*. Delft University of Technology, Delft.
- Visser, P., Kraak, A. W., Bakker, W. T., & Smit, M. J. (1995). A large scale breaching experiment on breaching in sand dikes. *Proceedings of coastal dynamics '95*, (pp. 583-594). Gdansk, Poland.

- Visser, P., Vrijling, J. K., & Verhagen, H. J. (1991). A field experiment on breach growth in sand-dikes. *Coastal Engineering 1990*, 2087-2100.
- Whipple, K. (2002). Surface processes and landforms (12.163/12.463).
- Whitlow, R. (1983). *Basic soil mechanics*. New York: Construction press.
- Zerihun, Y. T., & Fenton, J. D. (2006). A one-dimensional flow model for flow over trapezoidal profile weirs. *Advances in Water Resources 29(11)*, 1598-1607.
- Zhao, G., Visser, P. J., Ren, Y., & Uijtewaal, W. (2015). Flow hydrodynamics in embankment breach. *Journal of Hydrodynamics, Volume 27, Issue 6*, 835-844.
- Zhu, Y. (2006). *Breach growth in clay dikes, PhD*. Delft University of Technology, Delft, The Netherlands.
- Zonsopgang en zonsondergang Wetteren*. (2015, November 3). Retrieved from <http://www.sunrise-and-sunset.com/nl/sun/belgie/wetteren/2015/november/1>

# 11 Annexes

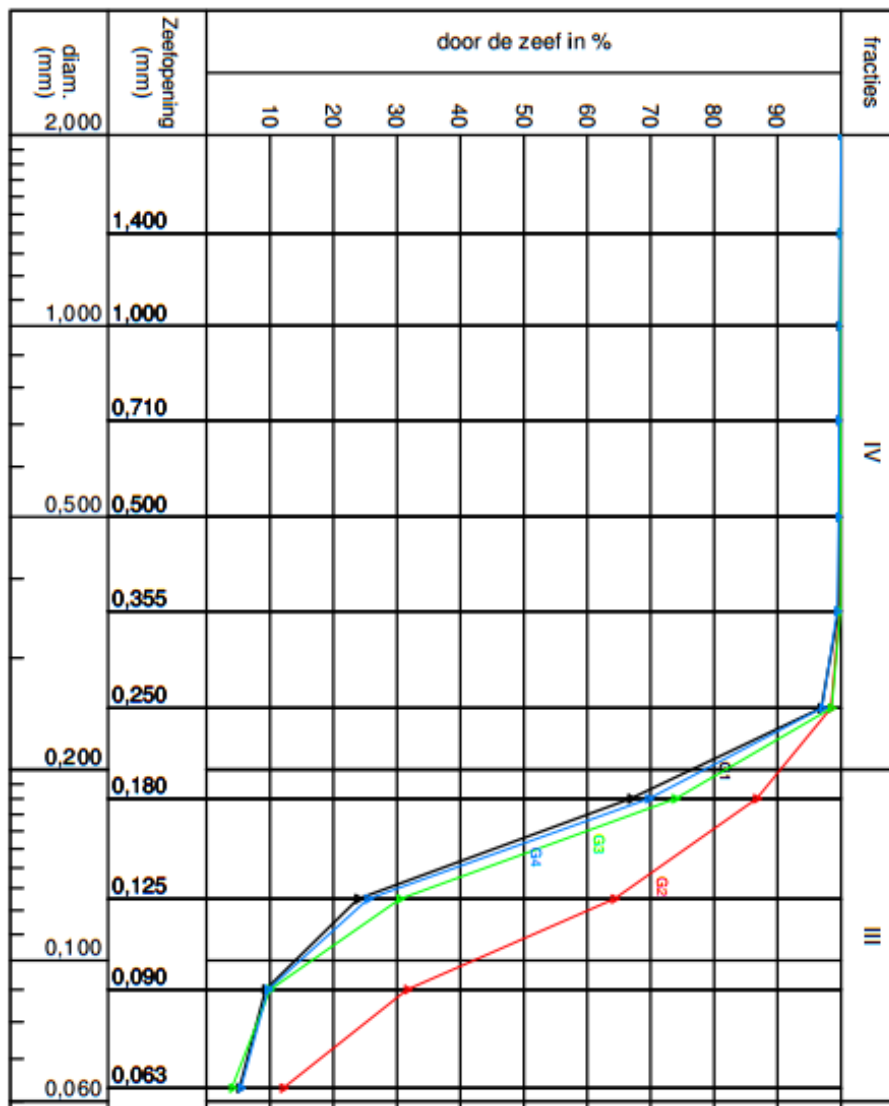
## Annex A: Soil characteristics dike

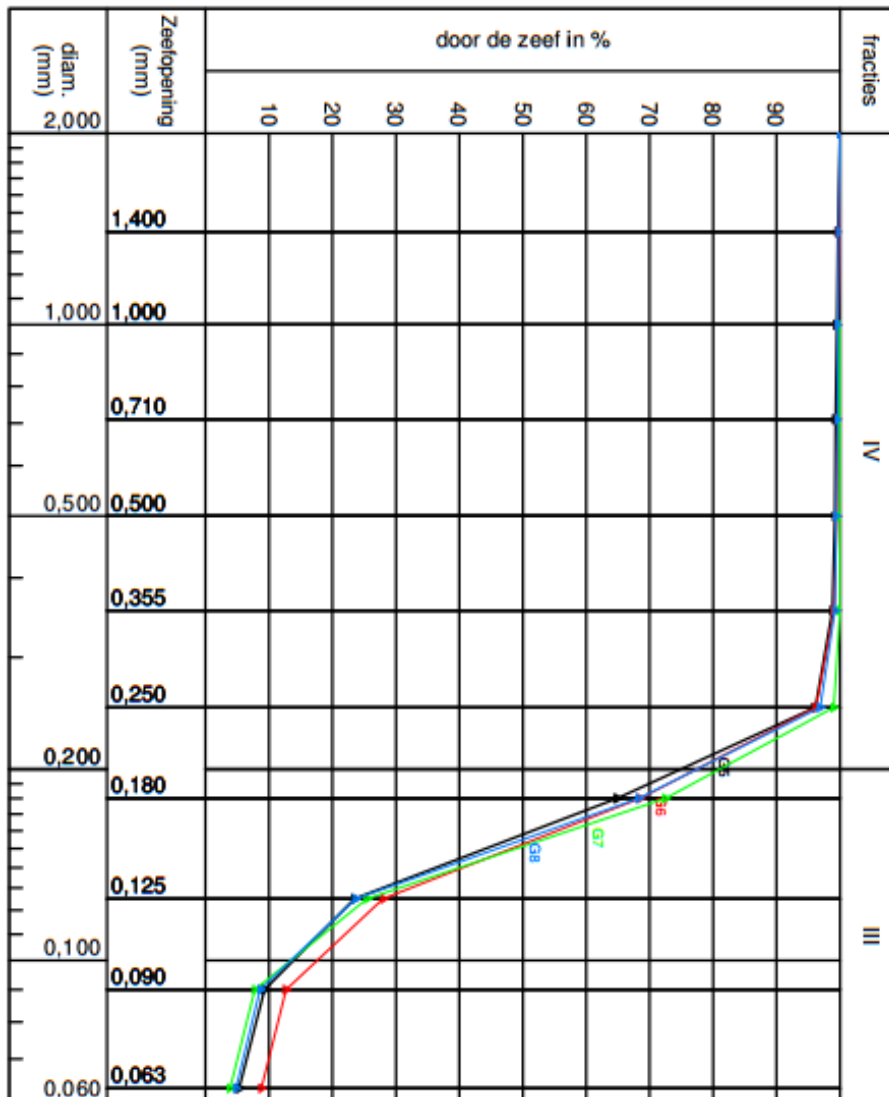
**JET HET test** (Irstea, 2015)

Soil tested	$\tau_c$ [N/mm <sup>2</sup> ]	$k_d$ [cm <sup>3</sup> /(sN)]
Sand core test 1	13,9-14,0	55,1-74,1
Sand core test 2	8,2-13,1	140,8-356,8
Clay lining	Not interpretable	Not interpretable

### Soil characteristics sand core

8 soil samples were taken of the central core, the results of a sieve test are displayed



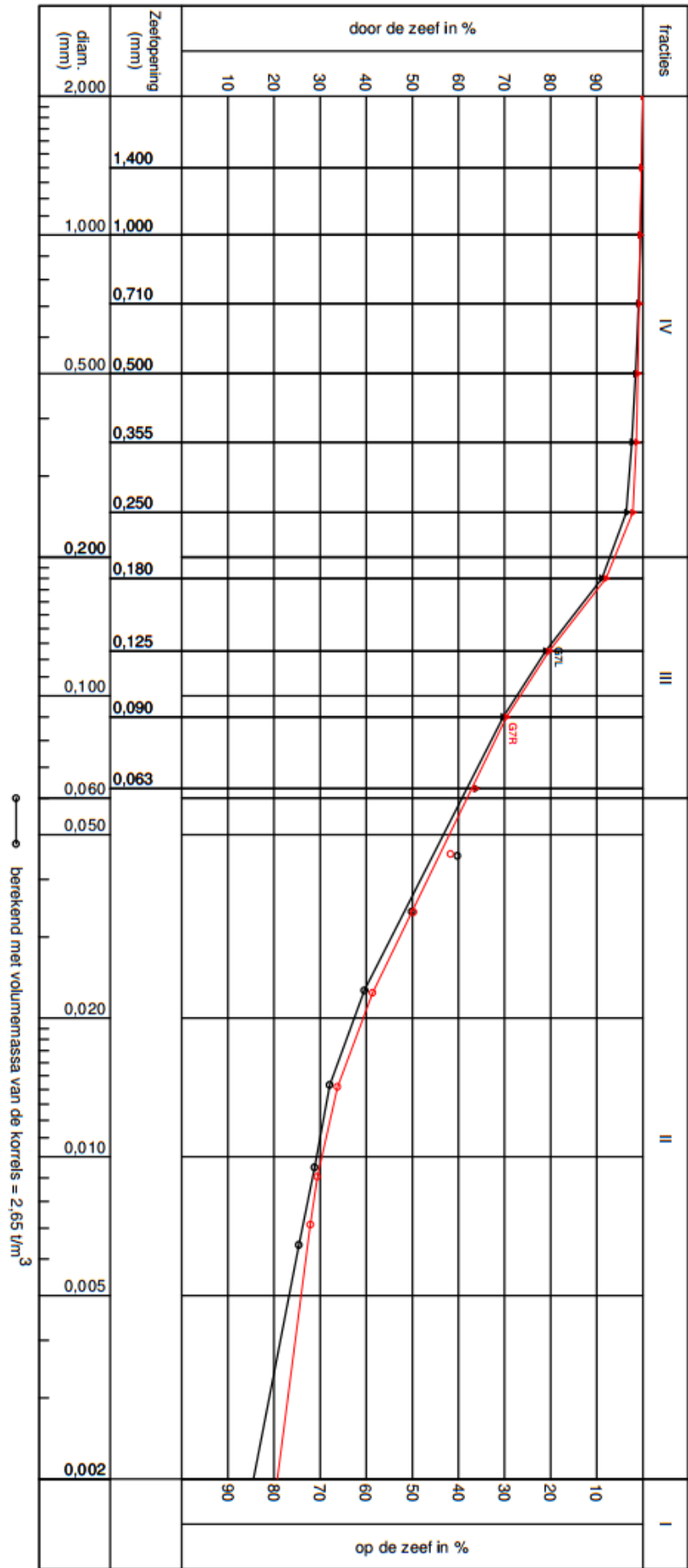


### Soil characteristics clay lining

herkomst & kenmerk	boringnr.	diepte (m)	monsternr.	grondsoort	korrelsamenstelling fractie					silbgehalte <0,02mm	vbeigrens	uitrolgrens	plasticijtsindex	humusgehalte	kalkgehalte	groepsymbool ASTM	activiteitsindex
					>IV	IV	III	II	I								
WICHELEN	nvt	0,1m	15/4146-nvt/G7L	weinig humush. zandh. klei	0,2*	7,3	32,0	45,2	15,5	37,4	66,6	27,4	39,2	4,6	3,2	CH	2,5
	nvt	0,1m	15/4147-nvt/G7R	weinig humush. zandh. klei	0,3*	6,2	32,0	41,1	20,7	39,3	58,6	21,7	36,9	2,5	3,4	CH	1,8

\* >2,000 mm in % t.o.v. korrels < 60 mm

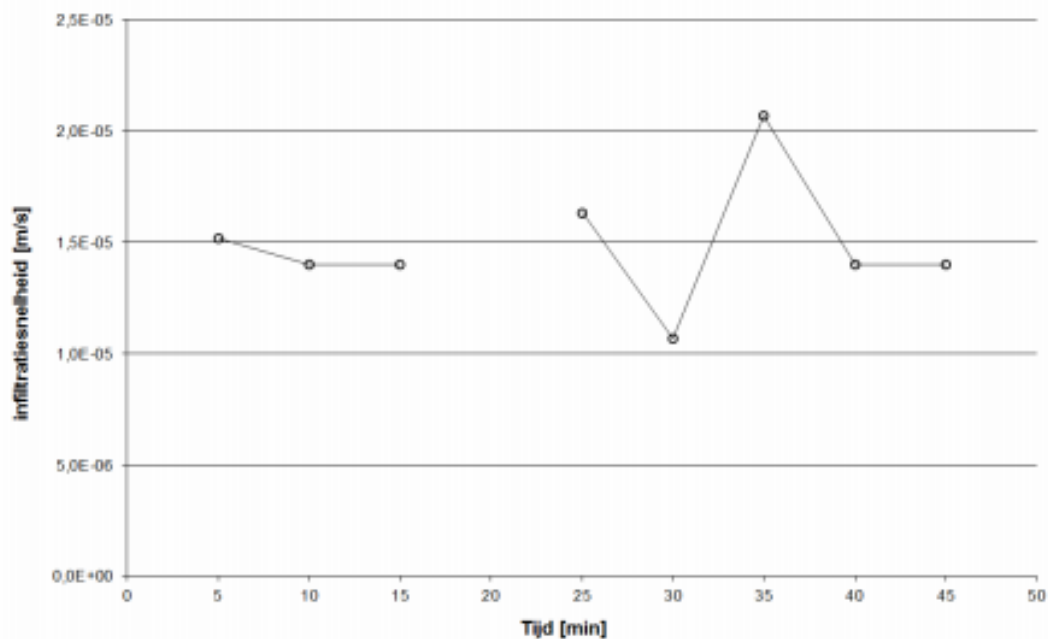




### Infiltration test in the breach

Opdracht <b>GEO- 15/144</b>	Datum <b>15/11/2015</b>	<b>WICHELEN</b> <b>x = 120157,5    y = 188564,0    z = 4,49</b>			Proef <b>INF BR</b>
--------------------------------	----------------------------	--	--	--	------------------------

Meting nr	Tijdsinterval	Cumulatieve tijd	Infiltratie	Infiltratiesnelheid	
				[cm/h]	[m/s]
1	5	5	325	5,46	1,52E-05
2	5	10	300	5,04	1,40E-05
3	5	15	300	5,04	1,40E-05
4	5	20	-	-	-
5	5	25	350	5,88	1,63E-05
6	5	30	371,4	3,84	1,07E-05
7	5	35	157,2	7,44	2,07E-05
8	5	40	300	5,04	1,40E-05
9	5	45	300	5,04	1,40E-05

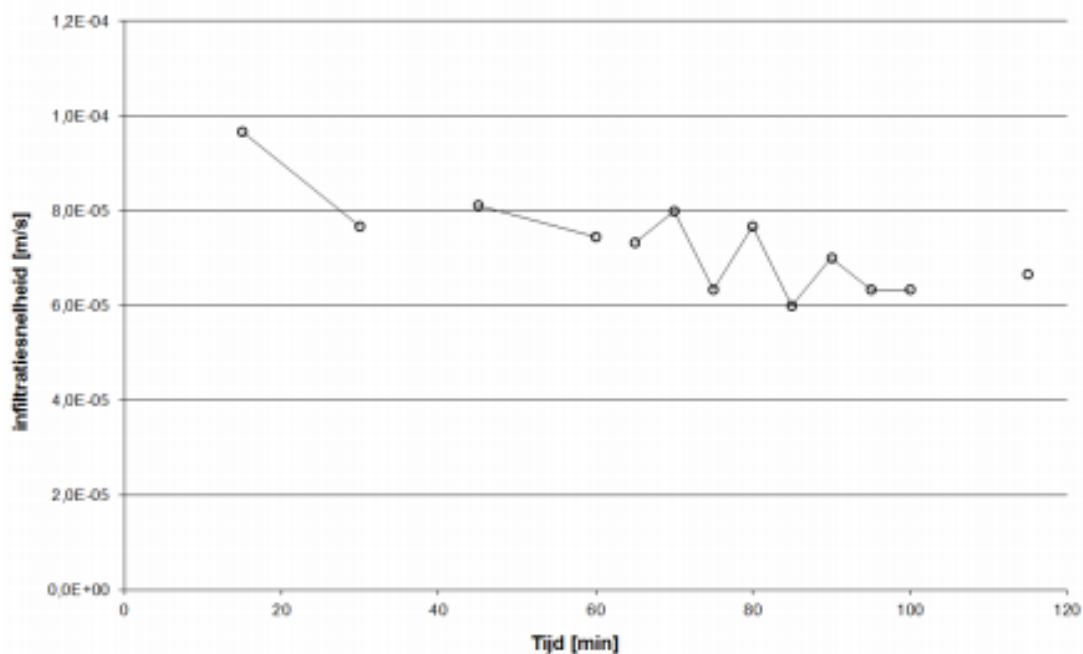


GEO-15/144  
Bijlage: 6/1

### Infiltration test on the dike slope

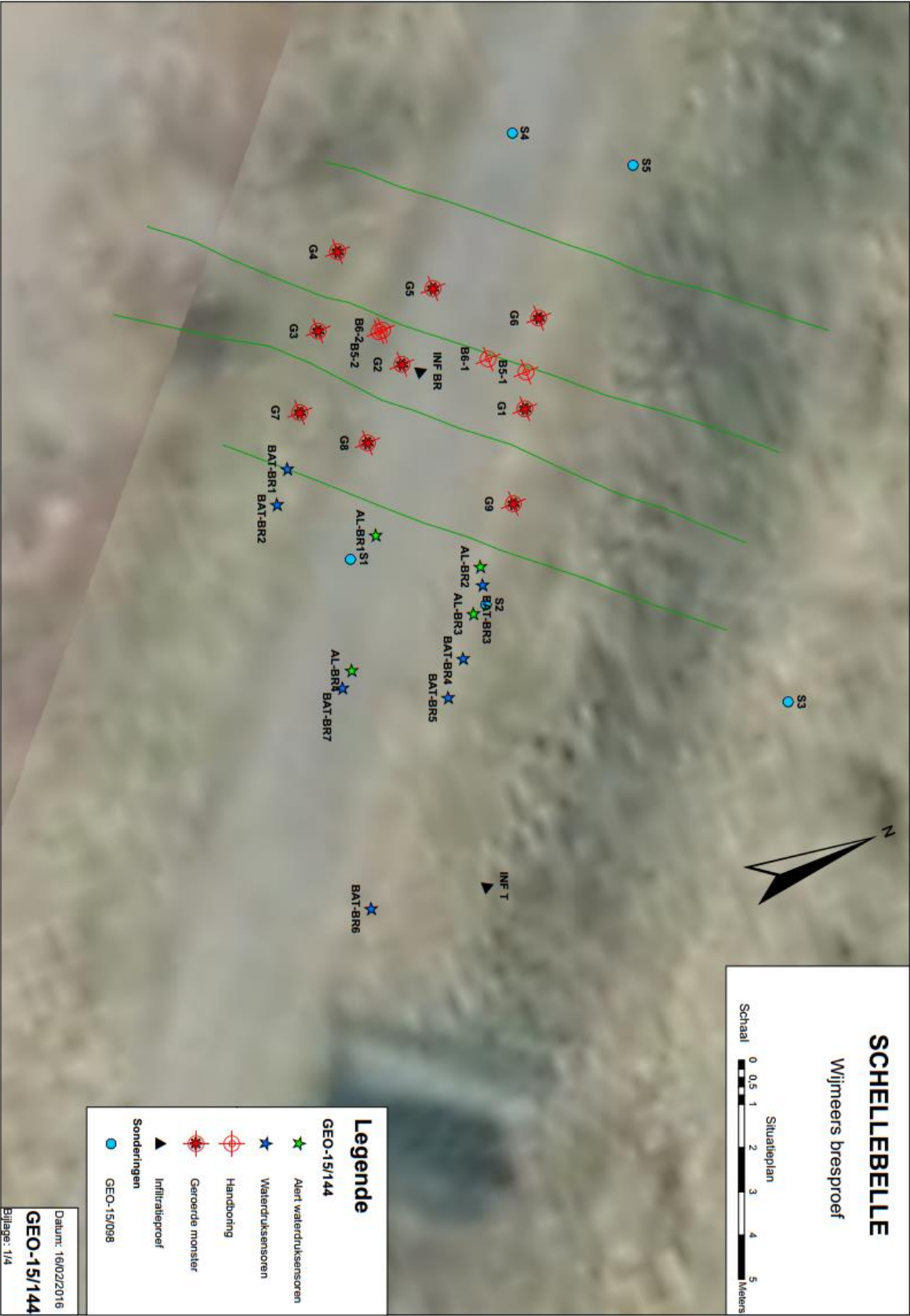
Opdracht <b>GEO- 15/144</b>	Datum <b>15/11/2015</b>	<b>WICHELEN</b> x = 120169,0    y = 188561,1    z = 6,23			Proef <b>INF T</b>
--------------------------------	----------------------------	---	--	--	-----------------------

Meting nr	Tijdsinterval	Cumulatieve tijd	Infiltratie	Infiltratiesnelheid	
				[cm/h]	[m/s]
1	15	15	9866,8	34,80	9,67E-05
2	15	30	7825,393	27,60	7,67E-05
3	0	30	-	-	-
4	15	45	8279,039	29,20	8,11E-05
5	15	60	7598,57	26,80	7,44E-05
6	0	60	-	-	-
7	5	65	2495,053	26,40	7,33E-05
8	5	70	2721,876	28,80	8,00E-05
9	5	75	2154,818	22,80	6,33E-05
10	5	80	2608,464	27,60	7,67E-05
11	5	85	2041,407	21,60	6,00E-05
12	5	90	2381,641	25,20	7,00E-05
13	5	95	2154,818	22,80	6,33E-05
14	5	100	2154,818	22,80	6,33E-05
15	10	110	-	-	-
16	5	115	2268,23	24,00	6,67E-05

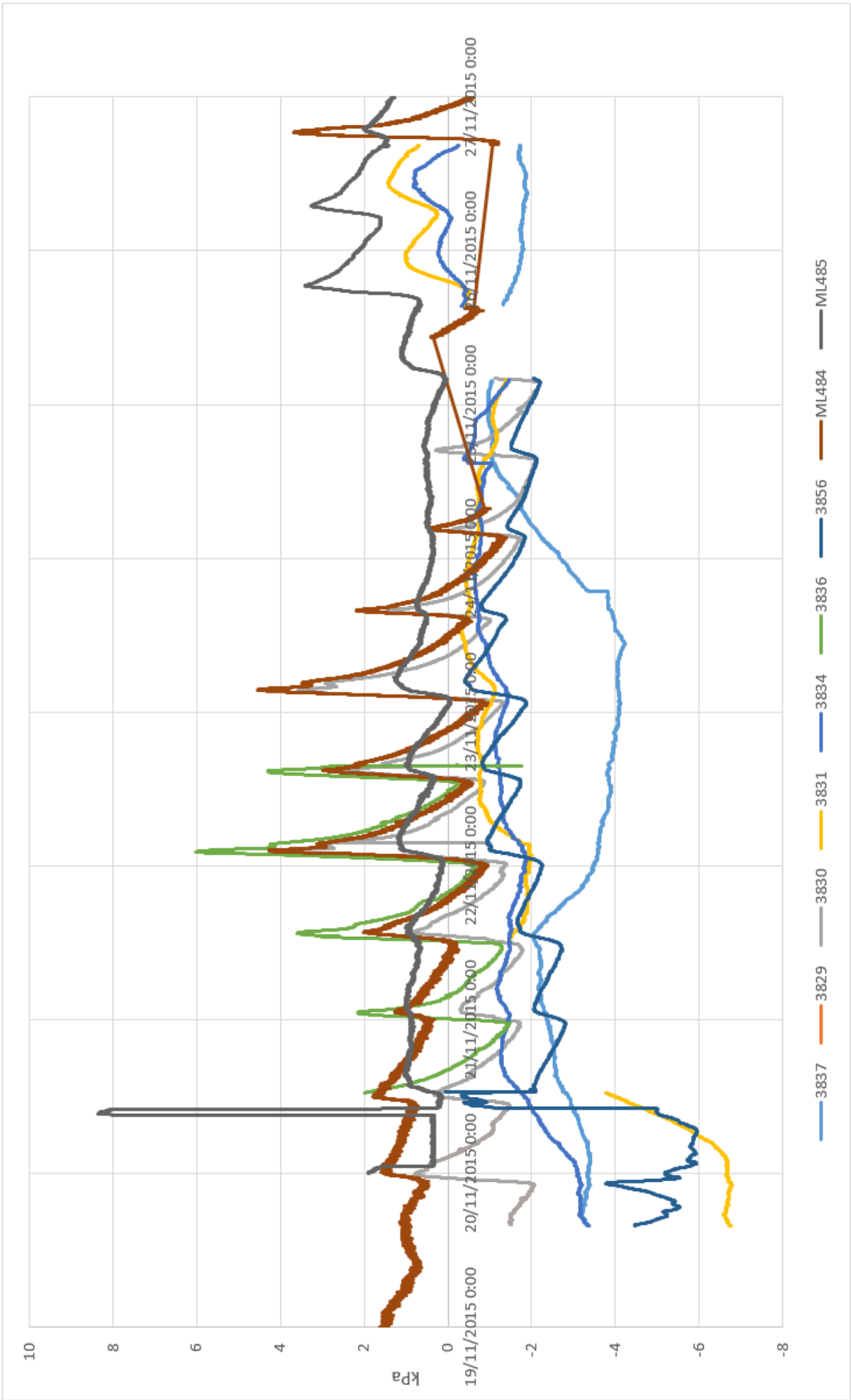


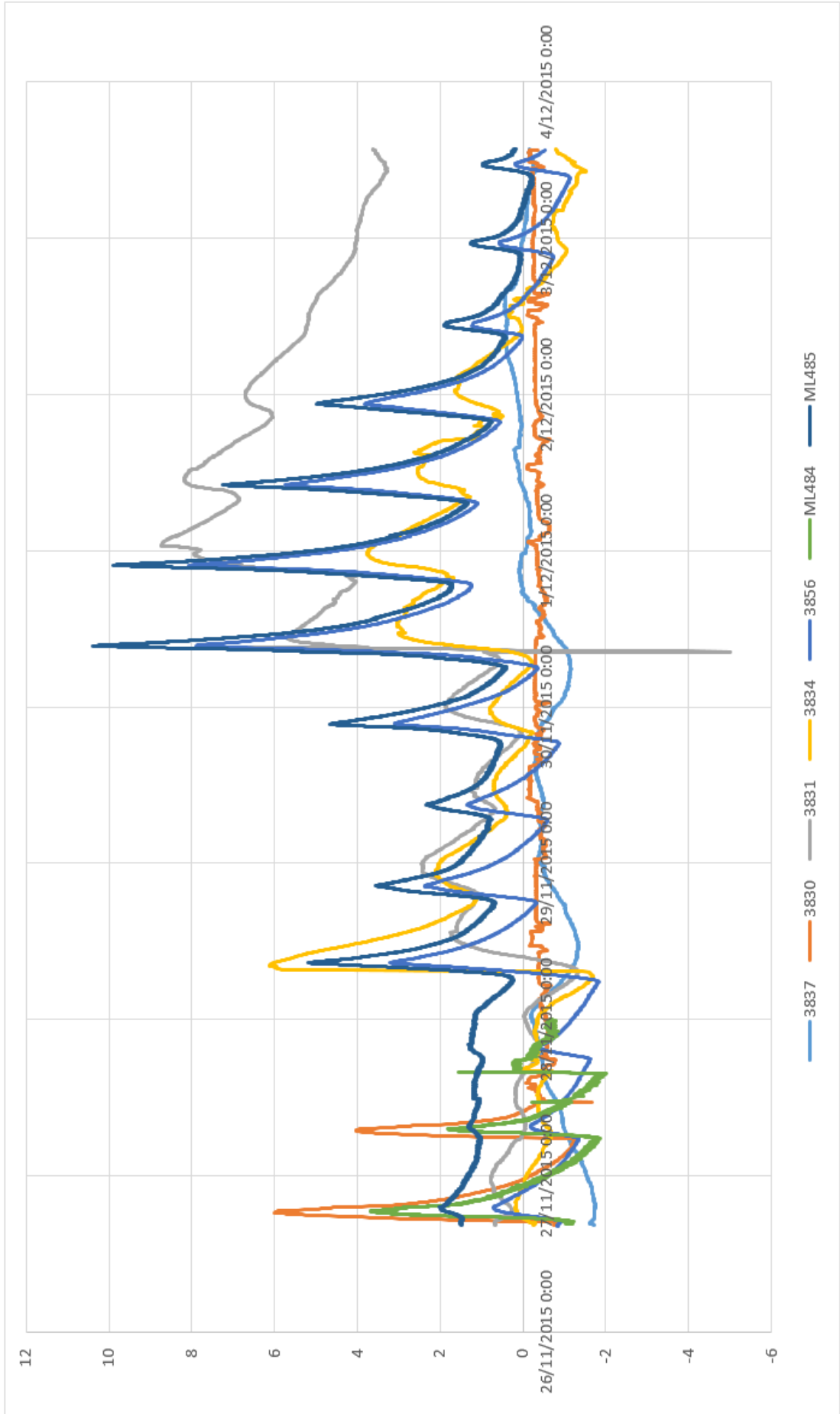
GEO-15/144  
Bijlage: 6/2

# Annex B: Plan of sensors and tests



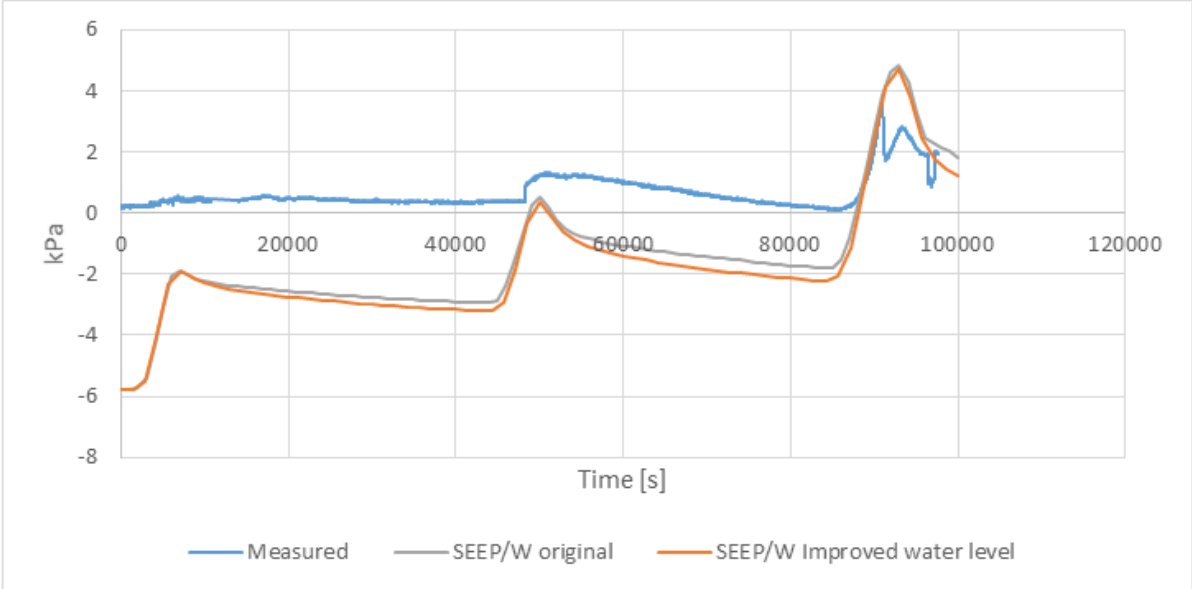
## Annex C: Water pressures recorded after the breach experiments



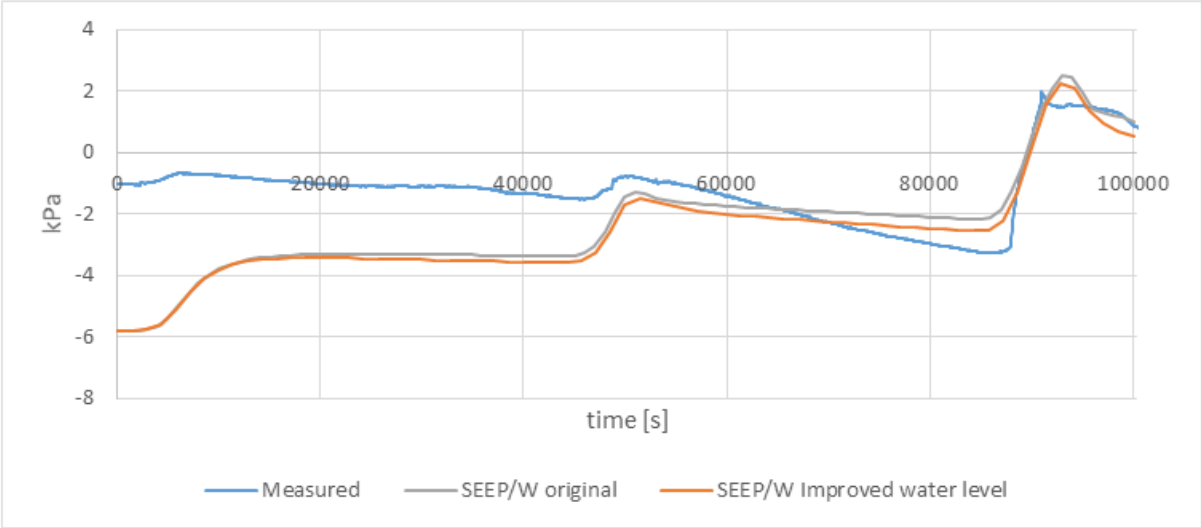


# Annex D: Calculated water pressures with lower water level

## ML 485 (only the non-eroded case is taken into account)

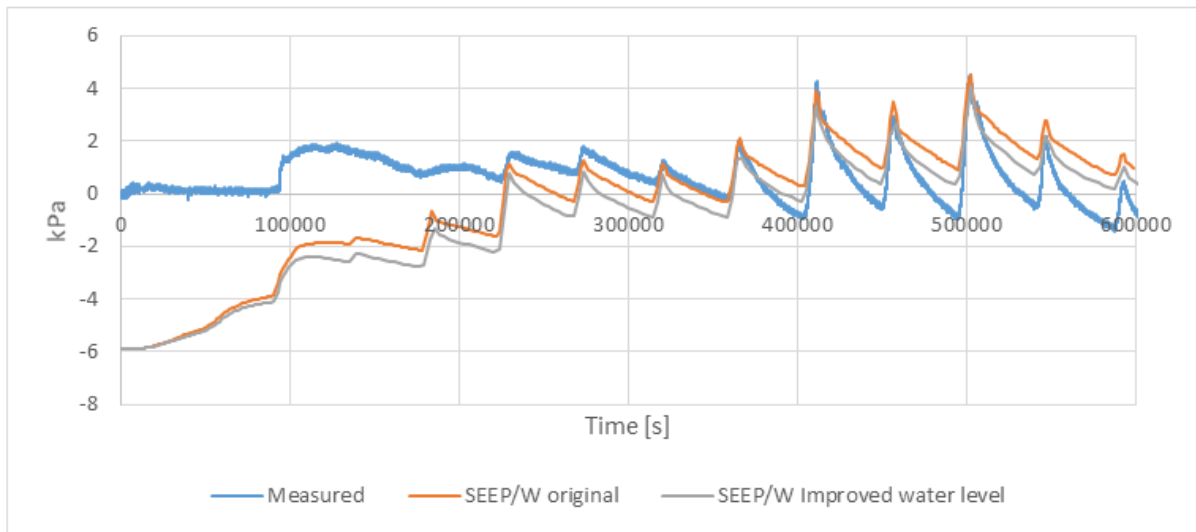


## BAT 3836 (only the non-eroded case is taken into account)

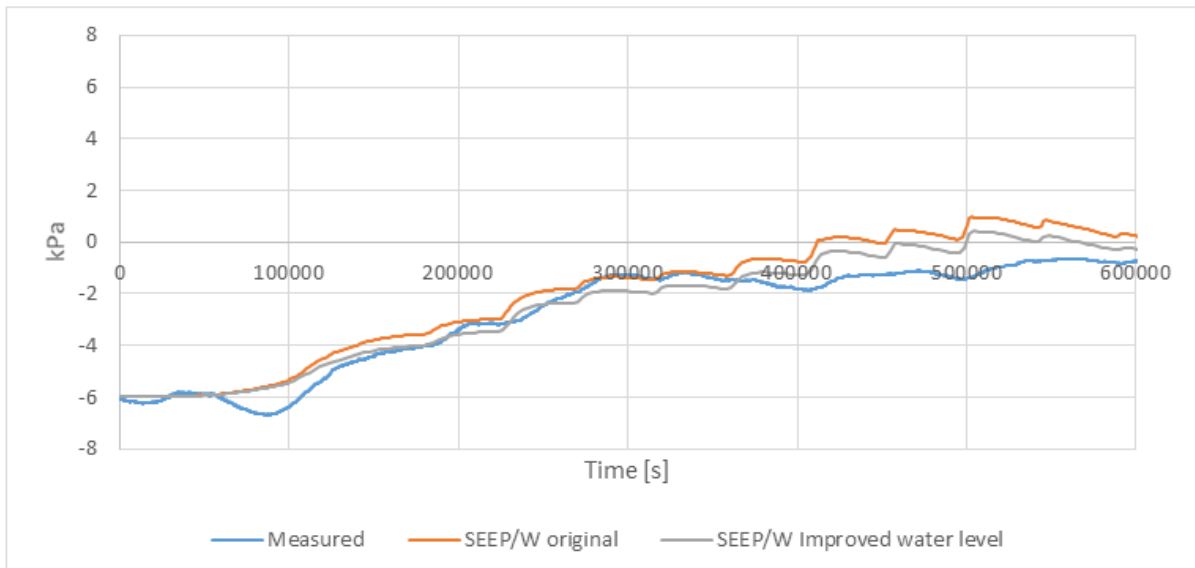




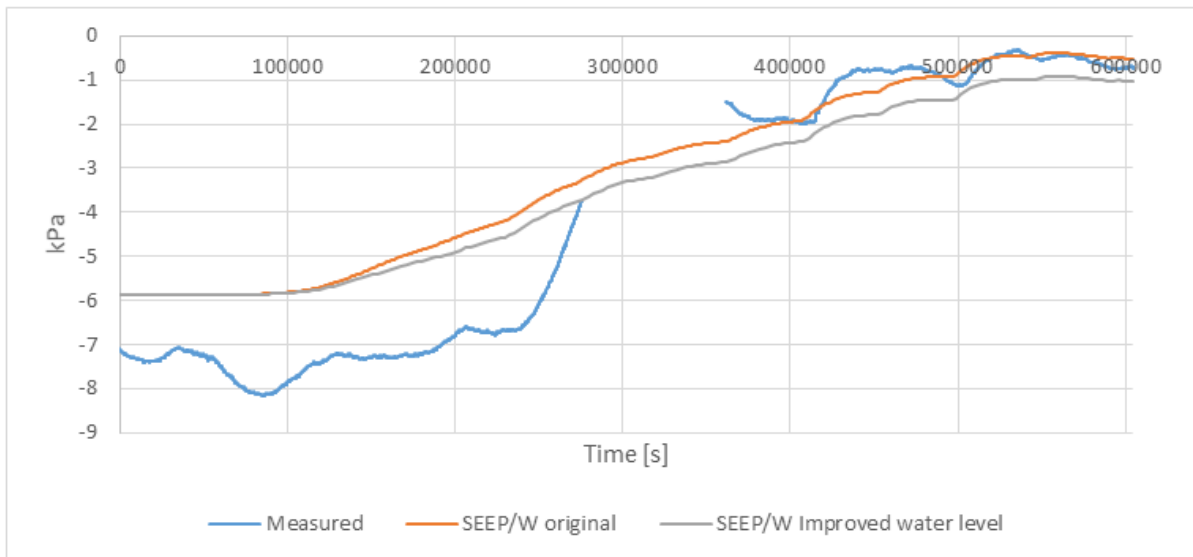
**ML 484**



**BAT 3834**



**BAT 3831**



**BAT 3837**

